TRAVELING WAVES IN PANCREATIC ISLETS

by

Heather Lyn Moreland

A dissertation submitted in partial fulfillment
of the requirements for the degree

of

Doctor of Philosophy

in

Mathematics

MONTANA STATE UNIVERSITY
Bozeman, Montana

August 2013

APPROVAL

of a dissertation submitted by

Heather Lyn Moreland

This dissertation has been read by each member of the dissertation committee and has been found to be satisfactory regarding content, English usage, format, citations, bibliographic style, and consistency, and is ready for submission to The Graduate School.

Dr. Jack D. Dockery

Approved for the Department of Mathematics

Dr. Tomáš Gedeon

Approved for The Graduate School

Dr. Ronald W. Larsen

STATEMENT OF PERMISSION TO USE

In presenting this dissertation in partial fulfillment of the requirements for a doctoral degree at Montana State University, I agree that the Library shall make it available to borrowers under rules of the Library. I further agree that copying of this dissertation is allowable only for scholarly purposes, consistent with "fair use" as prescribed in the U. S. Copyright Law. Requests for extensive copying or reproduction of this dissertation should be referred to Bell & Howell Information and Learning, 300 North Zeeb Road, Ann Arbor, Michigan 48106, to whom I have granted "the exclusive right to reproduce and distribute my dissertation in and from microform along with the non-exclusive right to reproduce and distribute my abstract in any format in whole or in part."

Heather Lyn Moreland

August 2013

DEDICATION

To my parents, Jim and Judy Moreland, who supported me through the dark times and celebrated the much brighter ones with me...All of my love and gratitude to my parents. They are some of the most understanding, accommodating, supportive, and loving parents any daughter could ever hope for.

ACKNOWLEDGEMENTS

First and foremost, I am particularly grateful to my advisor, Dr. Jack Dockery, for stepping in to assist me when I most needed it and for his uncanny ability to provide simple examples that make complicated ideas and concepts seem so much simpler. I also extend my gratitude to Dr. Lisa Davis for always being so supportive.

Several dear friends deserve special thanks for their assistance and encouragement throughout this process. To Mark and Heather Mathison: there are not words to describe how much your friendship means to me...I would never have persevered without your encouragement and support. To Jami Bartole: your willingness to be there at a moments notice for that needed pick-me-up is amazing. Hopefully I can reciprocate a small percentage of the comfort you have given me. To Derrick Cerwinsky: even from a distance you were helping me through the dark times and celebrating with me during the good times. And to Sarah Schaefer: you have been my personal cheerleader for the past many months and that has meant the world to me. Now it is my turn to cheer you on as you approach the finish line...

I am forever indebted to Dr. Stephen Bricher at Linfield College. You will never know how significantly you have influenced my career. You introduced to me this research area and continue to affect my teaching to this day. I look forward to our continued friendship.

TABLE OF CONTENTS

LIST OF TABLES

LIST OF FIGURES

Figure Page

LIST OF FIGURES - CONTINUED

Figure Page

LIST OF FIGURES - CONTINUED

Figure Page

LIST OF FIGURES - CONTINUED

Figure Page

ABSTRACT

In response to an increase in blood glucose levels, insulin is released into the bloodstream by the pancreatic islets of Langerhans. As a result of this influx of glucose, the islets start what are called bursting oscillations of the membrane potential and the intracellular calcium concentration. Time delays of several seconds in the activity of distant cells in the islets have been observed, indicating the presence of traveling waves through the islets.

By considering a robust model of a pancreatic islet in one dimension, we study the relationship between the wave speed and the model parameters for the existence of traveling wave fronts and traveling wave pulses. After a systematic reduction of the model equations, the wave fronts (or heteroclinic connection) are studied. Using the bi-stable equation, for which an exact expression of the heteroclinic connection can be computed, we use a homotopy parameter to move from this equation to an islet model. A relationship between the wave speed and the conductance of the ATP-modulated potassium channel is constructed. Upon the inclusion of the slow gating variable back into the model equations, we observe the presence of a traveling wave pulse (or homoclinic connection). Using a high period periodic orbit to approximate the homoclinic orbit, a similar relationship between these two parameters is constructed. We observe that the heteroclinic connection is a good approximation for a portion of the homoclinic connection. Comparisons of the speed of the wave traveling through the islet in the partial differential equation model and the model in traveling coordinates is carried out.

Since pancreatic islets are roughly circular, a two-dimensional model of an islet is also simulated on the unit disk. Due to the higher dimensionality of the problem, the numerics become more expensive. An alternating direction implicit (ADI) method for nonlinear parabolic differential equations is adapted for polar coordinates and mixed (Robin) boundary conditions. Using this method, we observe that the larger the portion of the boundary of the islet exposed to a stimulatory glucose concentration, the more rapidly the wave activity reaches the interior of the islet.

CHAPTER 1

INTRODUCTION

Background

The pancreas is an organ that regulates the body's metabolism by maintaining blood glucose levels through the secretion of hormones. In response to a rise in glucose levels in the blood plasma, such as after a meal, insulin is secreted by β-cells in the pancreas. The release of insulin signals target tissues, such as muscle and liver tissues, that glucose is available to be stored or used as fuel. As the glucose levels in the blood decline, the insulin secretion decreases and the cells in the target tissues return to using stored carbohydrates, fats, or proteins for energy. In effect, the pancreas acts as the body's thermostat. Defects in this glucose-insulin feedback loop can cause serious complications, the most well-known of which is diabetes.

In Type 1 diabetes, also known as early-onset or juvenile diabetes, the immune system in the body attacks and kills the pancreatic β-cells that produce insulin. People afflicted with Type 1 diabetes do not produce any insulin and, as a result, they must carefully monitor their blood sugar levels and inject insulin to control these levels. Type 1 diabetes has no cure and failure to control blood sugar levels can result in blindness, loss of appendages due to poor circulation and neuropathy, and early death.

Type 2 diabetes, also known as late-onset diabetes, can involve several components. One of the contributing factors is that the body does not properly respond to the insulin it produces. Defects in the β-cells or a deficit in β-cell mass resulting in decreased insulin levels is also associated with Type 2 diabetes. The majority of occurrences of diabetes are late-onset. Often Type 2 diabetes can be controlled through diet and exercise. If not, drugs can be used to increase insulin secretion or insulin injections are used to control the affliction.

With either form of diabetes, the importance of understanding insulin secretion motivates the study of pancreatic β-cells. β-cells are clustered in micro-organs in the pancreas called islets of Langerhans. When exposed to a stimulatory glucose concentration, the membrane potential of the β-cells exhibits a characteristic pattern of electrical activity called bursting. Electrical gap junctions connect most neighboring β-cells in the islet and act to synchronize the pattern of electrical activity. Bursting electrical activity, or "bursting" for short, is a periodic phenomenon characterized by a silent phase where the membrane potential changes slowly followed by an active phase where the membrane potential oscillates rapidly. As the glucose concentration increases, the active phase of the burst lengthens and the silent phase shortens. It is during the active phase that insulin is secreted. As a result, β-cell electrical activity is a critical component of the glucose induced insulin secretion process. The study of the electrical behavior of β-cells is motivated by gaining a better understanding of insulin release.

In the past, the bursting of β-cells in a single islet was thought to be synchronized across the whole islet due to the gap junction coupling between the cells. In reality, time delays of several seconds in the activity of distant cells are usually observed. This indicates that electrical/calcium wave propagation occurs in the islets of Langerhans. Aslanidi et al. [1] presented experimental evidence for this wave propagation and suggested these waves act as a signal which controls the insulin secretion inside the islet. In these experimental studies, an islet of Langerhans is secured to the bottom

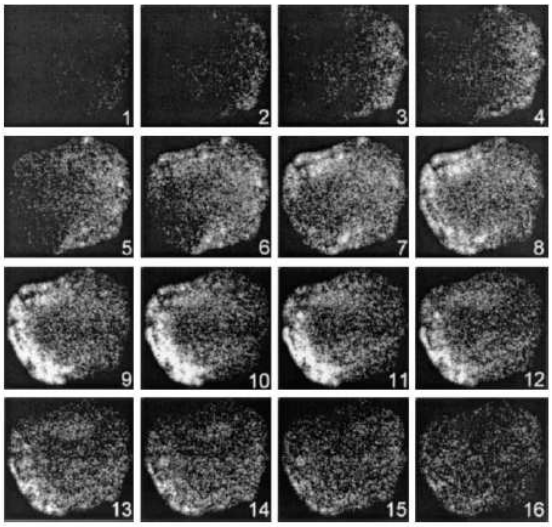

Figure 1: Pancreatic islet in a glucose bath showing the calcium wave propagating from the right edge to the left edge of the islet. The images are taken at one second intervals. First derivatives of the original images are shown to illuminate the temporal intensity changes. Taken from [1].

of a perifusion chamber. Through an inflow tube, substances such as glucose are introduced to the bath and the electrophysiological response of the β-cells inside is continuously observed. In Figure 1 we can see a calcium wave emerge from the right

side of the islet and travel leftward, terminating at the bottom left edge of the islet. These types of waves, with the activity initiated at the islet periphery, have been observed in 85% of the roughly 100 conducted experiments [1]. In the rest of the experiments the islets exhibited uniform oscillations. The waves emerging from the boundary of the islet can be explained by the fact that the glucose, which is responsible for the bursting oscillations, initially penetrates the islet along the boundary. In Figure 1 we see waves periodically emitted from the edge of the islet. This behavior was observed throughout the duration of the experiments, approximately 30 minutes. It should also be noted that the wave pattern is not symmetric. The waves initiated at distinct locations along the periphery which can be explained by the fact that there are some cells in the islet with a lower glucose response threshold as well as the the nonuniform distribution of the cell parameters in the islet. These two factors can also explain the emergence of waves from the inner regions of the islet.

The goal in this thesis is to gain a better understanding of the parameters responsible for the waves of electrical activity and, in particular, how these parameters affect the speed of propagation through the islet. We must first understand the β-cell electrophysiology and then proceed with a systematic reduction of the robust islet model to a system that is more amenable to analysis. The islet model will incorporate the latest β-cell model along with a model of glucose diffusion through an islet as proposed by Bertram and Pernarowski in 1998 [2]. The remainder of this introductory chapter is devoted to describing the necessary background information.

In Chapter 2, we will develop the model of the islet by first studying a single β-cell. This model can be extended to the islet by incorporating gap junctional coupling of β-cells and implementing the theories presented by Pernarowski [3]. The islet model is connected to the model of glucose diffusion through an expression that accounts for the known effects of glucose on electrical activity in β-cells. This combined model can be viewed in one or two dimensions.

The one-dimensional version of the model will be considered in Chapter 3. We investigate the presence of traveling wave fronts and pulses through a one-dimensional representation of a pancreatic islet. Using a systematic reduction of setting some of the kinetic variables to their stationary values, the model is simplified to an equation that is qualitatively the same as the bi-stable equation. For this equation, the exact representation of the traveling wave front can be computed. Using this exact expression as a starting point, we homotopy to an islet model equation and construct a continuation curve for the existence of a traveling wave front. We discuss how the wave speed for the traveling wave front is to leading order the wave speed for the associated traveling wave pulse present when the slow gating variable is reincorporated into the model. A similar continuation curve is constructed for the presence of the wave pulse and it is shown that there is good agreement between the wave front and pulse wave speeds. Finally, the wave speeds obtained from the system in traveling coordinates are compared to those obtained from simulations of the partial differential equation model. We note that the estimates from the PDE model are consistently

higher. Since the speed of the actual traveling wave is only being computed when the system is in traveling coordinates, we concluded that those speed computations are more accurate.

In Chapter 4, a two-dimensional distribution of β-cells on the unit disk will be presented. The increase in the dimensionality of the problem results in a much more computationally intensive simulation. Using Alternating Direction Implicit (ADI) methods first proposed by Peaceman, Rachford, and Douglas in 1955 [4, 5], the structure of the resulting equations allows for more efficient computations. In addition, because the islet model is nonlinear, we incorporate a modification of the ADI method for nonlinear parabolic partial differential equations proposed by Amiri and Hosseini in 2010 [6] that yields an unconditionally stable method that is second order in time and space. Using this nonlinear ADI method, numerical simulations of a two-dimensional islet are carried out. This provides a more realistic representation of the experimental observations. We consider different percentages of the boundary of the islet being exposed to a glucose concentration and observe how this affects the speed of the wave propagating through the islet. There appears to be a correlation, i.e., the more of the islet boundary exposed to glucose, the shorter the burst cycle. This relationship is logical since the larger the portion of the boundary exposed to glucose, the more β-cells will be exposed to the glucose concentration. As a result, the cascade of electrical activity will initiate over a larger range of boundary cells and cause the wave to propagate into the islet more quickly. In Chapter 5, we will

summarize the main results in this thesis.

Physiology

All cells are enclosed by a thin membrane made of phospholipid molecules. The membrane structure is formed by the phospholipids automatically lining up into two layers, that is, a bilayer. The hydrophobic fatty acid tails of the molecules are located on the inside layers and act as an impenetrable wall to water soluble molecules. Across the cell membrane boundary there exists an electropotential gradient referred to as the membrane potential which is measured on the scale of millivolts. The membrane potential arises from an imbalance of electrical charges across the cell membrane as well as the flow of ionic currents through the membrane. The principle mechanism for ionic movement through the cell membrane is the difference in the electric potential and the ionic concentrations across the membrane.

Cells can be divided into two groups: excitable cells and nonexcitable cells. When a sufficiently strong current is applied to excitable cells, the membrane potential goes through a large excursion called an action potential before eventually returning to its rest state. There are many examples of excitable cells, including cardiac cells, smooth and skeletal muscle cells, endocrine and secretory cells (including β-cells) and most neurons. In contrast, if a current is applied to a nonexcitable cell for a period of time, the potential will instantaneously return to rest once the stimulus is removed. One such example of nonexcitable cells are the epithelial cells in the gastrointestinal

system.

The composition of the cell membrane plays an important role in its electrophysiological dynamics. Many types of protein molecules can be found within the phospholipid bilayer. Some proteins are receptors for chemical signals or enzymes that catalyze reactions. Other proteins regulate the transport of ions across the cell membrane. These protein molecules form pores in the membrane called ionic channels which act as selective gates, only permitting a specific type of ion to pass through. The channels are not open at all times and are regulated primarily by changes in voltage and ionic concentrations. If a channel is activated by a change in the membrane potential, it is said to be voltage gated. Changes in ionic concentrations, either inside or outside the cell, can also affect the status of an ionic channel, and in this case, the channel is said to be ion gated. Chemicals such as ATP (adenosine triphosphate) can also affect the state of an ionic channel. The protein channels play a major role in the electrical activity seen in different types of cells.

The concentration gradient present across the cell membrane is due to differences in concentrations of ions inside and outside of the cell. Potassium ions are at a higher concentration inside the cell than outside, while sodium, calcium, and chloride ions are more abundant outside the cell. The movement of ions through open channels is driven by differences in electric potential and ionic concentration across a cell membrane as well as by the binding of ligands or messenger molecules. Since potassium ions are at a much higher concentration inside the cell, the concentration gradient

pushes these ions outward through open channels. In contrast, the electrical gradient tends to hold the positively charged potassium ions inside the cell membrane since the inside is about -60 mV with respect to the outside. The net forces are in opposition and it is not immediately apparent which influence, diffusional or electrostatic, is dominant. To compare the magnitude of these forces, the concentration gradient can be expressed as an equivalent electrical gradient using the Nernst equation. The Nernst potential for a particular ion, V_{ion} is as follows:

$$V_{ion} = \frac{RT}{Fz} \ln \frac{C_o}{C_i},$$

where

R = universal gas constant (8.31 Joules/mole/Kelvin)
F = Faraday's constant (96.487 Coulombs/milli-mole)
T = Temperature (Kelvin)
z = valence of the ion
C_o = concentration of the ion outside the cell
C_i = concentration of the ion inside the cell .

The potential difference calculated from the Nernst equation is referred to as the equilibrium potential for the ion. For the potassium ion, $V_{ion} = V_K \approx -75$ mV which means if the inside of the cell membrane was at this potential in relation to the outside, then the net diffusional and electrostatic forces would be balanced.

The flow of charged particles through the protein channels generates electrical currents affecting the membrane potential. In a nerve cell, potassium and sodium ions are responsible for action potentials during which the membrane potential is

briefly reversed. The voltage depolarizes rapidly from the rest state of approximately -65 mV, reaches a peak, then undershoots before returning to rest, as in Figure 2.

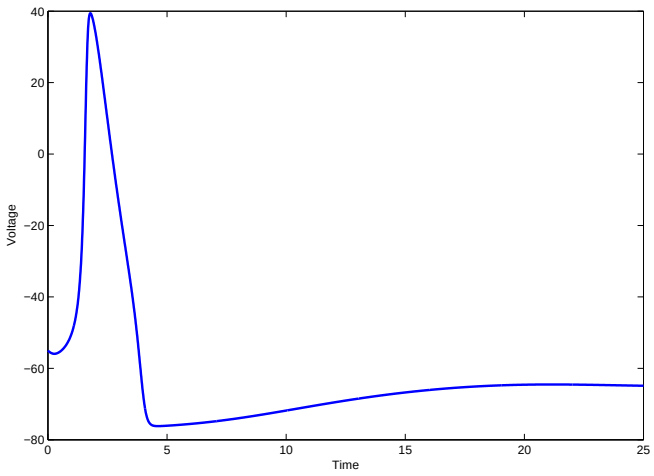

Figure 2: An action potential from the Hodgkin-Huxley neuron model of a squid giant axon. The Hodgkin-Huxley model will be discussed in detail in the next section.

The question of how to model these action potentials mathematically was answered in the 1950s with the profound work of Alan Hodgkin and Andrew Huxley [7] and their model of the membrane potential of a nerve cell.

Hodgkin-Huxley Model

The generation and propagation of action potentials has been studied by physiologists for the past one hundred years. However, it was not until the 1950s that the landmark work by Alan Hodgkin and Andrew Huxley broke the study of these phenomena wide open and resulted in the Nobel prize in medicine in 1963. Using the

giant axon from a squid, Hodgkin and Huxley developed the first quantitative model for the propagation of electrical signals along neurons. They modeled the nerve cell membrane as a leaky capacitor where current is passed through the membrane by the flow of ions or by charging the membrane capacity. Thus the total membrane current, I_m, is separated into a capacitive current and the ionic currents, given by the following equation

$$I_m = C_m \frac{dV}{dt} + I_{ion},$$

where C_m denotes the membrane capacitance, I_{ion} represents the sum of all ionic currents, V is the membrane potential and t represents time. In their experiments, Hodgkin and Huxley determined that there were two primary ionic currents: sodium and potassium. They also noticed that there were other types of currents but these were relatively small and could be lumped together in what was called a leak current. Thus, the total ionic current is given by

$$I_{ion} = I_K + I_{Na} + I_{leak}.$$

The difference between the concentration and electrical gradients for each ion produces a net driving force which is proportional to the difference between the membrane potential and the corresponding Nernst potential, $V - V_{ion}$. The ion carries a current which depends on this driving force as well as the permeability of the membrane to the ion, which is inversely proportional to resistance. According to Ohm's Law,

$$I_x = g_x \left(V - V_x\right)$$

where the conductance (the reciprocal of the resistance), g_x, is used as opposed to the resistance to remain consistent with the physiologists. Therefore, the potassium, sodium and leakage currents have the form

$$I_K = g_K\,(V - V_K)\,, \quad I_{Na} = g_{Na}\,(V - V_{Na})\,, \quad I_{leak} = g_{leak}\,(V - V_{leak})\,.$$

By Kirchoff's Law, the capacitive and ionic currents are in balance, that is, the total membrane current I_m is zero. The result is the current balance equation that is typical of a Hodgkin-Huxley type model

$$C_m \frac{dV}{dt} = -\sum_x I_x = -\left[\, g_K\,(V - V_K) + g_{Na}\,(V - V_{Na}) + g_{leak}\,(V - V_{leak})\,\right].$$

The dynamic nature of the ionic conductances means that the current balance equation is more complex than it appears. The conductance g_{ion} is essentially the permeability of the membrane or the ease with which the ion passes through the membrane. It has been observed experimentally that g_{ion} depends on the state of that particular ionic channel which in turn depends on the electrical and chemical gradients as well as the binding of messenger molecules. Hodgkin and Huxley thought of a channel as being composed of several gates each of which is either open or closed. As a result, each conductance is a dynamic variable depending on the status of the gates. As an example, the potassium channel was assumed to be regulated by four equal gates while the sodium channel was assumed to be regulated by three 'activation' gates and one 'inactivation' gate. The probability that a gate is open is

represented by 'gating' variables, h, m, and n, where h is the variable representing the status of the inactivation gate of the sodium channel and m and n variables represent the status of the activation gates of the sodium and potassium channel, respectively. Since these gating variables represent probabilities, their values range between 0 and 1. The individual ionic conductances are specified by the product of a maximal conductance, $\bar{g}_x$, which is realized if all the relevant channels are opened, and the product of the corresponding gating variables. For example, the potassium conductance is written as

$$g_K = \bar{g}_K \, n^4,$$

and the sodium conductance is written as

$$g_{Na} = \bar{g}_{Na} \, m^3 h,$$

where $\bar{g}_K$ and $\bar{g}_{Na}$ are the maximal conductances for the potassium and sodium channels, respectively. The exponents to which the gating variables are raised were chosen by Hodgkin and Huxley based on a fit to experimental data. Several years after their work was completed, it was discovered that the sodium channel is formed by a single protein molecule consisting of four subunits, three of which are identical and one, distinct from these three. The sodium channel is assumed to be open if three similar subunits ('particles') are active ('occupy certain positions') and one other subunit is inactive. This lends further credence to the model equations suggested by Hodgkin and Huxley.

The dynamics of the gating variables h, m, and n are described by

$$\frac{dx}{dt} = \alpha_x(V)(1-x) - \beta_x(V)x, \quad x = h,\, m,\, n, \tag{1.1}$$

where $\alpha_x(V)$ and $\beta_x(V)$ are rate constants. Consider the above equation for the gating variable n of the potassium channel. Interpreting the equation physically, we must assume the potassium ions can only cross the membrane if all four gates are open which occurs if four similar particles occupy a certain region of the membrane. The n represents the proportion of open gates and $(1-n)$ is the proportion of closed gates. The rate at which closed gates open is given by α_n and the rate at which open gates close is β_n. A similar interpretation can be made for m and the sodium channel. However, the sodium inactivation variable h represents the proportion of closed gates and thus the directions of the rate constants are reversed.

The kinetics of the gating variables in (1.1) are more often expressed in the equivalent form

$$\frac{dx}{dt} = \frac{x_\infty(V) - x}{\tau_x(V)}, \quad x = h,\, m,\, n, \tag{1.2}$$

where

$$x_\infty(V) = \frac{\alpha_x(V)}{\alpha_x(V) + \beta_x(V)}, \tag{1.3}$$

$$\tau_x(V) = \frac{1}{\alpha_x(V) + \beta_x(V)}. \tag{1.4}$$

Fits for x_∞ and τ_x, for $x = h, m, n$, were obtained by Hodgkin and Huxley using

experimental data. Details regarding the functional form and parameter values can be found in [7]. The functions τ_x can be interpreted as time constant functions and x_∞, for $x = h, m, n$, can be interpreted as the steady-state functions. As an example, suppose V were to suddenly move to V^* and be held there, then $x \to x_\infty(V^*)$ with time constant $\tau_x(V^*)$. The steady-state functions for the activation variables m and n increase with V while the inactivation variable h decreases with V as illustrated in Figure 3.

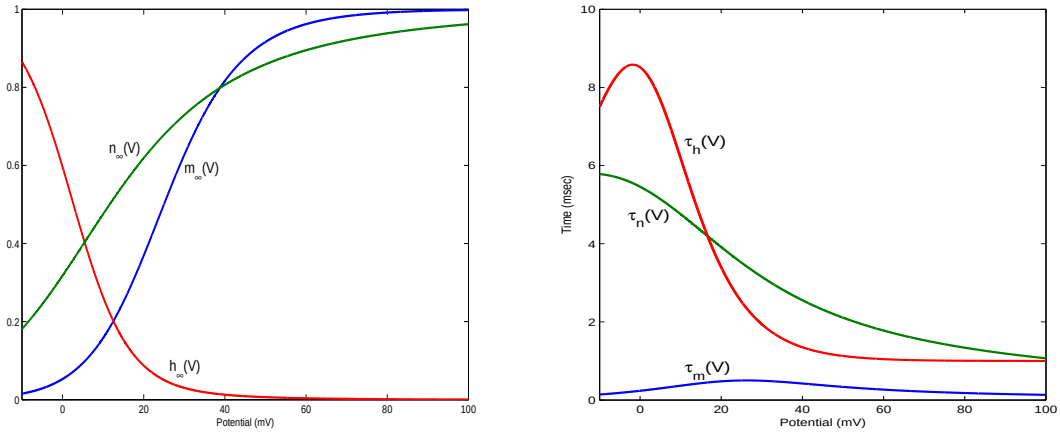

(a) The steady-state functions. (b) The time constant functions.

Figure 3: For the Hodgkin-Huxley Model, $m_\infty(V)$ and $\tau_m(V)$ are the blue curves, $n_\infty(V)$ and $\tau_n(V)$ are the green curves, and $h_\infty(V)$ and $\tau_h(V)$ are the red curves.

The complete four-dimensional system of equations is as follows:

$$C_m \frac{dV}{dt} = -\left[\bar{g}_K\, n^4\,(V - V_K) + \bar{g}_{Na}\, m^3 h\,(V - V_{Na}) + g_{leak}\,(V - V_{leak})\right],$$

$$\frac{dn}{dt} = \frac{n_\infty(V) - n}{\tau_n(V)},$$

$$\frac{dm}{dt} = \frac{m_\infty(V) - m}{\tau_m(V)},$$

$$\frac{dh}{dt} = \frac{h_\infty(V) - h}{\tau_h(V)}.$$

If the appropriate choice of model parameters is used, this system can produce a solution similar to the action potential in Figure 2. This system provides a basis for future mathematical models of membrane electrical activity. In other types of excitable cells, such as pancreatic β-cells, a similar modeling approach can be utilized by incorporating the particular ionic channels of these cells. The construction of a mathematical model for β-cells will be discussed in the next chapter.

CHAPTER 2

MODEL DEVELOPMENT

There are three principal types of cells in the pancreas: α-cells which secrete glucagon resulting in an increase in blood glucose levels, β-cells which secrete insulin causing a decrease in blood glucose levels, and δ-cells which secrete somatostatin which inhibits the production of both glucagon and insulin. These secretory cells are densely clustered together and coupled to their nearest neighbors by low resistance electrical pathways in functional units called islets of Langerhans. In human physiology, there are on the order of one million of these roughly spherical structures in the pancreas with a radius ranging from 50 to 250 μm. The α and δ cells combined number between 100 and 200 in each islet and are located mainly around the periphery of the islet. The β-cells have a diameter of 10 - 15 μm and there are on the order of $10^3 - 10^4$ cells per islet, comprising approximately 70 - 90 % of the islet [2].

Endocrine cells, such as β-cells, belong to the class of excitable cells. This excitability phenomenon was first reported in β-cells by Dean and Matthews [8]. As was observed in neurons, the electrical activity in the β-cells is a result of temporal changes in the permeability of the β-cell membrane to various ions. The most important ion channels in the β-cell membrane are selective to potassium and calcium ions and are both voltage-gated and ion-gated. The characteristic pattern of electrical

activity observed in β-cells alternates between a silent phase where the membrane potential changes very slowly, and an active phase during which the membrane potential oscillates rapidly, as shown in Figure 4. This phenomenon is called bursting.

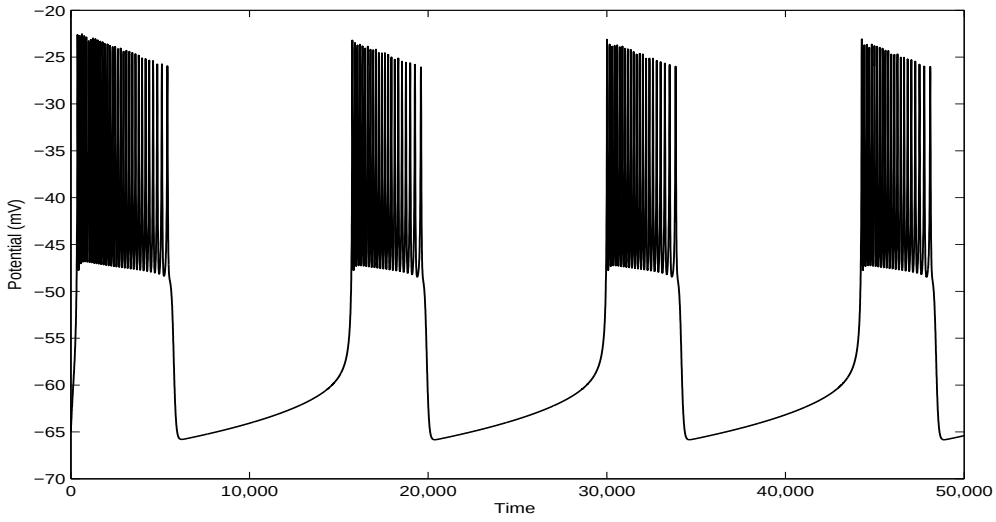

Figure 4: Bursting pattern in a pancreatic β-cell using the model of Sherman et. al. [9].

The plateau fraction is the ratio of the duration of the active phase to the period of the bursts.

The bursting exhibited by β-cells differs from that seen in neurons in that the action potentials of the active phase do not undershoot the membrane potential of the silent phase. The repetitive firing begins at a depolarized plateau. This pattern of bursting is called 'square-wave bursting'. The bursting behavior is induced by the introduction of glucose into the system. The addition of glucose in concentrations of up

to 5 mM results in a gradual depolarization of the membrane potential from the usual steady state ($\approx$ 65 mV) to a new steady-state level. In the presence of higher glucose concentrations, the membrane depolarizes past the threshold of approximately -55 mV where bursting is initiated. The bursting also facilitates an influx of calcium in the β-cells and as a result there is a periodic increase in the ionic calcium concentration. This initiates a complex sequence of events that eventually results in the secretion of insulin. It is through this mechanism that the electrical activity links the glucose signal and the resulting response of insulin secretion.

Single β-cell Model

The first mathematical model of bursting in β-cells was developed by Chay and Keizer [10]. This model was based upon the experimental observations of Atwater et al. [11] and their proposed qualitative model to explain the oscillations in the β-cell. This model included a potassium channel activated by intracellular calcium ions, a voltage-gated potassium channel, a voltage-gated calcium channel, and the cytoplasmic changes of intracellular calcium concentration that depend on the glucose concentration. Chay and Keizer adapted the Hodgkin-Huxley model to incorporate the known channels of the β-cell membrane and to allow bursting activity. The ionic channels incorporated in the Chay-Keizer model included voltage-gated potassium and calcium channels as well as calcium activated potassium channels. In this model, the influx of calcium through the voltage-gate calcium channels during the

active phase slowly increases the intracellular calcium concentration Ca. This, in turn, slowly activates the calcium-activated potassium channels. The active phase is ended when the repolarizing drive caused by the calcium-activated potassium channels is sufficiently large. During the silent phase, intracellular calcium ions are slowly removed from the cell using membrane pumps. As a result, the calcium-activated potassium channels deactivate which allows the repetitive firing stage to begin again. It was originally predicted that the ionic calcium concentration was responsible for the slow alternation between active and silent phases and would vary on a slow time scale, slowly accumulating during the active phase and then decreasing with the onset of the silent phase. As a first attempt, this model was remarkably successful at modeling the burst pattern and response to changes in glucose concentration. Once it became possible to image calcium during bursting it was shown that the intracellular calcium reaches a plateau almost simultaneously to the beginning of the active phase. Another variable or variables had to be incorporated into the model that could cause the switch between active and silent phases.

In 1989, Keizer and Magnus [12] proposed that the mechanism for bursting involved the ratio of cytoplasmic ATP (adenosine triphosphate) to ADP (adenosine diphosphate). When glucose enters a β-cell and is metabolized, ATP is synthesized from ADP. This increase in the ATP/ADP ratio decreases the conductance of the ATP-modulated potassium channels, $g_{K(ATP)}$, causing a depolarization of the cells. This depolarization opens the voltage-gated calcium channels which allows calcium

ions to enter, further depolarizing the cell and initiating excitable behavior such as bursting. As glucose is used, the production of ATP decreases which reduces the ATP/ADP ratio and increases the conductance $g_{K(ATP)}$. As the ATP-modulated potassium channels open, potassium ions flow out of the β-cells which decreases or repolarizes the membrane potential and terminates the active phase of the burst. By this mechanism, the slowly varying ATP/ADP ratio was considered to cause the transition between active and silent phases of bursting electrical activity.

Another possibility for the slow process could be the voltage-dependent inactivation of an excitatory calcium current [13]. However, their efforts to model the currents failed to produce bursting. While the inactivation of the calcium channels could terminate a burst, the threshold for the calcium current was too high for it to turn on again. As for the proposed mechanism that the bursts are driven by the ATP/ADP oscillations, there is no direct evidence that ADP oscillates as predicted. Smith et al [14] failed to find an oscillation in the KATP conductance during bursting. It should be noted however, that the predicted oscillation of less than 10% is likely below the resolution of current techniques [15]. Thus, none of the proposed mechanisms for bursting have been able to measure up to stringent experimental verification. Whatever the hypothesized slow process underlying the bursting, all models of β-cell electrical activity are based on the bistability of the cell membrane. The cell is either at a stable hyperpolarized membrane potential, the silent phase, or in a depolarized spiking state, the active phase. The slow process is responsible for

switching the cell between these two states.

Due to the uncertainty regarding the identity of the slow variable(s), Sherman and Rinzel [16] introduced the use of an abstract slow variable s acting through a slow current I_s. This slow variable is assumed to activate a voltage-independent potassium conductance. They use a simplified biophysical model in order to derive general results with a broad range of applications. We explain the mechanism of bursting with this generic model, describing the dynamics of a single β-cell which is assumed to be part of a perfectly synchronized islet. The system of (nondimensionalized) ordinary differential equations is

$$\tau \frac{dV}{dt} = -I_{Ca}(V) - I_K(V,n) - I_s(V,s), \tag{2.1}$$

$$\tau \frac{dn}{dt} = \lambda \left(n_\infty(V) - n \right), \tag{2.2}$$

$$\tau_s \frac{ds}{dt} = s_\infty(V) - s, \tag{2.3}$$

where the calcium, potassium and 'slow' currents are given by

$$I_{Ca}(V) = g_{Ca}\, m_\infty(V) \left(V - V_{Ca} \right),$$

$$I_K(V,n) = g_K\, n \left(V - V_K \right),$$

$$I_s(V,s) = g_s\, s \left(V - V_K \right),$$

and

$$x_\infty(V) = \frac{1}{1 + exp\left(\left(V_x - V \right) / \theta_x \right)} \quad \text{for } x = m,\, n,\, s.$$

Note that the conductances g_{Ca}, g_K, and g_s have been scaled by a typical instantaneous conductance in order to define τ and thus are dimensionless. This model has been simplified from the Hodgkin-Huxley model as it contains one less variable. The sodium contribution to the current balance equation has been replaced by the calcium current to reflect β-cell physiology. The inactivation variable h has been completely eliminated and the calcium activation variable m is assumed to act instantaneously and is therefore replaced by its steady state value $m_\infty(V)$. The exponents for all the gating variables have been removed and the voltage dependence of the time constants τ and τ_s have been removed. It is critical for the dynamics of the system that the two independent time constants have the relationship $\tau << \tau_s$ since the slow wave and fast spike generating mechanisms must operate on different time scales. The spikes during the active phase are due to the calcium and potassium currents as given by the equations for V and n. During the active phase, s slowly accumulates which causes the membrane potential to become less excitable by raising the threshold for bursting. A typical bursting solution for this model is shown in Figure 5 along with slow oscillation in the variable s. The parameter values for the Sherman/Rinzel model are found in Table 1.

It has become more common to write the Sherman/Rinzel model in a form where the conductances are dimensional. This gives

$$C_m \frac{dV}{dt} = -I_{ion}(V,n,s) = -I_{Ca}(V) - I_K(V,n) - I_s(V,s), \tag{2.4}$$

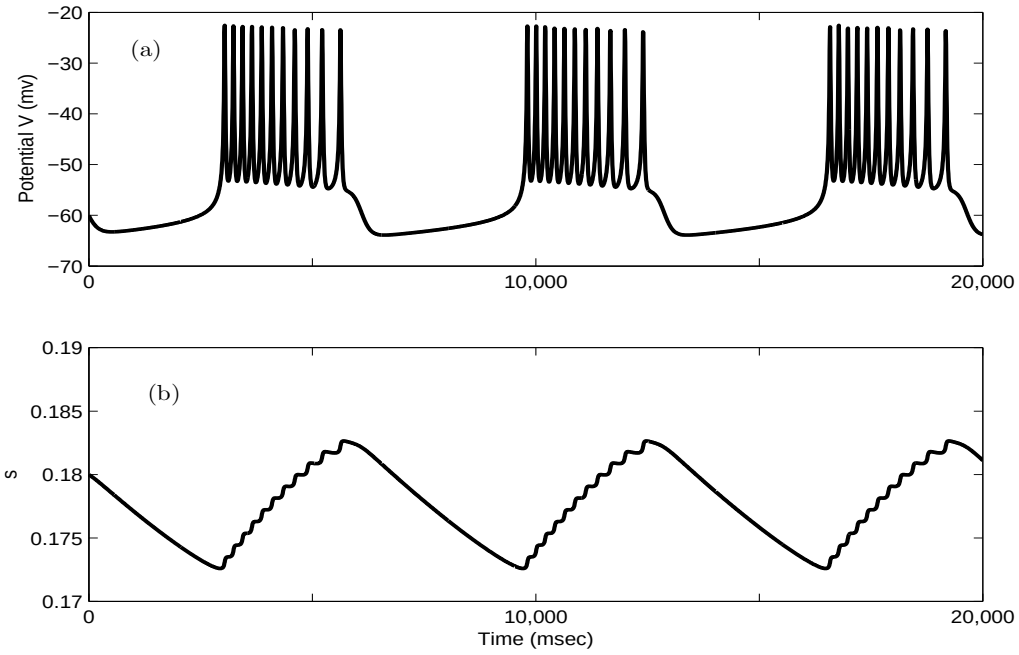

Figure 5: (a) Characteristic bursting pattern of the β-cell, (b) Dynamics of the slow variable s during the bursting in (a).

$$\frac{dn}{dt} = \frac{n_\infty(V) - n}{\tau_n}, \tag{2.5}$$

$$\frac{ds}{dt} = \frac{s_\infty(V) - s}{\tau_s}. \tag{2.6}$$

Electrophysiological Effects of Glucose

Glucose stimulated insulin secretion is of great importance in the maintenance of glucose homeostasis. Defects in this process are a critical component of Type 2 diabetes. Recall that glucose metabolism causes a rise in the ATP/ADP ratio which results in a closure of the ATP-modulated potassium channels and the eventual influx of calcium ions. The best biophysical candidate for an electrical glucose sensor is

Symbol	Value	Symbol	Value
g_{Ca}	3.6	θ_m	12 mV
g_K	10	V_m	-20 mV
g_s	4	θ_n	5.6 mV
τ	20 msec	V_n	-17 mV
τ_s	35000 msec	θ_s	10 mV
V_{Ca}	25 mV	V_s	-38 mV
V_K	-75 mV	λ	0.9 mV

Table 1: Parameter values for the Sherman/Rinzel single β-cell model [16].

the conductance of this current, $g_{K(ATP)}$, since the closure of these channels implies a decrease in $g_{K(ATP)}$. Therefore, increased glucose concentration corresponds to a decrease in the conductance $g_{K(ATP)}$. This provides a connection between glucose metabolism and the influx of calcium ions into the β-cell which is necessary for insulin secretion.

In the absence of glucose, G, the β-cell would be inactive or quiescent. If the concentration of glucose is increased towards 5 mM, the membrane potential depolarizes. Additional glucose stimulation initiates the bursting electrical activity in the β-cell. As G increases, so does the plateau fraction until it reaches 1 which corresponds to continuous spiking when the islet is exposed to a very high glucose concentration (> 20 mM) [17].

To incorporate the glucose sensing into the Sherman/Rinzel model, we must include the contribution of the the ATP-modulated potassium channels or $K(ATP)$

channel in the current balance equation (2.1) which becomes

$$C_m \frac{dV}{dt} = -I_{Ca}(V) - I_K(V, n) - I_s(V, s) - I_{K(ATP)}(V),$$

where

$$I_{K(ATP)}(V) = g_{K(ATP)} (V - V_K)$$

and the other currents are unchanged. We can view the ratio of $g_{K(ATP)}$ to g_s as the glucose sensing parameter R. Decreasing $g_{K(ATP)}$, and thus R, is interpreted as an increase in glucose [17]. Changes in R, or equivalently G, affect the plateau fraction as shown in Figure 6. Small changes in R result in substantial changes in the plateau

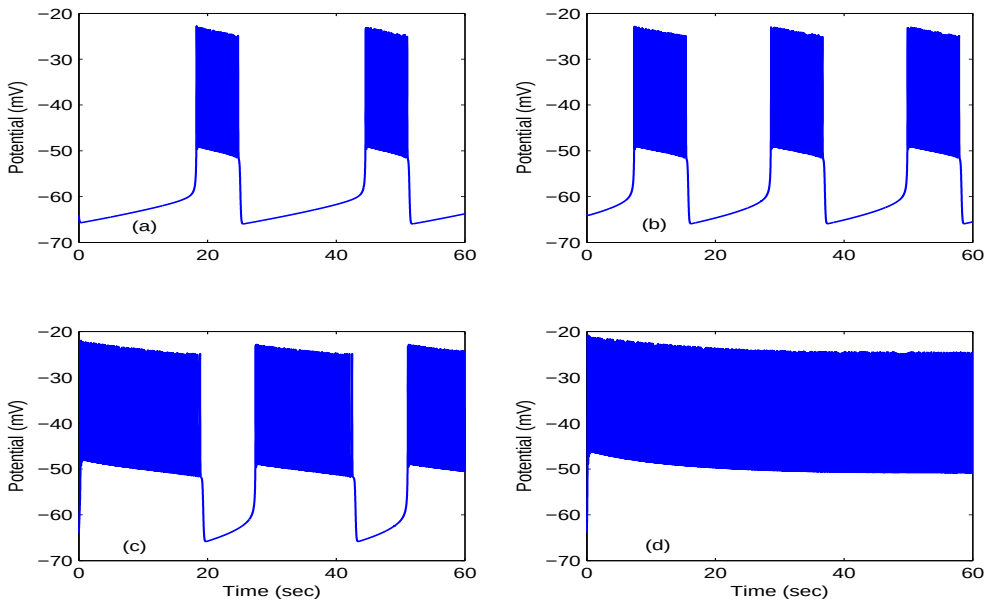

Figure 6: Bursting of the membrane potential for the following values of the glucose sensing parameter. A decrease in R corresponds to an increase in glucose concentration. (a) $R = 0.65$, (b) $R = 0.6$, (c) $R = 0.5$, (d) $R = 0.4$.

fraction. Thus, it is apparent that changes in glucose, represented as changes in R, have a significant effect on β-cell electrical activity. The process of glucose diffusion into an islet will be discussed in detail in the next section.

Thus far, we have not discussed the biophysical meaning for the slow current s. Many β-cell models have been constructed [10, 18, 13] that hypothesize various possibilities for this current as well as for the glucose sensing mechanism, but the issue remains unresolved. In [10], the concentration of free cytosolic calcium Ca^{2+} played the role of s and the rate of removal of Ca^{2+} by the pumps and exchangers, k_c, was the glucose sensor. As a result, with Ca being the concentration of free calcium, the calcium balance equation had the form

$$\frac{dCa}{dt} = f\left[\alpha I_{Ca}(V) - k_c\, Ca\right], \tag{2.7}$$

where α is a factor to convert current to concentration changes and f is the fraction of free cytosolic calcium. Most of the calcium that enters the cells is rapidly bound to proteins. As a result, f is a small parameter and the intracellular calcium concentration was plausible as the slow variable. This model led to a prediction that the free calcium concentration would show a sawtooth oscillation like s in Figure 5. When fluorescence measurements were done, it was found that calcium had a time course that was closer to a square-wave, demonstrating that the hypothesis of calcium as the slow variable s was false [19]. The change in calcium concentration was not slow enough to pace bursts with the necessary period because the parameter f is closer to

0.01 than the 0.001 needed. If we append the calcium equation (2.7) to our model and use the larger value of f, we obtain a roughly square-wave time course. Even though calcium was ruled out as the slow variable, it is still an important mechanism to include in the model. The importance of calcium is the link it provides between the electrical activity in a β-cell and insulin secretion.

Glucose is the primary stimulus for β-cells. However, secretion can also be initiated by acetylcholine (ACh) provided adequate glucose is present [20]. ACh works by binding to muscarinic receptors on the β-cell plasma membrane which leads to the production of 1,4,5-trisphosphate (IP_3) and diacylglycerol (DAG). The latter mechanism does not affect electrical activity and thus will not be considered in the model [21]. The IP_3 diffuses into the endoplasmic reticulum (ER) where it activates ligand-gated Ca^{2+} channels, releasing calcium into the cytosol. The ER can be viewed as a large organelle inside the cell that is a calcium reservoir. ER equations are added to the model. These include fluxes into (J_{in}) and out of (J_{out}) the ER that are incorporated into the intracellular calcium concentration. Additionally, there is an equation for the ER calcium concentration, Ca_{er}. The equations for the calcium dynamics become

$$\frac{dCa}{dt} = f\left[\alpha I_{Ca}(V) - k_c\, Ca\right] + \frac{1}{\mu}\left(J_{out} - J_{in}\right),$$

$$\frac{dCa_{er}}{dt} = \frac{1}{\sigma}\left(-J_{out} + J_{in}\right).$$

The factor σ accounts for the difference in the ER and cytosolic volumes as well as the Ca^{2+} buffering capacity. The parameter μ sets the ER time scale.

Two new ionic currents are needed to couple the events in the ER to the membrane potential. There is experimental evidence to suggest the existence of a calcium-activated potassium channel, I_{KCa}, in β-cells [22]. The mechanism through which muscarinic agonists (chemicals which bind to receptors of a cell and trigger a response by that cell) open membrane channels and depolarize the β-cell is unknown. In [20], it is hypothesized that a calcium-release-activated-current, I_{CRAC}, activated by the depletion of calcium stores in the endoplasmic reticulum is present in β-cells. The conductance of this current increases as the ER empties. When the ER calcium becomes too low, a messenger is released that diffuses outward to the cell membrane where it opens calcium channels. This results in an increase in the intracellular calcium and replenishes the ER calcium stores. The existence of this 'CRAC' current is less clearly established by direct measurement. However, its inclusion explains a variety of phenomena, lending credence to its existence. The agreement between experiments and the simulations supports the hypothesis that ACh works through the I_{CRAC} current [20]. The precise form of these currents as well as the fluxes into and out of the ER can be found in [21] and are summarized here

$$I_{KCa}(V, Ca) \;=\; \bar{g}_{KCa}\left(\frac{Ca^5}{Ca^5 + k_d^5}\right)(V - V_K)\,,$$

$$I_{CRAC}\left(V, Ca_{er}\right) = \bar{g}_{CRAC}\, z_{\infty}\left(Ca_{er}\right)\left(V - V_{CRAC}\right),$$

$$z_{\infty}\left(Ca_{er}\right) = \frac{1}{1 + exp\left(\left(Ca_{er} - \overline{Ca_{er}}\right)/s_c\right)},$$

$$J_{in}(Ca) = \frac{\nu_p}{\mu}\frac{Ca^2}{Ca^2 + k_p^2},$$

$$J_{out}\left(Ca, Ca_{er}\right) = \frac{1}{\mu}\left(p_l + p_{ip3}\right)\left(Ca_{er} - Ca\right).$$

The $z_{\infty}\left(Ca_{er}\right)$ represents the ER calcium dependent activation. Since data on the kinetics of this current are unknown, it is modeled as instantaneous. The p_l term in J_{out} accounts for the leakage of calcium out of the ER and the p_{IP3} term accounts for the IP_3 receptor channel.

We can now summarize our model equations for the electrical activity in a single β-cell:

$$\frac{\partial V}{\partial t} = -\frac{1}{C} I_{ion}\left(V, n, s, Ca, Ca_{er}\right),$$

$$\frac{dn}{dt} = \frac{n_{\infty}(V) - n}{\tau_n},$$

$$\frac{ds}{dt} = \frac{s_{\infty}(V) - s}{\tau_s},$$

$$\frac{dCa}{dt} = f\left(\alpha\, I_{Ca}(v) - k_c\, Ca\right) + \left(J_{out} - J_{in}\right),$$

$$\frac{dCa_{er}}{dt} = \frac{1}{\sigma}\left(J_{in} - J_{out}\right),$$

where

$$I_{ion} = I_s(V,s) + I_{Ca}(V) + I_K(V,n) + I_{KATP}(V) + I_{KCa}(V,Ca) + I_{CRAC}\left(V, Ca_{er}\right).$$

Values for the parameters are given in Appendix A. Using the dynamical system software XPPAUT [23], we can simulate the model equations for a single β-cell, shown in Figure 7. Note that this simulation was carried out on the nondimensionalized version of the model equations which will be discussed later in this chapter. We can see that the electric potential V, the gating variable n and the intracellular calcium concentration Ca are fast variables. That is, they exhibit rapid oscillations during the active phase of bursting. The gating variable s and the endoplasmic reticulum calcium concentration Ca_{er} are what are referred to as slow variables. We now turn our attention to the process of glucose diffusion into the islet.

Glucose Diffusion

In experimental studies, an islet of Langerhans is secured to the bottom of a perifusion chamber. Through an inflow tube, substances such as glucose are introduced to the bath and the electrophysiological response of the β-cells inside the islet

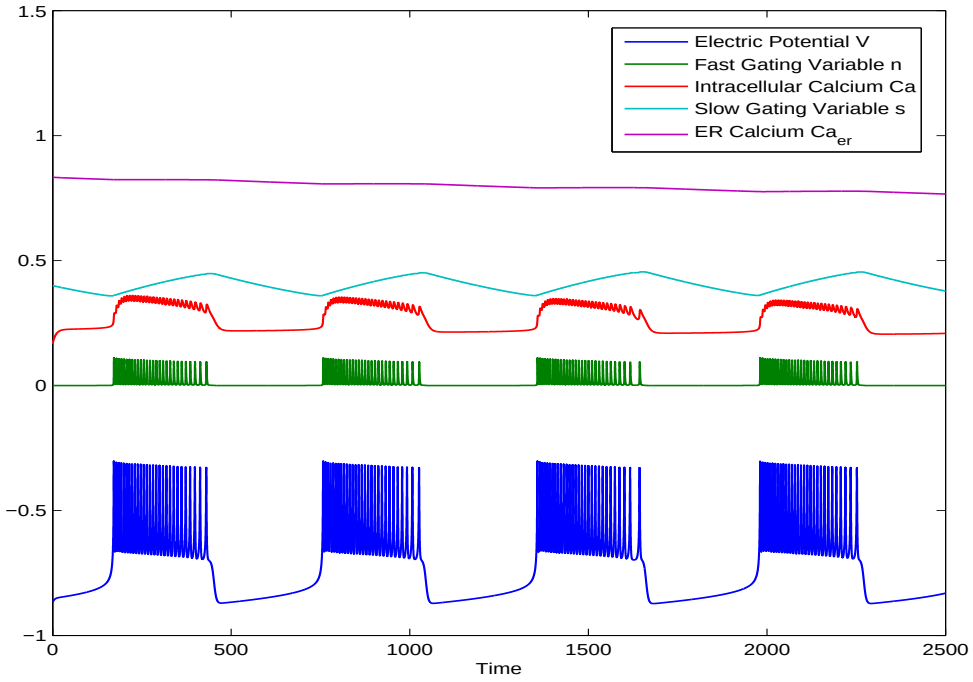

Figure 7: Dynamics of the Single β-cells model. From bottom to top, the curves are the electric potential V, the fasting gating variable n, the intracellular calcium Ca, the slow gating variable s, and the ER calcium Ca_{er}. Note that the Ca_{er} variable has been rescaled by a factor of 3. Also, note that these simulations were carried out for the nondimensionalized system discussed later in this chapter.

is continually observed. A common experimental protocol is to study the response of an islet to stepped changes in the glucose concentration. In these experiments, the glucose bath is continually refreshed to keep the concentration at a constant level. As glucose diffuses into the islet, the electrically excitable β-cells depolarize which initiates bursting electrical activity when the glucose concentration reaches a certain threshold.

When an isolated islet is exposed to a stimulatory concentration of glucose, there

is a 1-2 minute delay before the islet electrical activity begins [14]. Bertram and Pernarowski hypothesized that this delay is due in part to the delay in penetration of the glucose into the inner portions of the islet [2]. They tested this hypothesis by formulating a model of hindered glucose diffusion. The main focus of their work was to determine the glucose distribution in the islet after exposure to a stimulatory concentration of glucose at a time when islet electrical activity is likely present. For a relatively small islet of radius 100 μm and a glucose bath concentration of 10 mM, it was observed that the islet was not near a uniform glucose concentration 2 minutes after the bath was applied which is when electrical activity is usually occurring. Near the center of the islet the glucose concentration was less than 5 mM. It has been documented that isolated β-cells exposed to a glucose concentration of 7 mM or greater will become electrically active [24]. Even for high values of porosity and the permeability of the membrane used in the numerical approximations, only the cells near the periphery of the islet would have been exposed to a sufficient glucose concentration to become electrically active. The cells near the center would remain silent. These experimental results indicate that the synchronized electrical activity observed in islets occurs when just some of the cells are exposed to a stimulatory glucose concentration. The cells on the periphery that become active influence the cells with sub-stimulatory glucose levels and the islet bursts in synchrony.

In the model developed by Bertram and Pernarowski [2] to simulate the diffusion

process, it is assumed that the islet consists entirely of β-cells. This simplifying assumption is reasonable because there are roughly $10^3 - 10^4$ β-cells in a single islet and only 100 - 200 other secretory cells. Glucose diffusion through the islet is affected by several factors. It is assumed that the glucose diffuses mainly through the space between the β-cells. This property is incorporated into the model through the use of an 'effective' diffusion rate taking into account the porosity of the islet. Therefore, if the islet is tightly packed with β-cells or less porous, the diffusion will be hindered which is reflected in a decreased rate of diffusion. The glucose diffusion is also impeded by a thick layer of cells, known as the acinar layer, surrounding the islet. The permeability of this layer is incorporated into the model and the effects of varying this permeability are investigated.

As glucose penetrates through the acinar layer into the islet and comes in contact with β-cells, some of the glucose is transported into the β-cells by a GLUT-2 transporter. This slows down the penetration of glucose into the islet. Using transport values obtained experimentally [25], the effect of GLUT-2 transporters on the glucose diffusion is incorporated into the model, assuming the transport is uniform throughout the islet. Analysis of the model demonstrated the strong impact on diffusion made by the transportation of glucose into the β-cells. In a simulated islet of radius 200 μm exposed to a glucose bath of 10 mM, approximately 5 minutes were required for the center of the islet to reach 90% of the bath concentration when the GLUT-2 transport is included. When this transport is excluded, the glucose would reach 90%

of the bath concentration at the center of the islet after only 1 minute.

Once glucose has been transported inside a β-cell, a cascade occurs that initiates electrical activity. First, the glucose is metabolized to produce ATP which increase the ratio of ATP to ADP. This increase in ATP inactivates the K(ATP) channels in the cell membrane and the cell becomes depolarized. The time it takes for glucose to be metabolized may also contribute to the 1-2 minutes delay that is observed between the exposure of the islet to the glucose concentration and the initiation of electrical activity. The metabolism of glucose by the β-cells is not incorporated into the model since experimental results have indicated that the glucose concentration inside a β-cell equilibrates very quickly to a slightly lower concentration than the concentration outside the cell [26].

The gap junctions that electrically couple β-cells tend to synchronize electrical activity through the islet. Thus, as glucose diffuses into the islet, cells on the periphery are stimulated and become electrically active. These cells may be restrained by the majority of cells in the interior that still remain inactive. This implies that the entire islet will not exhibit synchronized bursting until the glucose has diffused into the islet sufficiently far to activate, i.e., excite, a sufficient number of β-cells. The exact ratio of active to silent cells necessary for the islet to burst is not known. This supports the hypothesis that the delay can be attributed in part to the time it takes for glucose to diffuse into the islet.

The glucose in the extracellular space between the β-cells is called the extracellular

glucose, Ge. The glucose concentration within the β-cells is called the intracellular glucose, Gi. In [2], the glucose diffusion process for an islet of radius a is modeled using spherical coordinates and assuming spherical symmetry. The partial differential equation for Ge is

$$\frac{\partial Ge}{\partial t} = p\, D_G \frac{1}{r^2}\frac{\partial}{\partial r}\left(r^2 \frac{\partial Ge}{\partial r}\right) - \frac{1}{\rho}\, F(Ge, Gi), \quad r < a, \quad t > 0. \tag{2.8}$$

The 'effective' glucose diffusion is given by the product of the porosity $p \in [0, 1]$ and the diffusion coefficient of glucose in water D_G. The GLUT-2 transport mechanism is represented by the function $F(Ge, Gi)$ and depends on both the extracellular and intracellular glucose concentrations. The precise form of this transport function will be specified later. The number of β-cells in the islet will affect the amount of glucose transported from the extracellular space inside the β-cells. This is accounted for by the parameter $\rho = V_e/V_i$, the volume fraction of the total volume of extracellular space, V_e, to the total β-cell volume, V_i. It was shown in [27] that the extracellular volume is only 1-2 % of the total islet volume, so the value $\rho = 0.02$ is used for the volume fraction. In the model, the inverse of the volume fraction accurately reflects the property that an increase in β volume (V_i) would result in a further reduction of extracellular glucose due to GLUT-2 transport and as a result, diffusion would be slowed.

The glucose concentration in the islet is initially assumed to be zero

$$Ge(r, 0) = 0, \quad r \in [0, a]. \tag{2.9}$$

Boundary conditions are obtained by assuming that the acinar layer is a passive membrane. Thus, the chemical gradient across the surrounding layer is the only source of flux. If the glucose bath concentration is given by G and the permeability of the acinar layer is given by k, then the appropriate boundary condition is

$$\frac{\partial Ge}{\partial r} = k(G - Ge), \quad r = a, \quad k > 0. \tag{2.10}$$

Additionally, the glucose concentration at the center of the islet is assumed to be bounded:

$$|Ge(0,t)| \leq M < \infty, \quad t \geq 0. \tag{2.11}$$

The dynamics of the intracellular glucose concentration, Gi, are modeled by assuming that glucose enters the β-cells only via GLUT-2 transport. Diffusion through gap junctions is not considered although there is some evidence that this is possible [28]. This results in the following equation

$$\frac{\partial Gi}{\partial t} = F(Ge, Gi). \tag{2.12}$$

The initial glucose concentration inside the β-cells is assumed to be zero, yielding the initial condition

$$Gi(r,0) = 0, \quad r \in [0,a]. \tag{2.13}$$

The derivation of the GLUT-2 transport is complex and the reader is directed to

[2] and [29] for details. The glucose flux into the cell is represented by

$$F(Ge, Gi) = V_{max} \frac{K_m(Ge - Gi)}{(Ge + K_m)(Gi + K_m)}, \tag{2.14}$$

where V_{max} and K_m are the maximum transport rate and the transporter dissociation constants, respectively. The values for these parameters were determined in studies of glucose uptake in dispersed rat islet cells [25]. The values for the parameters in the model given by equations (2.8)-(2.14) are found in Table 2. Before

Symbol	Description	Value
D_G	Glucose diffusivity in water	$0.673 \times 10^{-5} \frac{\text{cm}^2}{\text{sec}}$
a	Islet radius	100 μm
ρ	Volume fraction	0.02
K_m	GLUT-2 dissociation constant	17 mM
V_{max}	GLUT-2 maximum uptake rate	0.53 $\frac{\text{mM}}{\text{sec}}$
k	Acinar layer permeability	0.02-1.0 $\frac{1}{\mu\text{m}}$
p	Islet porosity	0.02-1

Table 2: Parameter values for the glucose diffusion model [2].

analyzing this coupled nonlinear system, the transformations $\zeta_e = Ge\, r$ and $\zeta_i = Gi\, r$ are applied to handle the removable singularity at the islet center. In Figure 8, the spatial distribution of the extracellular and intracellular glucose concentrations after a simulated bath application of 10 mM is shown. As we would expect from our discussion, Gi increases more slowly than Ge at all locations since diffusion occurs only in the interstitial spaces. After 1 minute, only cells near the islet boundary ($r =$

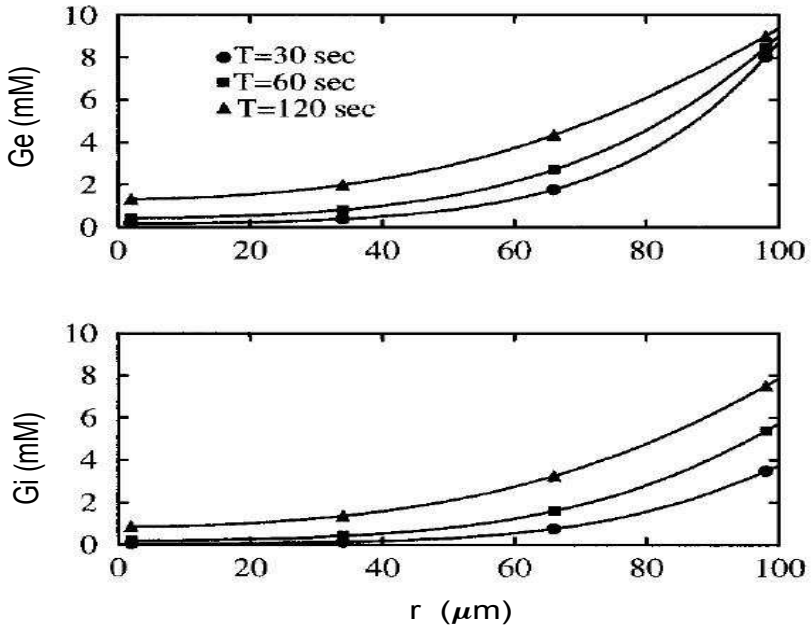

Figure 8: Extracellular (Ge) and intracellular (Gi) glucose concentrations in the islet 30 seconds, 1 minute and 2 minutes after exposure to a 10 mM glucose bath. Computations were made using permeability and porosity values of $k = 0.3\,\mu\text{m}^{-1}$ and $p = 0.03$. Initially $Ge = Gi = 0$ throughout the islet. Other parameter values are as in Table 2. Taken from [2].

$100\,\mu$m) have a glucose concentration of more than 50% of the bath concentration. After 2 minutes, only cells approximately 20 μm from the islet boundary have reached a glucose concentration of more than 50% of the glucose bath concentration. Thus, we observe that after 2 minutes, the glucose levels in the islet are far from the equilibrium value of 10 mM. However, islet electrical activity is typically observed approximately 2 minutes after the stimulatory glucose concentration is applied. This indicates that the electrical activity is occurring long before the glucose concentration inside the islet has reached equilibrium. In [2] it is proposed that the time required for glucose to

equilibrate throughout the islet is on the order of several minutes, long after electrical activity is likely to have commenced inside the β-cells of the islet.

In order to model the electrical activity in an pancreatic islet, the single β-cell model developed by Sherman [21] is modified by incorporating gap junctional coupling β-cells and implementing the theories presented by Pernarowski in [3]. The islet model is then connected to the model of glucose diffusion [2] through an expression that accounts for the known effects of glucose on electrical activity in β-cells as suggested by Aslanidi [30].

Gap Junction Coupling

β-cells are electrically coupled together by gap junctions which are formed by protein molecules in the cell membrane. The protein pores make an electrical connection between most adjacent cells. Electrical recordings of β-cell pairs extracted from an islet indicated that 65% of cell pairs were electrically coupled and the coupling conductance, g_c, was measured at 215 ± 110 pS [31]. It is thought that islets depend on gap junctions to produce a coordinated electrical response to glucose stimulation. Coupling has effects on β-cell activity other than aiding in synchronization. Sherman and Rinzel [32] have shown that the length of time the cells spend bursting is maximized for an intermediate coupling strength. When the cells are coupled strongly enough together to synchronize the bursts but not the spikes, the spikes are out of phase which causes their potentials to be pulled together. This reduces the amplitude

of the spikes and as a result, the slow variable must increase further to end the burst, thereby increasing the burst period. An increased burst period, or higher plateau fraction, results in an increase in the average intracellular calcium concentration which translates to an increase in insulin secretion [33].

Gap junction coupling has also been shown to aid in stabilizing the effects of noise and parameter variability on electrical activity patterns in islets [34]. Bursting is rarely observed experimentally in isolated β-cells. It is seen far more commonly in sufficiently large and tightly coupled clusters of cells. A typical islet burst ranges from 10 - 30 seconds depending on the concentration of glucose to which the islet is exposed. Conversely, single cells tend to burst on a much longer scale of up to several minutes or they burst much faster [35]. It is not clear which properties of islet electrical behavior are inherent to isolated cells or emergent features of coupling. However, it is well documented that electrical coupling between the cells exists and as a result it is important to examine the behavior of coupled β-cells in an islet model.

In [3], Pernarowski introduces a continuum model for islet electrical activity. Consider a linear string of cells coupled by gap junctions. If cell i, for $i = 1 \dots M$, is located at $x_i = i\Delta x$, where Δx is the β-cell diameter, then the coupling current, I_c, affecting the i-th cell would be given by the sum of the contributions from the cells to the left and right. Let V_i represent the electrical potential at the i-th cell. Then we have

$$I_c = g_c\left(V_{i+1} - V_i\right) + g_c\left(V_{i-1} - V_i\right) = g_c\left(V_{i+1} - 2V_i + V_{i-1}\right).$$

The coupling current can be seen to be a discretization of a diffusion term by letting

$$g_c = \frac{D}{\Delta x^2}$$

which implies

$$D\frac{\partial^2 V}{\partial x^2} \approx \frac{D}{\Delta x^2}\left(V_{i+1} - 2V_i + V_{i-1}\right).$$

In the continuum limit for a cell located at $x_i \in \mathbb{R}$ and homogeneous nearest neighbor gap junction coupling, we have

$$D\nabla^2 V\Big|_{x=x_i} \approx \sum_{j=1}^{M} g_c\left(V_j - V_i\right).$$

Thus, the gap junction coupling of β-cells in an islet can be modeled as a diffusion term. Since cells on the boundary of the islet are not connected by gap junctions to any cells outside the cluster, there will be no current across the boundary. Thus we have a no flux boundary condition

$$\frac{\partial V}{\partial n} = 0, \quad x \in \partial\Omega,$$

where $\hat{n}$ is the outward unit normal vector to the islet domain Ω.

We can now formulate the model equations for a pancreatic islet. In the $K(ATP)$ current, we recognize that R is related to the glucose concentration of the bath, G. The bursting electrical response of β-cells is mediated through the conductance $g_{K(ATP)}$ of this current. Therefore, by varying the value of $g_{K(ATP)}$ we can account for the glucose effects on the electrical activity of β-cells. This establishes a connection

between the islet model and the glucose diffusion model. From the work of Bertram and Pernarowski [2], it is believed that glucose penetrates into the islets slowly, only high initially at the periphery of the islet. As a result, only the cells on the boundary of the islet have a glucose concentration high enough to decrease the conductance $g_{K(ATP)}$. In the rest of the islet, the value of this conductance remains relatively high. Thus, a natural way to account for these effects of an inhomogeneous distribution of glucose inside the islets is to allow $g_{K(ATP)}$ to vary. In particular, it is treated as a function of the intracellular glucose concentration. The exact form of this dependency is unknown. Using some reasonable assumptions, Aslanidi et.al. [30] hypothesized the functional form. The conductance $g_{K(ATP)}$ is chosen to be a sigmoid function of the intracellular glucose concentration, Gi,

$$g_{K(ATP)}(Gi) = \bar{g}^{(o)}_{K(ATP)} + \bar{g}^{(c)}_{K(ATP)}\, h(Gi),$$

$$h(Gi) = \frac{1}{1 + exp\left(\left(Gi - G_{th}\right)/s_g\right)}.$$

The parameter $\bar{g}^{(c)}_{K(ATP)}$ corresponds to the fraction of channels which close upon glucose treatment and $\bar{g}^{(o)}_{K(ATP)}$ corresponds to the fraction of channels remaining open. The parameter G_{th} is a glucose threshold for the activation of the β-cells. This value is chosen to be 5 mM based upon the fact that there is a threshold value of about 7 mM for the external glucose concentration and that the intracellular glucose concentration is somewhat lower [2]. Putting everything together results in the following islet model

equations:

$$\begin{aligned}
\frac{\partial V}{\partial t} &= D\left(\nabla^2 V\right) - \frac{1}{C} I_{ion}(V, n, s, Ca, Ca_{er}, Ge, Gi), \\
\frac{dn}{dt} &= \frac{n_\infty(V) - n}{\tau_n}, \\
\frac{ds}{dt} &= \frac{s_\infty(V) - s}{\tau_s}, \\
\frac{dCa}{dt} &= f\left(\alpha\, I_{Ca}(V) - k_c Ca\right) + \left(J_{out} - J_{in}\right), \\
\frac{dCa_{er}}{dt} &= \frac{1}{\sigma}\left(J_{in} - J_{out}\right), \\
\frac{\partial Ge}{\partial t} &= pD_g\left(\nabla^2 Ge\right) - \frac{1}{\rho} F(Ge, Gi), \\
\frac{\partial Gi}{\partial t} &= F(Ge, Gi),
\end{aligned}$$

where

$$I_{ion} = I_s(V, s) + I_{Ca}(V) + I_k(V, n) + I_{KATP}(V, Gi) + I_{KCa}(V, Ca) + I_{CRAC}(V, Ca_{er}).$$

We summarize the model equations along with the auxiliary equations and parameter values in Appendix A. This model accounts for the dynamics of the electric

potential and ionic currents across the cell membranes and the changes in the intracellular calcium concentration. The resulting model equations consist of two reaction-diffusion equations (for the electric potential V and the extracellular glucose Ge) coupled with five ordinary differential equations (for the gating variables n and s, the intracellular and endoplasmic reticulum calcium Ca and Ca_{er}, and the intracellular glucose Gi). This model can be used to simulate a one- or two- dimensional array of β-cells depending on the form of the diffusion (Laplacian) operator. We will consider both cases: a one-dimensional linear array of cells and a two-dimensional array of cells on the unit disk. In the latter case, the Laplacian operator will be expressed in polar coordinates. These model equations represent the most robust model of a pancreatic islet currently referenced in the literature. More recent studies have been concerned with understanding the multiple slow processes present in β-cells [36] as well as incorporating spatially dependent coupling to account for the inhomogeneities present in pancreatic islets [37]. Typically the mathematical models of β-cells have been based on rodent data. More recently, work has also been done in studying the differences between the electrophysiological characteristics of β-cells in rodents versus that of humans [38]. Before any analysis of this model is carried out, the model equations will be nondimensionalized.

Nondimensionalization

The model equations are nondimensionalized with the independent variables being

rescaled so that the length of the array of cells in one dimension or the islet radius in two dimensions is 1. We will also rescale to make the coupling coefficient, $D = 1$. Let

$$x = \frac{r}{a}, \qquad \tau = \frac{Dt}{a^2},$$

where a is the dimensional array length or islet radius. Furthermore, the dependent variables are rescaled in the following manner:

$$u = -\tfrac{V}{V_K},$$

$$w = n, \qquad z = s,$$

$$ci = \tfrac{Ca}{k_d}, \qquad cr = \tfrac{Ca_{er}}{Ca_{er}},$$

$$ge = \tfrac{Ge}{G}, \qquad gi = \tfrac{Gi}{G}.$$

A summary of the exact form of the nondimensional functions n_∞, m_∞, s_∞, z_∞, and g_{KATP} and the definition of the dimensionless parameters and their values are in Table 3. For convenience, the nondimensional system and its parameters are also summarized in Appendix B. The nondimensional equations in two dimensions are given by

$$\frac{\partial u}{\partial \tau} = \nabla^2 u - I_{ion}(u, w, z, cr, ci, ge, gi), \tag{2.15}$$

$$\frac{dw}{d\tau} = \lambda_2 \left(n_\infty(u) - w\right), \tag{2.16}$$

$$\frac{dz}{d\tau} = \lambda_3 \left(s_\infty(u) - z\right), \tag{2.17}$$

$$\frac{dcr}{d\tau} = \alpha_1 \frac{ci^2}{ci^2 + \delta_2^2} - \alpha_2 \left(cr - \alpha_3\, ci\right), \tag{2.18}$$

$$\frac{dci}{d\tau} = -\delta_1\, \gamma_{Ca}\, m_\infty(u)\, (u - u_{Ca}) - \delta_3 ci + \delta_4 (cr - \alpha_3\, ci) - \delta_5 \frac{ci^2}{ci^2 + \delta_2^2}, \tag{2.19}$$

$$\frac{\partial ge}{\partial \tau} = \Delta_2\, \nabla^2 ge - \frac{\lambda_1\, \alpha_4}{\rho} \frac{ge - gi}{(ge + \alpha_4)(gi + \alpha_4)}, \tag{2.20}$$

$$\frac{\partial gi}{\partial \tau} = \lambda_1\, \alpha_4 \frac{ge - gi}{(ge + \alpha_4)(gi + \alpha_4)}, \tag{2.21}$$

where

$$I_{ion} = \gamma_s\, z\, (u + 1) + \gamma_{Ca}\, m_\infty(u)\ (u - u_{Ca}) + \gamma_K\, w\, (u + 1) + \frac{a^2}{CD}\, g_{KATP}(gi)\, (u + 1) + \gamma_{KCa} \left(\frac{ci^5}{ci^5 + 1}\right) (u + 1) + \gamma_{CRAC}\, z_\infty(cr)\ (u + u_{CRAC})\,.$$

We are now prepared to look at simulations of these model equations in one and two dimensions. We begin with the one-dimensional array of cells in the next chapter.

Parameter	Value	Parameter	Value
$u_{Ca} = -\frac{V_{Ca}}{V_K}$	$\frac{1}{3}$	$u_{CRAC} = \frac{V_{CRAC}}{V_K}$	0.4
$\gamma_s = \frac{\bar{g}_s a^2}{CD}$	800	$\gamma_K = \frac{\bar{g}_K a^2}{CD}$	10800
$\gamma_{Ca} = \frac{\bar{g}_{Ca} a^2}{CD}$	4000	$\gamma_{KCa} = \frac{\bar{g}_{KCa} a^2}{CD}$	4000
$\gamma_{CRAC} = \frac{\bar{g}_{CRAC} a^2}{CD}$	160	$\lambda_1 = \mathbb{T}_u \frac{a^2 V_{max}}{DG}$	1.02145
$\lambda_2 = \frac{a^2}{D\tau_n}$	1060	$\lambda_3 = \frac{a^2}{D\tau_s}$	1.06
$\delta_1 = \frac{\alpha f C V_K}{k_d}$	0.029813	$\delta_2 = \frac{k_p}{k_d}$	$\frac{1}{6}$
$\delta_3 = \frac{f a^2 k_c}{D}$	42.4	$\delta_4 = \frac{a^2 (p_l + p_{ipi3}) \overline{Ca_{er}}}{k_d D \mu}$	11.3067
$\delta_5 = \frac{a^2 \nu_p}{k_d D \mu}$	33.92	$\alpha_1 = \frac{a^2 \nu_p}{\sigma D \mu \overline{Ca_{er}}}$	1.0176
$\alpha_2 = \frac{a^2 (p_l + p_{ip3})}{\sigma D \mu}$	0.3392	$\alpha_3 = \frac{k_d}{\overline{Ca_{er}}}$	0.15
$\alpha_4 = \frac{K_m}{G}$	1.54545	$\Delta_2 = \mathbb{T}_u \frac{p D_g}{D}$	0.107007

Table 3: Definitions and values of the dimensionless parameters in the model equations.

CHAPTER 3

1D MODEL AND TRAVELING WAVES

In this chapter, we consider a one-dimensional string of β-cells and we seek to investigate the presence of traveling wave fronts and pulses through the one-dimensional islet. After some reductions in the model equations, we note that the model is qualitatively the same as the bi-stable equation, for which the exact representation of the traveling wave front can be computed. Using this as a starting point, we homotopy to the reduced islet model equations and construct a continuation curve for the existence of a traveling wave front. We discuss how the wave speed for the traveling wave front is, to leading order, the wave speed for the associated traveling wave pulse present when the slow gating variable is reincorporated into the model. A similar continuation curve is constructed for the presence of the wave pulse and it is shown that there is good agreement between the wave front and wave pulse speeds. Finally, the speeds of the traveling wave trains obtained from the system in traveling coordinates are compared to those obtained from simulations of the partial differential equation model. We note that the estimates from the PDE model are consistently higher. This may be a result of the numerical method used to simulated the PDE model. Since the speed of the actual traveling wave is only being computed when the system is in traveling coordinates, we concluded that those speed computations

are more accurate. For the traveling coordinate system, the continuation software AUTO was used which incorporates collocation and adaptive mesh methods. The adaptive nature of the numerics in AUTO would also support the conclusion that the speed computations from the traveling coordinate model would be more accurate than those from the PDE model.

Traveling Wave Fronts

Consider a one-dimensional string of β-cells on the interval $0 \leq x \leq 1$. These cells are coupled together through gap junctions. Numerical simulations of the model equations (2.15)-(2.21) are shown in Figure 9. Looking closely at the figure, we can see that the electrical activity in the distribution of cells begins at the right boundary $x = 1$ and propagates inward through the cells. We can better see this wave of electrical activity by projecting the three-dimensional representation onto the tx-plane and focusing on one cycle of the electrical activity. This is shown in Figure 10. The other dependent variables are shown in Figure 11. We can see that the gating variable w and the intracellular calcium concentration ci exhibit rapid oscillations (Figures 11a, 11c) in phase with those of the electrical potential. The gating variable z and the endoplasmic reticulum calcium concentration exhibit slow variations (Figures 11b, 11d). In the glucose system variables, (Figures 11e, 11f), we see the extremely slow process of glucose diffusing into the islet. We would like to investigate how the speed of this wave through the islet is affected by variations in

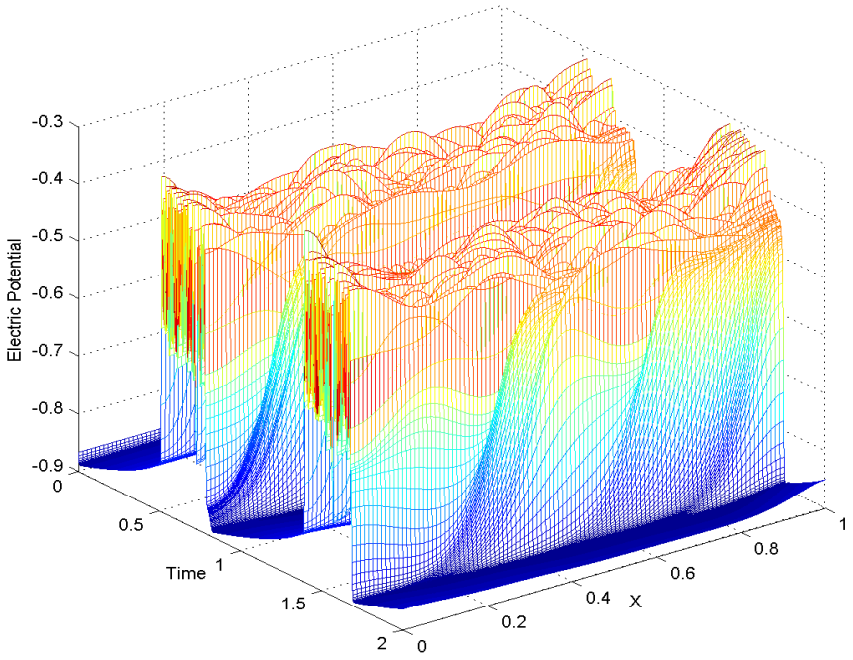

Figure 9: Islet model equations simulated with MATLAB's ode15s routine. Looking at the last bursting cycle, we can see that the electrical activity has commenced at the $x = 1$ boundary, but has not yet reached the $x = 0$ boundary, thus indicating the presence of a wave of activity propagating through the islet.

certain model parameters.

The Bistable Equation

When an excitable membrane is incorporated into a nonlinear cable equation, traveling waves of electrical excitation can emerge. Hodgkin and Huxley [7] showed that this action potential should propagate along an axon with fixed speed, which could be calculated. In our discussion, the term traveling wave refers to solutions that travel at constant velocity c with fixed shape. The two most important types of

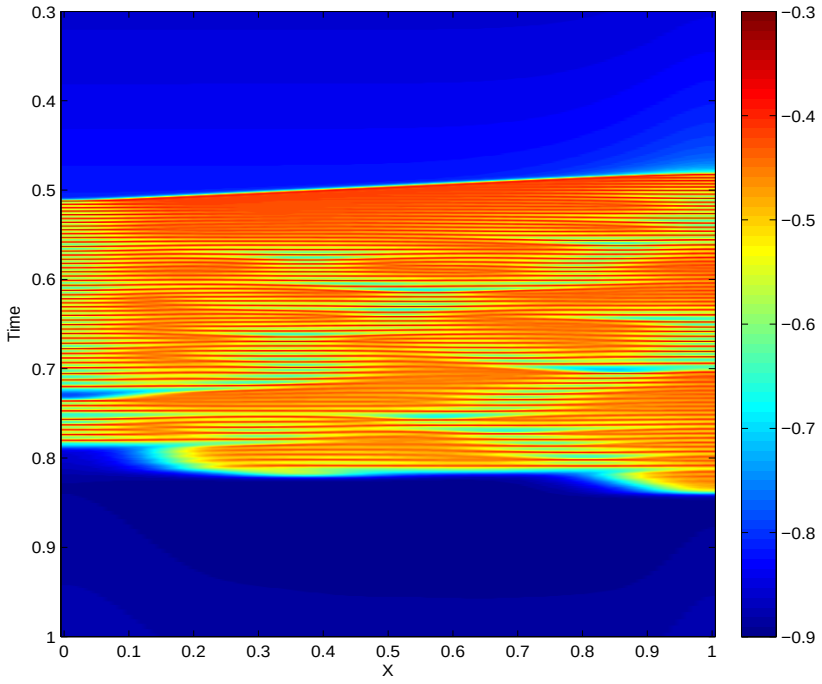

Figure 10: Projection of one bursting cycle from Figure 9 onto the tx-plane to better visualize the wave of electrical activity propagating through the islet.

traveling waves in excitable systems are traveling fronts and traveling pulses. Examples of these are shown in Figure 12. The former looks like a moving plateau. In front of the wave, the wave variable v is at some low value and behind the wave, it is steady at a higher value. In a traveling pulse, the wave begins and ends at the same value and resembles a moving pulse. Mathematically, these can be described in the following way. The traveling front depends on the excitation variable, for our model the electrical potential. When the recovery or slow variable is at steady-state, the excitation variable has two stable steady states, i.e., it is bistable. Under appropriate

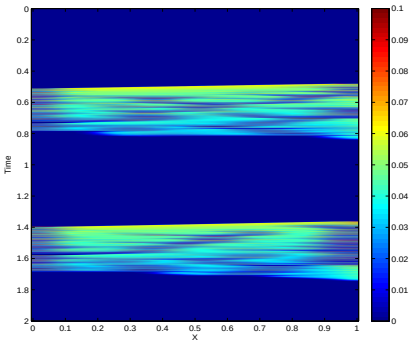

(a) The fast gating variable w.

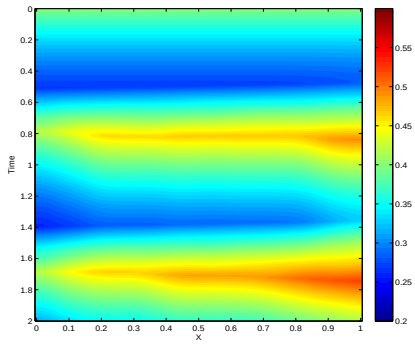

(b) The slow gating variable z.

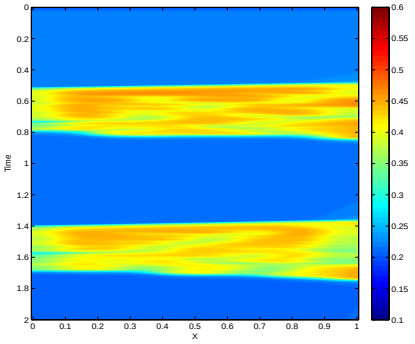

(c) The intracellular calcium ci.

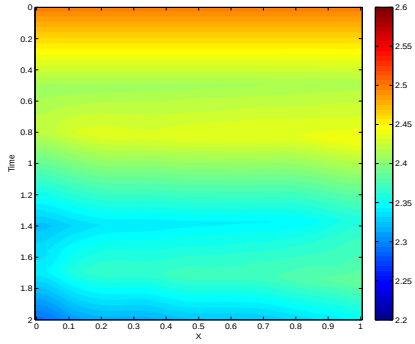

(d) The ER calcium cr.

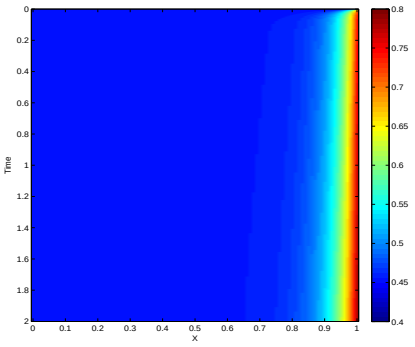

(e) The extracellular glucose ge.

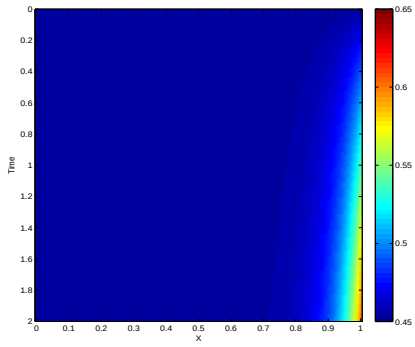

(f) The intracellular glucose gi.

Figure 11: 2D plots of the other six dependent variables. Note the fast variation in the gating variable w and the intracellular calcium ci and the slow variation in the gating variable z, the ER calcium cr, and both glucose variables.

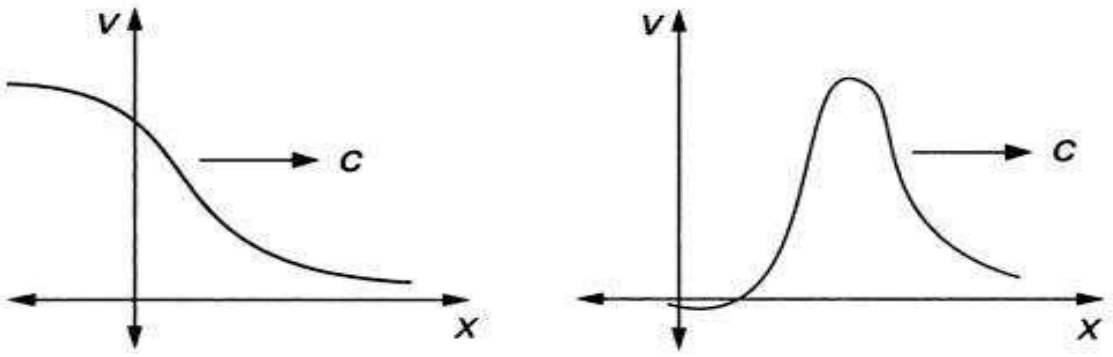

Figure 12: Examples of traveling fronts (on the left) and traveling pulses (on the right). Taken from [39].

conditions, there is a traveling front acting like a zipper changing the excitation variable from the resting to the excited state. If the recovery (slow) variable is included, a more complex model results, the Fitzhugh-Nagumo model [40, 41]. In this model, for certain parameter values and initial conditions, the solution will be forced back to the resting state and the traveling front becomes a pulse.

The bistable equation is a nonlinear partial differential equation which has two stable rest points and is of the form

$$V_t = V_{xx} + F(V), \tag{3.1}$$

where $F(V) = V(V-1)(\alpha - V)$ has three zeros at 0, α, and 1. The values $V = 0$ and $V = 1$ are stable steady solutions of the ordinary differential equation $\dot{V} = F(V)$. Here $[\dot{}]$ represents the time rate of change. A traveling wave solution is a translation invariant solution of (3.1) that provides a transition between the the stable rest states $V = 0$ and $V = 1$ and travels with constant speed. When numerical simulations of

(3.1) are done with certain initial conditions, a traveling wave front can be seen propagating through the domain in Figure 13. As a result, we seek solutions of

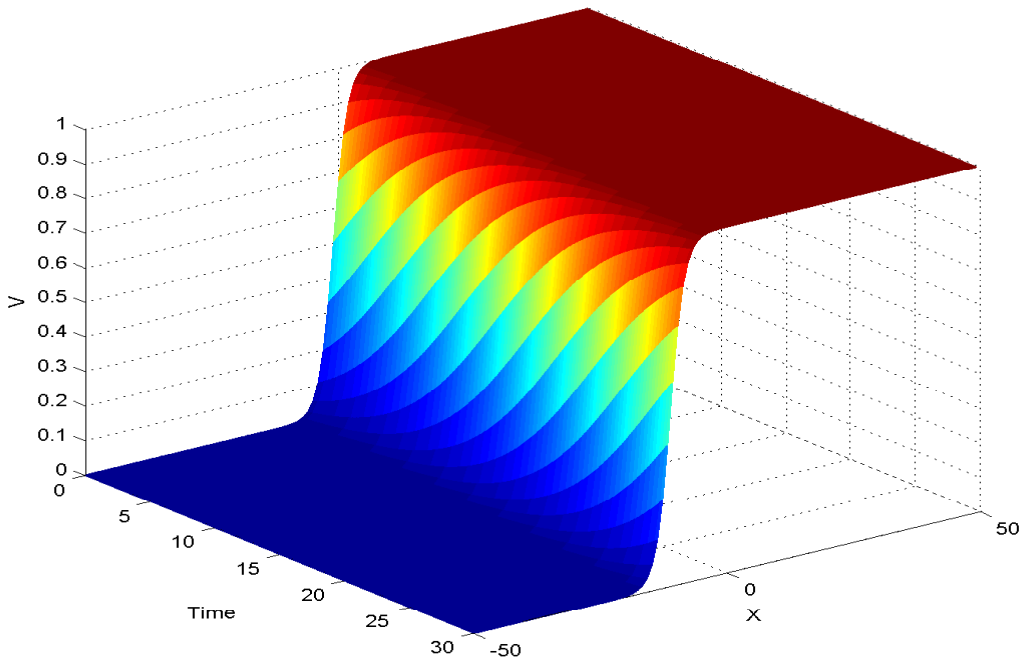

Figure 13: Numerical simulation of the bistable equation. We can see the wave front propagating through the domain.

(3.1) of the form $V(x,t) = U(x+ct) = U(\zeta)$ for some value of c. This new variable $\zeta = x + ct$ is called the traveling coordinate and has the property that fixed values move in space-time with a fixed speed c. When written in terms of the variable ζ, the wave appears stationary. This conversion to traveling coordinates converts (3.1) into the ordinary differential equation

$$U'' - cU' + U(\alpha - U)(U - 1) = 0, \tag{3.2}$$

where $[\cdot]' = \frac{d}{d\zeta}$. For $U(\zeta)$ to be a transition between steady states, we must require that $F(U(\zeta)) \to 0$ as $\zeta \to \pm\infty$. Consider the equivalent system of first order equations

$$u_1' = u_2 \tag{3.3}$$

$$u_2' = cu_2 - u_1(\alpha - u_1)(u_1 - 1). \tag{3.4}$$

Traveling wave front solutions for the bistable equation will be a heteroclinic trajectory that connects the rest points $(u_1, u_2) = (0, 0)$ and $(u_1, u_2) = (1, 0)$. The steady states $u_1 = 0$ and $u_1 = 1$ are both saddle points. For the steady state $u_1 = \alpha$, the real part of both eigenvalues have the same sign: negative if $c > 0$ and positive if $c < 0$, so this equilibrium is a node or a spiral. To find a traveling wave front, we need to determine if there is a value of the parameter c such that the trajectory leaves $u_1 = 0$ at $\zeta = -\infty$ and connects with the saddle point $u_1 = 1$ at $\zeta = \infty$. An example of this is shown in Figure 14 for $\alpha = 0.5$ and $c = 0$. Note that looking for the 'forward' wave from $u_1 = 0$ to $u_1 = 1$ is a choice as we could look for the other heteroclinic trajectory from $u_1 = 1$ to $u_1 = 0$, or the 'backward' wave. If such a monotone increasing connecting trajectory exists, that is $U' > 0$, we can multiply (3.2) by U' and integrate from $\zeta = -\infty$ to $\zeta = \infty$. Assuming $U'(\pm\infty) = 0$, this yields

$$c\int_{-\infty}^{\infty} (U')^2 \, d\zeta = \int_0^1 f(U)\, dU. \tag{3.5}$$

Thus, if a traveling wave solution exists with $U(-\infty) = 0$ and $U(\infty) = 1$, the sign of c is the same as the sign of the area under the curve $F(U)$ between them. If this

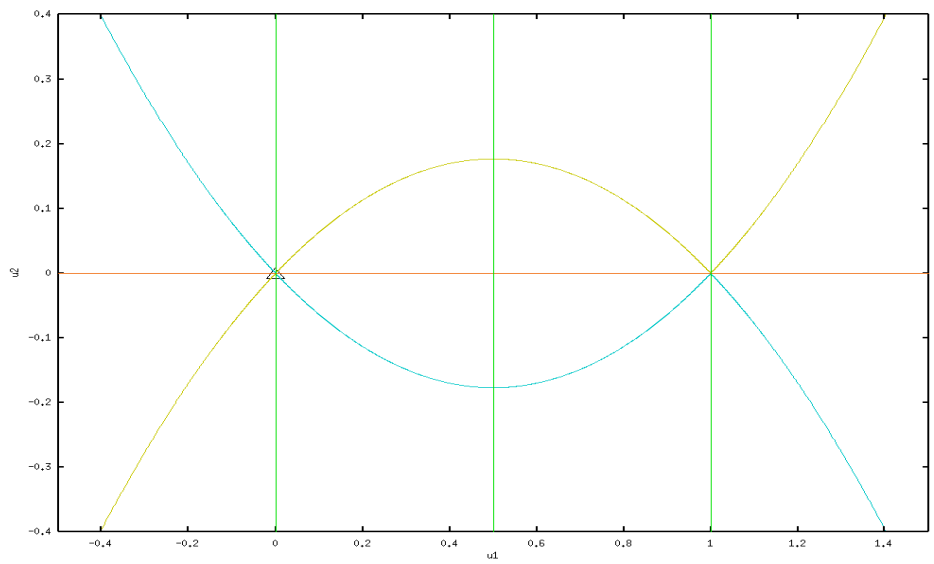

Figure 14: Phase portrait of the bistable equation for $\alpha = 0.5$ and $c = 0$.

area is positive, the traveling wave front moves U from 0 to 1. We can deduce a physical interpretation of the middle root α and the wave speed c by considering the bistable equation in terms of a mass-spring system. In traveling coordinates (3.2) looks like the equation of motion for a nonlinear spring with damping coefficient c. The potential energy of the system is given by

$$PE(u) = \int_0^u f(s)\,ds = \int_0^u s(\alpha - s)(s-1)\,ds.$$

By plotting $f(u)$ and $PE(u)$ we can see that a potential well is present, see Figure 15. Suppose we have a marble at $(0, 0)$ and we want to apply the appropriate initial velocity so that the marble stops at $u = 1$. If $c = 0$ and $\alpha = 0.5$, the area under the curve $f(u)$ is zero and there is an initial velocity that will cause the marble to roll through the potential energy well and stop at exactly $u = 1$. However, if α is

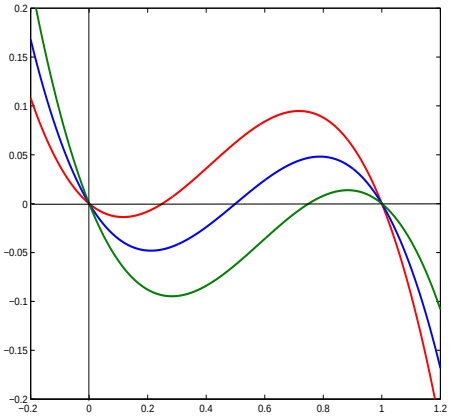

(a) The cubic forcing term $f(u)$ of the mass-spring system.

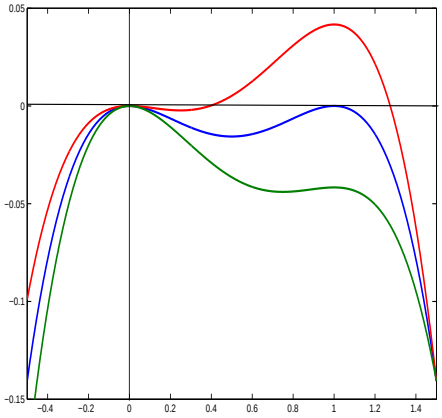

(b) The potential energy of the mass-spring system.

Figure 15: The forcing and potential energy functions for the bistable equation. The red curves are for $\alpha = 0.25$, the blue curves are for $\alpha = 0.5$, and the green curves are for $\alpha = 0.75$.

decreased, the area under $f(u)$ becomes positive and more energy will need to be added to push the marble up the potential energy hill to reach and stop at $u = 1$. We can think of this additional energy as anti-friction added to the system in the form of anti-damping, $c > 0$. Similarly, if α is increased, the area under $f(u)$ becomes negative and we will need to slow the marble down to get it to stop at $u = 1$. This can be accomplished by adding friction, $c < 0$, to the system in the form of damping. For most forcing functions, the speed of the traveling front must be calculated numerically. However, for the bi-stable equation and $f(u)$ being a cubic polynomial, the traveling wave can be computed explicitly. Consider the forcing function

$$f(u) = (u - \alpha)(u - \beta)(\gamma - u), \tag{3.6}$$

where the zeros of the cubic are ordered as $\alpha < \beta < \gamma$. The speed of propagation of the wave can be computed explicitly by considering the ordinary differential equation [39]

$$u'' - cu' + (u - \alpha)(u - \beta)(\gamma - u) = 0. \tag{3.7}$$

We require that $u'(\alpha) = u'(\gamma) = 0$. Thus, we look for a solution with the property that

$$u' = P(u) = B(u - \alpha)(\gamma - u). \tag{3.8}$$

Then we have that

$$u'' = \frac{dP(u)}{du}P = B^2(u - \alpha)(\gamma - u)(\gamma - 2u + \alpha). \tag{3.9}$$

Substituting (3.8) and (3.9) into (3.7) yields

$$B^2(u - \alpha)(\gamma - u)(\gamma - 2u + \alpha) - cB(u - \alpha)(\gamma - u) + (u - \alpha)(\gamma - u)(u - \beta) = 0,$$

so,

$$B^2(\gamma - 2u + \alpha) - cB + (u - \beta) = 0.$$

This linear function of u is identically zero only if we choose

$$B = \frac{1}{\sqrt{2}} \qquad \text{and} \qquad c = \frac{1}{\sqrt{2}}(\alpha - 2\beta + \gamma)$$

and, thus, we have an explicit formula for the speed of propagation. Returning to (3.8), we have that

$$\frac{du}{d\zeta} = \frac{1}{\sqrt{2}}(u - \alpha)(\gamma - u),$$

which is a separable differential equation whose solution is given by

$$u(\zeta) = \frac{K\gamma + \alpha e^{\frac{1}{\sqrt{2}}(\alpha-\gamma)\zeta}}{K + e^{\frac{1}{\sqrt{2}}(\alpha-\gamma)\zeta}}. \tag{3.10}$$

This represents a family of traveling wave solutions. We select the solution that passes through $u(0) = \beta$ and thus we determine that

$$K = \frac{\beta - \alpha}{\gamma - \beta}.$$

For this instance of a cubic polynomial, we can explicitly determine the equation for the heteroclinic connection between the two stable steady states

$$u_1(\zeta) = \frac{K\gamma + \alpha e^{\frac{1}{\sqrt{2}}(\alpha-\gamma)\zeta}}{K + e^{\frac{1}{\sqrt{2}}(\alpha-\gamma)\zeta}} \quad \text{with} \quad K = \frac{\beta - \alpha}{\gamma - \beta} \tag{3.11}$$

where this representation is for the heteroclinic orbit. The exact expression for the heteroclinic orbit from 1 to 0 can be obtained through the change of variables $c \to -c$ and $\zeta \to -\zeta$.

These two exact solutions can be used as starting points to carry out parameter continuation for each of the heteroclinic orbits in the parameters β (the middle root) and c (the wave speed). This continuation can be carried out using the bifurcation program AUTO developed by Doedel [42, 43, 44]. This program utilizes algorithms for the numerical bifurcation analysis of differential equations. Using the algorithm outlined by Doedel and Friedman in 1989 [45], we compute the heteroclinic cycle connecting two saddle points in $\mathbb{R}^2$. This cycle can be computed to high accuracy due to an integral phase condition and the adaptive discretization capabilities of

AUTO. In the case of the bistable equation with $\alpha = 0$, $\beta = 0.5$, and $\gamma = 1$, the exact expression for a heteroclinic connection (3.11) becomes

$$u_1(\zeta) = \frac{e^{\frac{1}{\sqrt{2}}\zeta}}{1 + e^{\frac{1}{\sqrt{2}}\zeta}}. \tag{3.12}$$

The phase plane representation of the system of differential equations for this case is shown in Figure 16 for $c = 0$. We can see a family of periodic orbits. As the period

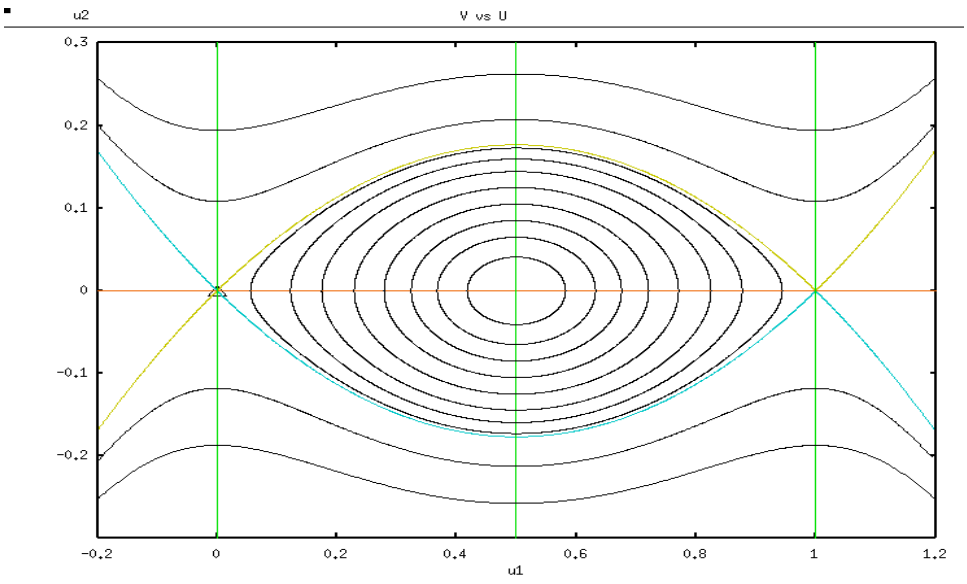

Figure 16: Phase portrait of the bistable equation for $\beta = 0.5$ and $c = 0$ showing a series of periodic orbits of increasing period. As $T \to \infty$, these orbits approach a heteroclinic cycle.

$T \to \infty$, this family of orbits approaches a heteroclinic cycle. The heteroclinic connection was continued in the parameter β and wave speed parameters. The resulting two branches are shown in Figure 17. The orbits remain unchanged along the two

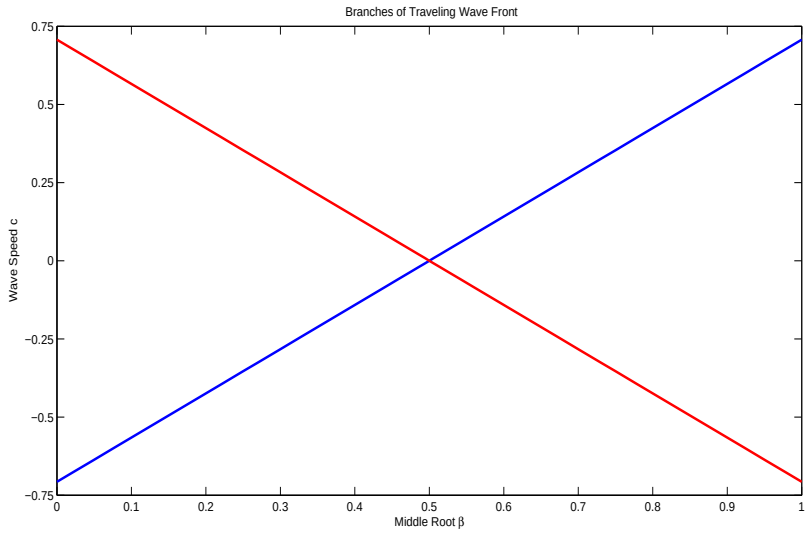

Figure 17: Continuation curves for each heteroclinic connection in the bistable equation.

branches and have the analytical representation

$$c = \pm\sqrt{2}\left(\beta - \frac{1}{2}\right).$$

For $\beta = 0.5$, if $c \neq 0$, the periodic orbits vanish. If $c > 0$, the middle singular point becomes an unstable spiral node and if $c < 0$, this singular point is a stable spiral node.

The pancreatic islet model equations exhibit the same qualitative behavior as the bistable equation. We would like to use the well known properties of the bistable equation to facilitate our analysis of traveling wave fronts in a one-dimensional pancreatic islet.

Pancreatic Model Reduction

Often to facilitate the analysis of complex biological systems, a systematic reduction of the model equations is carried out. The first simplification we carry out is to decouple the glucose system by assuming that the parameter g_{KATP} is a constant and is not a function of the intracellular glucose concentration. Following Sherman [21], we exclude the additive currents i_{KCa} and i_{CRAC} from the total ionic current i_{ion}. These two currents depend on the intracellular and endoplasmic reticulum calcium concentrations. Excluding these currents results in the ionic current function no longer being dependent on these variable since the calcium system is now decoupled. After these simplifications, we are left with two kinetic variables, w and z and a generic three variable model which is comparable to the β-cell models developed since the original work of Chay and Keizer [10]. The model equations now have the form

$$\frac{\partial u}{\partial \tau} = u_{xx} - i_{ion}(u, w, z), \tag{3.13}$$

$$\frac{dw}{d\tau} = \lambda_2 \left(n_\infty(u) - w\right), \tag{3.14}$$

$$\frac{dz}{d\tau} = \lambda_3 \left(s_\infty(u) - z\right), \tag{3.15}$$

where

$$i_{ion}(u,w,z) = \gamma_s\, z\,(u{+}1){+}\gamma_{Ca}\, m_\infty(u)\,(u-u_{Ca}){+}\gamma_K\, w\,(u{+}1){+}\gamma_{KATP}\,(u{+}1), \quad (3.16)$$

and

$$\gamma_{KATP} = \frac{a^2 g_{KATP}}{CD}. \quad (3.17)$$

Heteroclinic Connection

In general, the velocity of a nonlinear wave propagation is defined by the velocity of its front. As a result, to measure the wave velocity we can reduce the description of the wave to the description of its front only. Based upon the fact that the variable w is fast and the variable z is slow, in comparison with the rate of change of the electric potential at the wave front, we reduce the model equations by setting these kinetic variables to their stationary values. These types of model reductions are common in excitable systems such as nerve axons and β-cells. While the electric potential at the wave front is changing, the value of w at each moment in time is close to the stationary value $n_\infty(u)$ and the value of z remains close to the stationary value $s_\infty(u)$. With these reductions, the model of the pancreatic islet now has the form

$$\frac{\partial u}{\partial \tau} = u_{xx} - i_{ion}(u), \quad (3.18)$$

where

$$i_{ion}(u) = \gamma_s\, s_\infty(u)\,(u+1) + \gamma_{Ca}\, m_\infty(u)\,(u-u_{Ca}) + \gamma_K\, n_\infty(u)\,(u+1) + \gamma_{KATP}\,(u+1). \tag{3.19}$$

The function $i_{ion}(u)$ has the form of an N-shaped curve with three zero-crossings (Figure 18) which is typical for excitable media with two stable steady states. Similarly to the bistable equation, changes in the parameter γ_{KATP} will shift this curve up or down and result in a change in the wave speed.

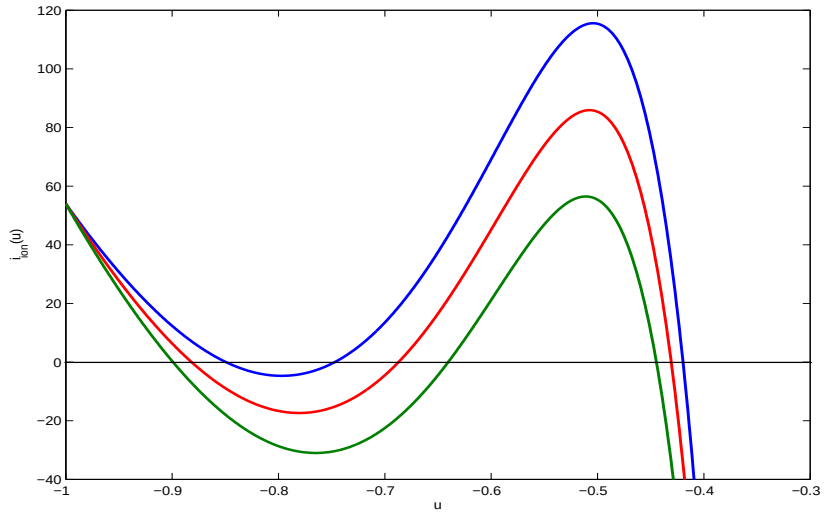

Figure 18: The function $-i_{ion}(u)$ for various values of the parameter γ_{KATP}. The blue curve is for $\gamma_{KATP} = 480$, the red curve is for $\gamma_{KATP} = 540$, and the green curve is for $\gamma_{KATP} = 600$. We can see that changes in this parameter affect the wave speed in much the same way as the location of the middle root in the bistable equation affected the speed of the wave.

The reduced pancreatic model and the bistable equation have the same qualitative behavior. Using the bistable equation as a starting point, we can homotopy the

heteroclinic connection in this model to a heteroclinic connection in the pancreatic model. The equilibria of the bistable equation will be shifted to better match those of i_{ion}. We choose the roots of the bistable equation $\alpha < \beta < \gamma$ to be -0.9, -0.675, and -0.45, respectively, and we consider the differential equation

$$\frac{\partial u}{\partial \tau} = u_{xx} - \lambda i_{ion}(u) + (1-\lambda)(u-\alpha)(u-\beta)(\gamma-u), \tag{3.20}$$

or, equivalently in traveling coordinates

$$\begin{aligned} u_1' &= u_2, \\ u_2' &= cu_2 + \lambda i_{ion}(u) - (1-\lambda)(u-\alpha)(u-\beta)(\gamma-u), \end{aligned}$$

where λ is the homotopy parameter. Using AUTO and the exact expression for the heteroclinic connection in the bistable equation, we use parameter continuation to move from $\lambda = 0$ to $\lambda = 1$. The homotopy curve is shown in Figure 19. We can now use the $\lambda = 1$ data as a starting point and continue in the parameter γ_{KATP} which will demonstrate the set of parameters values (wave speed c and γ_{KATP}) for which there is a heteroclinic connection and thus a traveling wave front through the pancreatic islet. This continuation curve is shown in Figure 20. In this figure, we have kept $z = s_\infty(u)$. The traveling front will be present for the values of γ_{KATP} for which the intersection of the nullcline and this curve occurs on the left branch of the cubic nullcline and the z value of this intersection is not greater than the z value at the local maximum of the nullcline. For this reason, the continuation curve has a

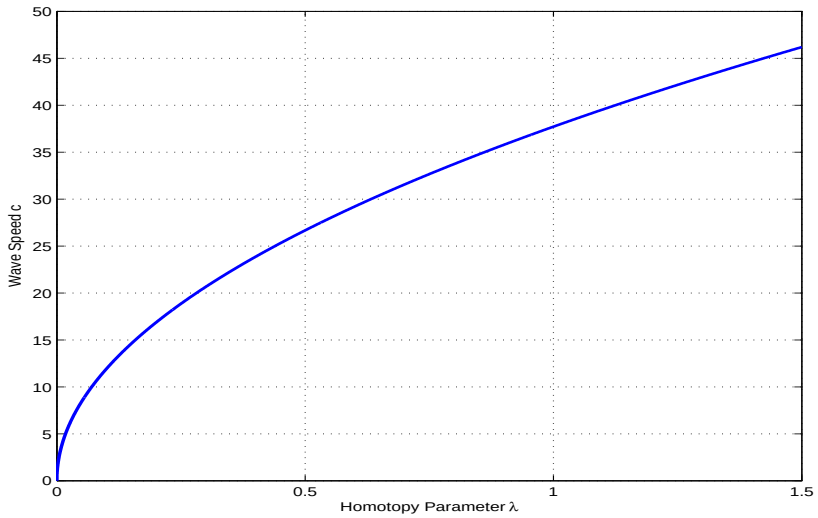

Figure 19: The homotopy curve for continuing the heteroclinic connection in the bistable equation to the reduced pancreatic model.

domain of approximately $600 \leq \gamma_{KATP} \leq 950$.

Traveling Fronts Versus Pulses

In this section, we describe the connection between a traveling wave front (heteroclinic connection) and a traveling wave pulse (homoclinic orbit). A traveling pulse is a traveling wave solution that starts and ends at the same steady state of the model equations. For our purposes of understanding the relationship between traveling fronts and pulses, we will consider the Fitzhugh-Nagumo model equations

$$\varepsilon \frac{\partial v}{\partial t} = \varepsilon^2 \frac{\partial^2 v}{\partial^2 x} + f(v, w), \tag{3.21}$$

$$\frac{\partial w}{\partial t} = g(v, w), \tag{3.22}$$

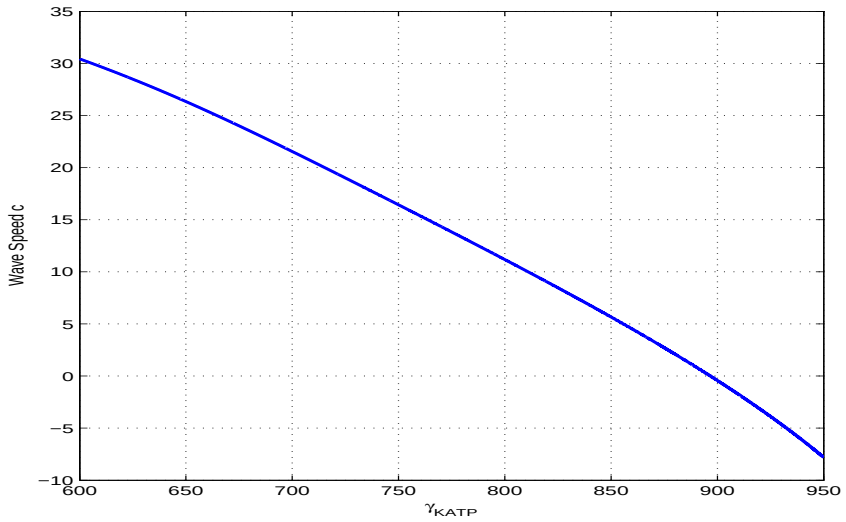

Figure 20: Continuation of the heteroclinic connection in the γ_{KATP} and wave speed parameters.

and follow the analysis in [39], where ε is assumed to be a small positive number. Here space has been scaled so that the diffusion coefficient of v is ε^2. The variable v represents the membrane potential and w represents a slow gating variable. We assume that the nullcline $f(v, w) = 0$ is of 'cubic' shape and the nullcline $g(v, w) = 0$ is assumed to have precisely one intersection with the cubic nullcline (see Figure 21). As before, the equations (3.21)-(3.22) are converted to traveling coordinates ($\zeta = x - ct$) and have the form

$$\varepsilon^2 v'' + c\varepsilon v' + f(v, w) = 0,$$

$$cw' + g(v, w) = 0,$$

where the derivative here is with respect to ζ. By exploiting the smallness of the

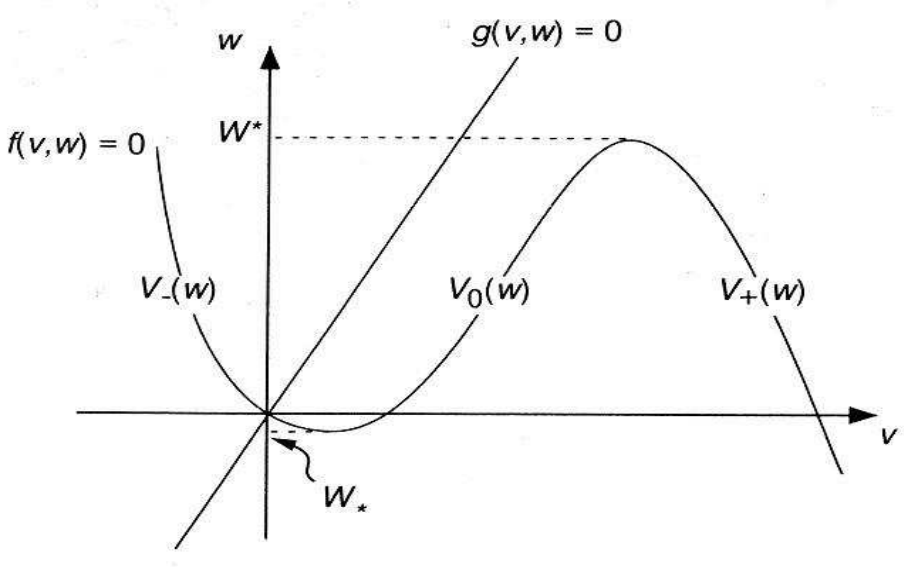

Figure 21: The generalized Fitzhugh-Nagumo phase plane. Taken from [39].

parameter ε, we can gain insight into the traveling pulse solution. Taking $\varepsilon = 0$ in (3.21)-(3.22) we obtain the outer equations

$$w_t = g(v, w), \qquad f(v, w) = 0. \tag{3.23}$$

Since the cubic nullcline $f(v, w) = 0$ is assumed to have three solutions and only two of these equilibria are stable (the left and right solution branches), the outer equations (3.23) reduce to

$$\frac{\partial w}{\partial t} = g\left((V_{\pm}(w), w\right) = G_{\pm}(w). \tag{3.24}$$

The region in which $v = V_+(w)$ is called the excited region and the region where $v = V_-(w)$ is called the recovery region. The outer equation is valid whenever the diffusion is not large, but there are interfaces where the diffusion is large and (3.24)

is not valid. To determine the behavior in these cases, we rescale space and time. Let $y(t)$ denote the position of the wave front. We rescale as follows

$$\tau = t, \qquad \zeta = \frac{x - y(t)}{\varepsilon},$$

and (3.21)-(3.22) become

$$\begin{aligned} v'' + \dot{y}(\tau)v' + f(v,w) &= \varepsilon \frac{\partial v}{\partial \tau}, \\ -\dot{y}(\tau)w' &= \varepsilon \left(g(v,w) - \frac{\partial w}{\partial t} \right), \end{aligned}$$

where $[\dot{}]$ represents the derivative with respect to τ. By setting $\varepsilon = 0$, we obtain the inner equations

$$v'' + \dot{y}(\tau)v' + f(v,w) = 0, \tag{3.25}$$

$$\dot{y}(\tau)w' = 0. \tag{3.26}$$

Since τ only appears as a parameter in these equations and the traveling wave is stationary in the traveling coordinate system ζ, τ, they can be solved as ordinary differential equations. We observe that w is independent of ζ. The inner equation provides a transition layer between the regions where the outer dynamics hold. Thus, we require the matching condition that $f(v,w) \to 0$ as $\zeta \to \pm\infty$.

We observe that (3.25) is the bi-stable equation for which there are heteroclinic orbits. For fixed w, if the nullcline $f(v,w) = 0$ has three roots, two of which are

stable, then there is a number (the wave speed) $c = c(w)$ for which the equation

$$v'' + c(w)v' + f(v, w) = 0, \tag{3.27}$$

has a heteroclinic orbit connecting the two stable roots of $f(v, w) = 0$. This orbit corresponds to a moving transition layer, traveling with speed c. Since the roots of $f(v, w) = 0$ are functions of w, c is also a function of w. The function $c(w)$ is the unique parameter value for which (3.27) has a solution with $v \to V_-(w)$ as $\zeta \to \infty$ and $v \to V_+(w)$ as $\zeta \to -\infty$. If $c(w) > 0$, this transition is described as an 'upjump' moving to the right while if $c(w) < 0$ then the transition is a 'downjump' moving to the left.

A general picture of wave propagation can now be described. In most of space, the outer dynamics (3.24) are satisfied. At any transition between the two types of outer dynamics, the continuity of w is maintained by a sharp transition in v that travels at the speed $\dot{y}(t) = c(w)$ if $v = V_-(w)$ on the right and $v = V_+(w)$ on the left or $\dot{y}(t) = -c(w)$ if $v = V_+(w)$ on the right and $v = V_-(w)$ on the left where w is the value of the recovery variable in the interior of the transition layer. Now we can examine in more detail the traveling wave pulse. The phase portrait for a solitary pulse is shown in Figure 22. The pulse consists of a single excitation front followed by a single recovery back. Furthermore, we observe that the wave speed for the traveling wave front is, to leading order, the wave speed for the homoclinic orbit. This homoclinic orbit, in the singular limit, consists of a (excitation) front, a

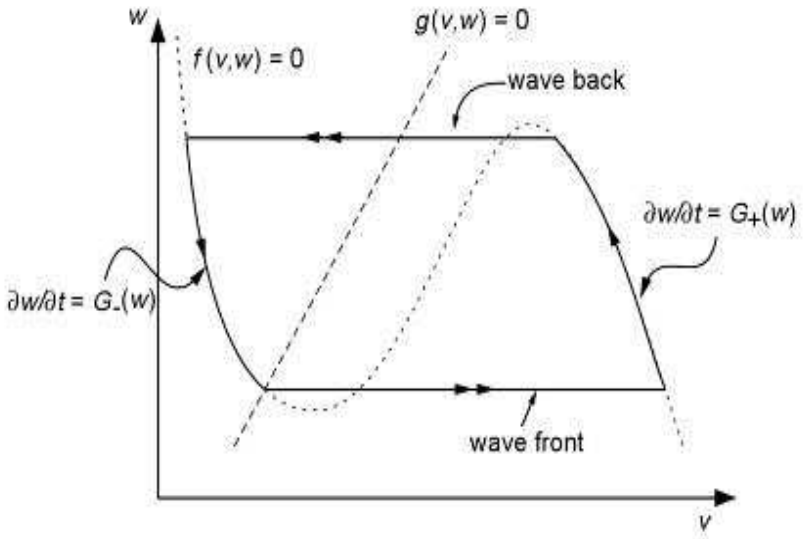

Figure 22: The phase portrait of the fast traveling pulse for Fitzhugh-Nagumo dynamics in the singular limit $\varepsilon \to 0$. Taken from [39].

(recovery) back and two slow pieces.

We have seen that the reduced pancreatic model equations are qualitatively the same as the Fitzhugh-Nagumo equations. Thus, we would expect to see the same type of dynamics for the islet model. This is addressed in the next section.

Homoclinic Connection

When the slow gating variable z is added back into the reduced model equations, a homoclinic orbit will result which corresponds to a traveling wave pulse through the islet. As before with the heteroclinic connection, we would like to determine for which values of the parameters γ_{KATP} and wave speed c there is a homoclinic connection.

In traveling coordinates, the system of equations becomes

$$\begin{aligned} u_1' &= u_2, \\ u_2' &= cu_2 + i_s(u_1, z) + i_{Ca}(u_1) + i_K(u_1) + i_{KATP}(u_1), \\ z' &= \frac{\lambda_3}{c}(s_\infty(u_1) - z), \end{aligned}$$

where

$$\begin{aligned} i_s(u_1, z) &= \gamma_s z(u+1), \\ i_{Ca}(u_1) &= \gamma_{ca}\, m_\infty(u)(u - u_{Ca}), \\ i_K(u_1) &= \gamma_K\, n_\infty(u)(u+1), \\ i_{KATP}(u_1) &= \gamma_{KATP}(u+1). \end{aligned}$$

It should be noted that this reduced islet model is qualitatively the same as the Morris-Lecar biological neuron model for oscillatory behavior in the giant barnacle muscle fiber [46].

As the parameter γ_{KATP} varies, the equilibrium point moves along different branches of the cubic nullcline as seen in Figure 23. When the equilibrium is on the left branch, we will observe the presence of a homoclinic orbit. A high period periodic orbit will be used to approximate the homoclinic orbit [47]. Beginning with the equilibrium on the middle branch of the cubic nullcline, we use AUTO to continue in the wave speed parameter. Upon the detection of a Hopf bifurcation, periodic orbits are computed. A periodic orbit with period $T \approx 45$ is selected and is continued

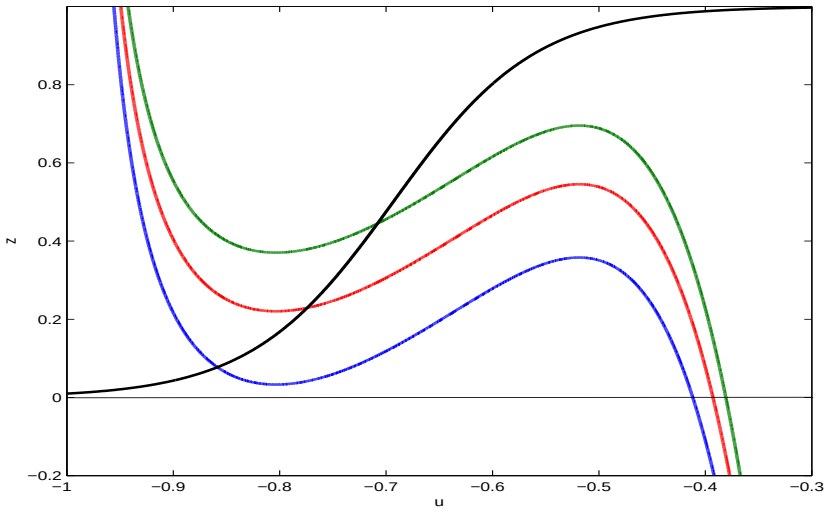

Figure 23: Nullclines for the two variable system. The cubic-like curves correspond to various values of the parameter γ_{KATP}. From bottom to top: $\gamma_{KATP} = 480$ (blue), $\gamma_{KATP} = 600$ (red), $\gamma_{KATP} = 750$ (green). The other curve (black) is the nullcline $z = s_\infty(u)$.

in the wave speed c and γ_{KATP} parameters, see Figure 24. By selecting an orbit corresponding to the equilibrium being on the left branch and continuing in the period and the wave speed we can obtain a good approximation for the homoclinic orbit. We select the orbit located at the value $\gamma_{KATP} = 750$. The resulting dispersion curve is shown in Figure 25. There appear to be two values of the wave speed for which there is a homoclinic orbit. In the Fitzhugh-Nagumo model, the dispersion curve also has two branches, one denoting fast waves and the other slow. The solutions on the fast branch are typical of action potentials and are usually stable while the solutions on the slow branch are small amplitude oscillations and are unstable [39] and are thus not observed. For the islet model, we see the same behavior. Plots of a small and

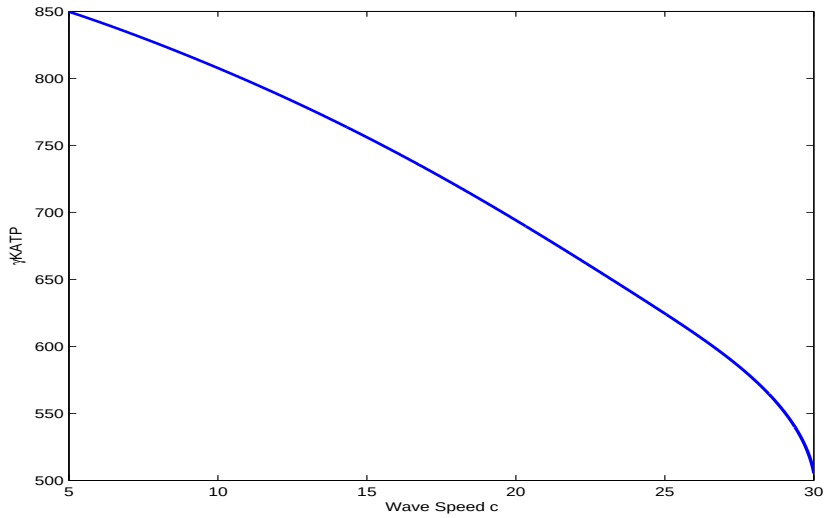

Figure 24: Continuation of a high period periodic orbit in the wave speed c and γ_{KATP}.

large amplitude oscillation are shown in Figure 26. In Figure 27 the small and large oscillations are overlayed on the nullclines of the system. We consider the higher wave speed orbit, i.e., the large amplitude stable traveling waves.

By selecting a high period orbit on the upper branch of the dispersion curve, the homoclinic orbit can be approximated and continued in the wave speed and γ_{KATP} parameters, shown in Figure 28. From our previous discussion, we would expect that the wave speeds obtained from the heteroclinic connection would be a good approximation to the speeds for a traveling pulse. In Figure 29 we compare these two curves. In the region of the equilibrium on the left branch, we see that there is good agreement.

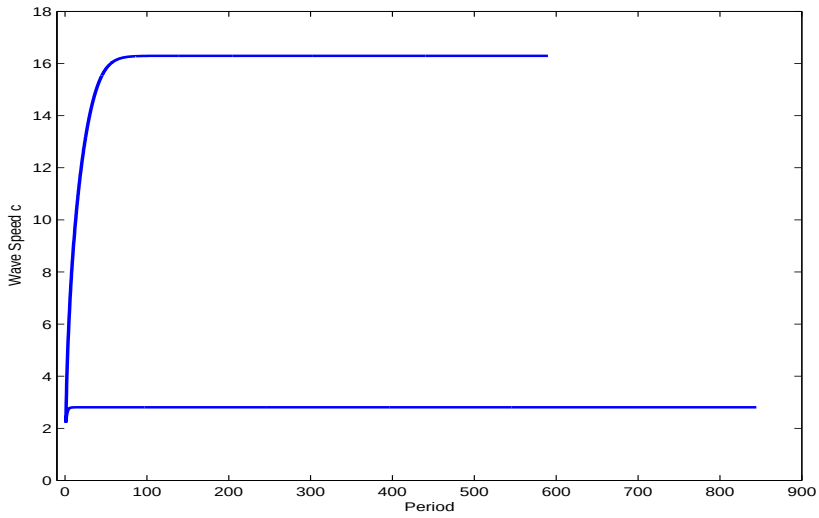

Figure 25: The dispersion relation for $\gamma_{KATP} = 750$.

Comparison of Wave Speeds

We have obtained estimations of the wave speed for the reduced two variable model of the pancreatic islet in traveling coordinates. The partial differential equation was simulated on a length scale of $L = 20-50$. To compare the results of the traveling wave system with those seen in the partial differential equation two variable model, we reduced the length of the spatial interval. The wave activity in the PDE model is initiated by imposing a flux condition on one end of the distribution of cells. Once the wave has commenced, periodic boundary conditions will be imposed and the wave speed can be estimated. For a length scale $L = 50$ and for $\gamma_{KATP} = 700$, the initial wave and and the propagation on a ring are shown in Figure 30. The wave speed is estimated to be 15.61. To compare this to the computation of the wave speed in

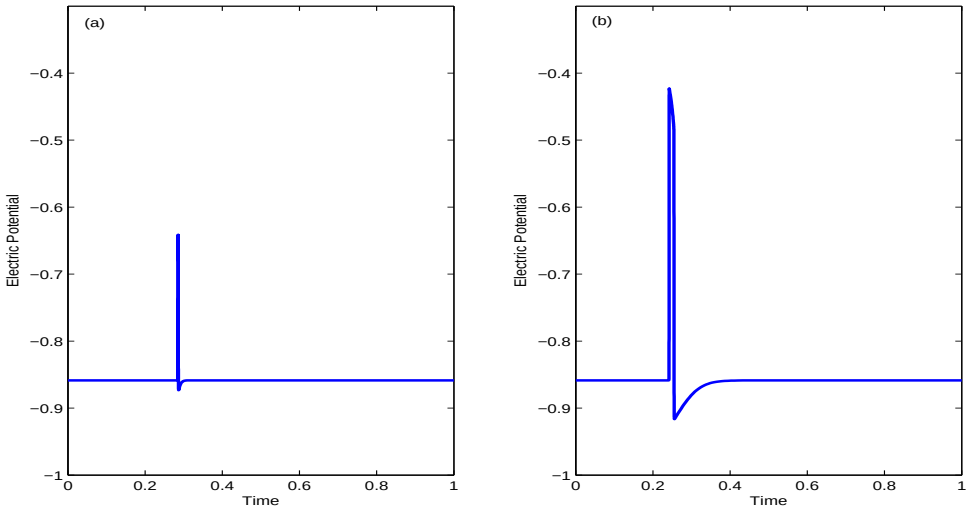

Figure 26: (a) Plot of a small amplitude oscillation on the lower branch of the dispersion curve. (b) Plot of a large amplitude oscillation on the upper branch of the dispersion curve.

traveling coordinates, the AUTO numerics must be carried out again, but for a short period, i.e., length scale. Returning to the dispersion relation (Figure 25), we select the orbit on the upper branch corresponding to a period of 50 and continue this orbit in the wave speed and γ_{KATP} parameters. The results are shown in Figure 31. For the value $\gamma_{KATP} = 700$, we see a wave speed of 20.17. Similarly we can obtain wave speeds for $\gamma_{KATP} = 725$ and 750. Proceeding in the same way, estimations of the wave speed for the other values of the γ_{KATP} and the corresponding length scales can be computed. The results are summarized in Table 4.

We can see from Table 4 that the estimations of the wave speeds from the partial differential equation two variable reduced model and the reduced model in traveling

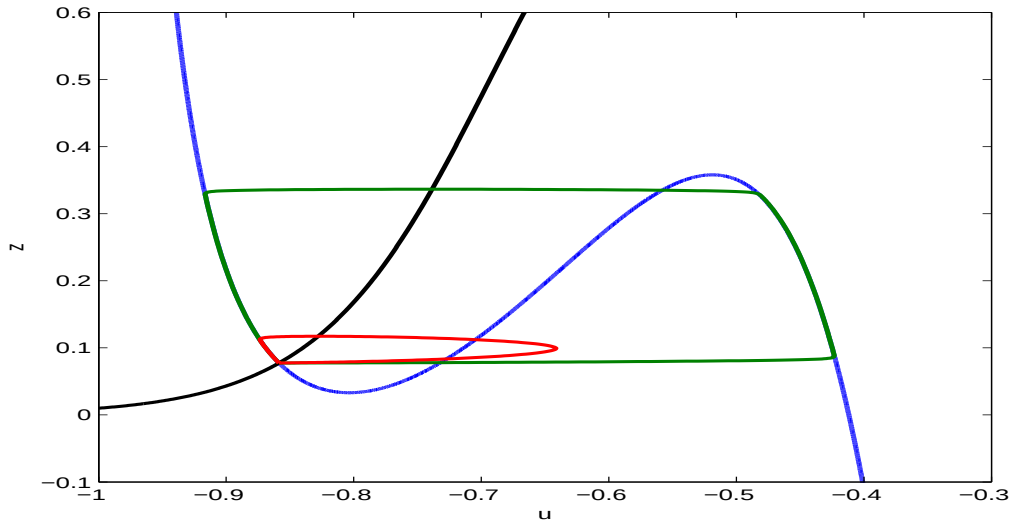

Figure 27: Plots of the small and large oscillations overlayed on the nullclines of the system (shown in black and blue). The small amplitude oscillation is shown in red and the large amplitude oscillation is shown in green.

coordinates differ by a considerable amount. This leads one to ask which of these two estimations is more accurate? If we could run simulations of the islet model to infinite accuracy, we would expect the values of the wave speed to better match those obtained from AUTO. It is only in the traveling coordinates that we are actually computing the wave speed of the traveling pulse. AUTO also incorporates collocation and adaptive mesh methods into its computations. As a result, we should trust the computations and values for the wave speed from the traveling coordinate system over the approximations from numerical simulations of the partial differential equation. In their 2001 paper, Aslanidi et. al. [1] estimated the wave speed using numerical simulations of the partial differential equation model. They also obtained an explicit

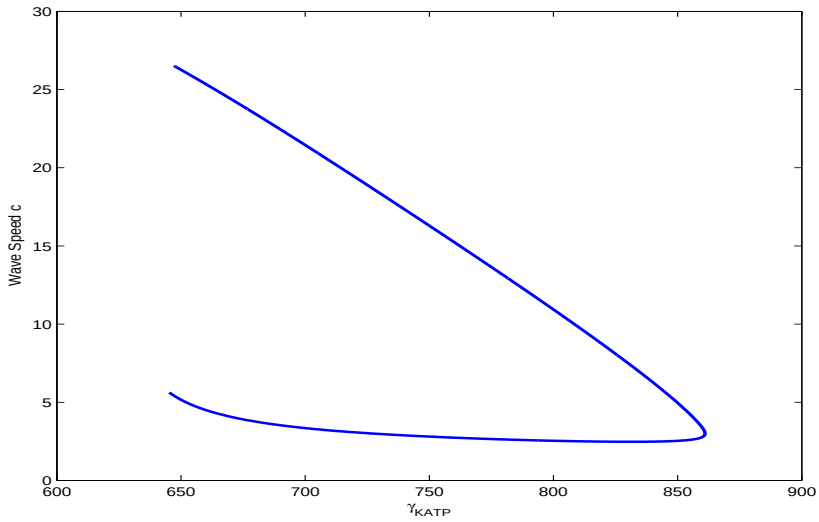

Figure 28: The continuation of the homoclinic orbit with the higher wave speed in γ_{KATP}.

formula for the speed of the traveling front. However, in their formula they introduced a factor of 1.5 to achieve better correspondence with the results of the numerics. By considering the model in traveling coordinates, we have obtained a better estimation for the speed of the traveling wave through the pancreatic islet.

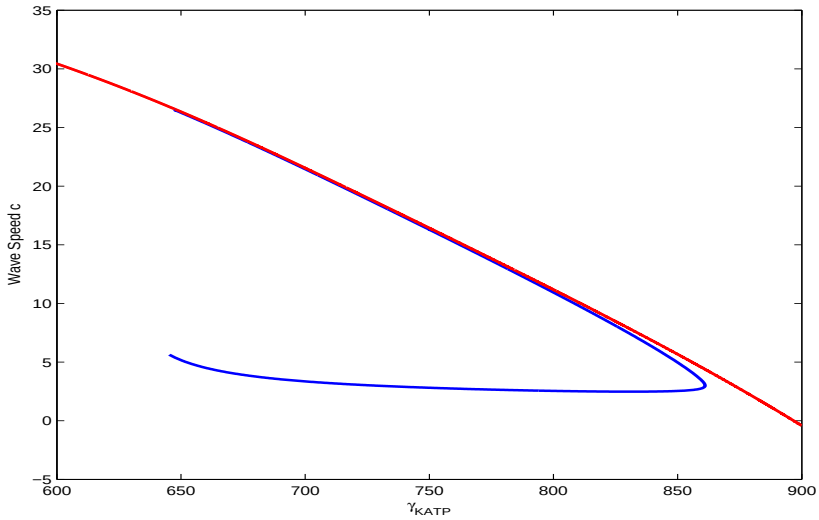

Figure 29: Comparsion of the front (upper) heteroclinic and homoclinic connection wave speeds for the two variable model. The homoclinic connection is shown in blue and the heteroclinic connection is shown in red. We see agreement in the region where the equilibrium lies on the left branch of the nullcline.

γ_{KATP}	Length Scale	Wave Speed - TC	Wave Speed - PDE
700	50	15.61	20.17
725	50	12.41	18.03
750	50	9.12	15.80
775	40	11.02	13.07
800	30	7.85	10.30
825	25	6.37	7.74
850	20	4.34	4.86

Table 4: Comparison of wave speeds for the traveling coordinate model and the numerical simulation of the PDE model.

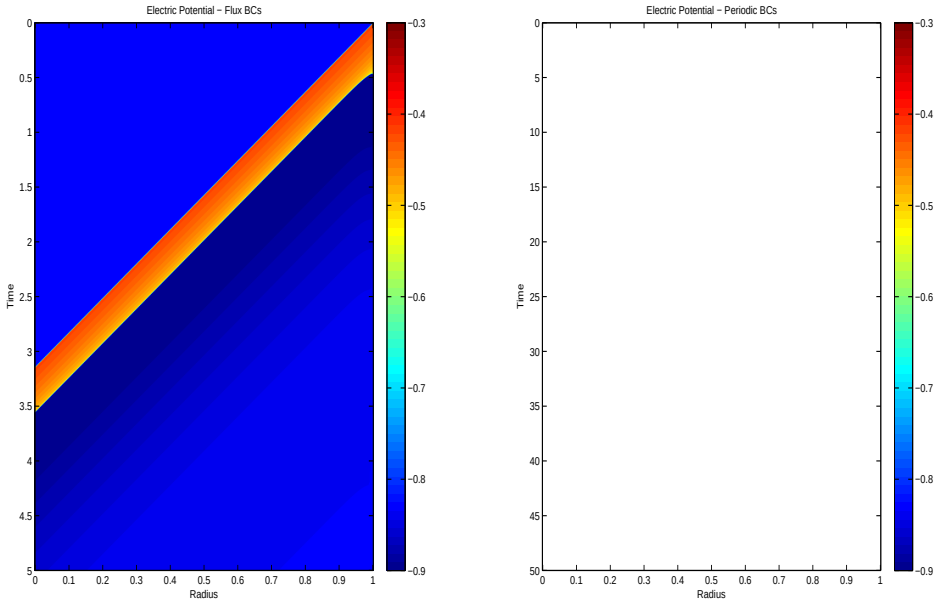

Figure 30: On the left is the initial wave propagating through the distribution of cells. On the right, the data from the initial wave at time=2.5 is used and periodic boundary conditions are imposed.

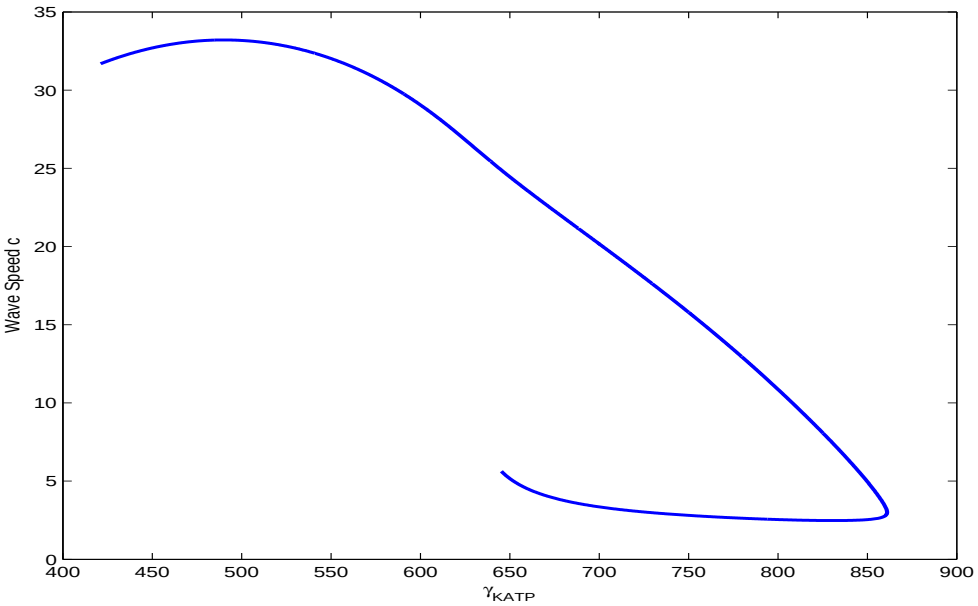

Figure 31: The continuation of a period 50 orbit on the upper branch of the dispersion relation in the wave speed and γ_{KATP} parameter.

CHAPTER 4

2D MODEL AND ADI METHODS

Two-Dimensional Islet Model

While the one-dimensional model exhibits the wave phenomenon through the distribution of β-cells, it is not geometrically realistic. Pancreatic islets are roughly circular and, thus, we will think of a distribution of β-cells over the unit disk and utilize polar coordinates. The formulation for discretizing the Laplacian is modeled after Thomas [48]. However, adjustments must be made to account for the Robin boundary condition. These higher dimensional discretizations become numerically expensive to simulate. However, by using alternating direction implicit numerical methods (ADI) introduced by Douglas, Peaceman and Rachford in 1955 [4, 5], the banded structure of the discretization matrices is re-established allowing for more efficient solvers to be utilized. The complication with the pancreatic islet model is that the partial differential equations are nonlinear. The standard ADI method must be adapted to allow for this nonlinearity and not sacrifice numerical accuracy. We adapt a new nonlinear ADI method proposed by Amiri and Hosseini in 2012 [6] to the pancreatic model equations. This new method is second order in both time and space as well as unconditionally stable.

Discretizing the Laplacian

Let $D(r,\theta) = \{(r,\theta) : 0 \leq r \leq 1, 0 \leq \theta \leq 2\pi\}$ and consider a distribution of β-cells over D. The grid points will be labeled as (r_j, θ_k) for $j = 0, \ldots, M$ and $k = 0, \ldots, N$ with $r_0 = 0$, $r_M = 1$, $\theta_0 = 0$, and $\theta_N = 2\pi$ as shown in Figure 32. There is only one point corresponding to $j = 0$ and we will denote this point by u_0.

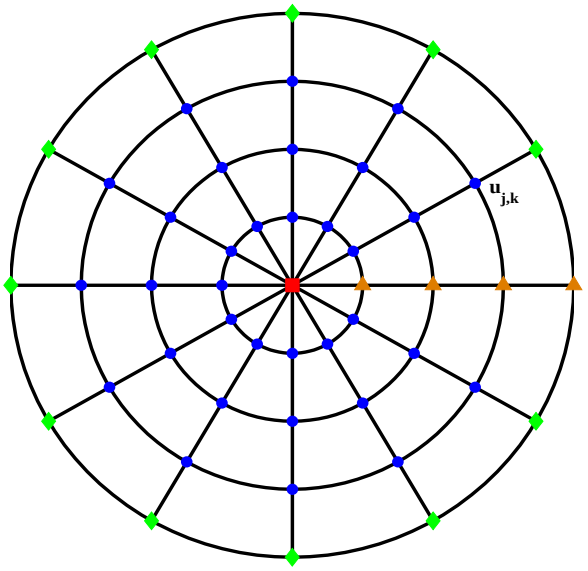

Figure 32: An example of the polar discretization. The blue round nodes are the interior nodes, the green diamond nodes are the boundary nodes, the red square node is the origin node, and the orange triangle nodes are the θ periodicity condition nodes.

Additionally, a continuity condition will be prescribed, $u_{j,N} = u_{j,0}$, to account for the

periodicity in θ. We recall the Laplacian operator in polar coordinates given by

$$\nabla^2 u = \frac{1}{r}\left(r u_r\right)_r + \frac{1}{r^2} u_{\theta\theta} = u_{rr} + \frac{1}{r} u_r + \frac{1}{r^2} u_{\theta\theta}. \tag{4.1}$$

There are four cases to consider (see Figure 32):

Case 1: Interior Nodes $j = 1, \ldots, M-1$ and $k = 1, \ldots, N-1$

Case 2: Boundary Nodes $j = M$ and $k = 1, \ldots, N-1$

Case 3: θ Periodicity Condition Nodes $j = 1, \ldots, M-1$ and $k = 0$

Case 4: Origin Node $j = 0$

For the interior nodes, that is for $j = 1, \ldots, M-1$ and $k = 1, \ldots, N-1$, we have that (4.1) becomes

$$\begin{aligned}
\nabla^2 u_{j,k} &\approx \frac{1}{r_j}\left(\frac{\left(r u_r\right)_{j+1/2,k} - \left(r u_r\right)_{j-1/2,k}}{\Delta r}\right) + \frac{1}{r_j^2}\left(\frac{u_{j,k+1} - 2\,u_{j,k} + u_{j,k-1}}{\left(\Delta\theta\right)^2}\right), \\
&= \frac{1}{r_j\,\Delta r}\left[r_{j+1/2}\left(\frac{u_{j+1,k} - u_{j,k}}{\Delta r}\right) - r_{j-1/2}\left(\frac{u_{j,k} - u_{j-1,k}}{\Delta r}\right)\right] \\
&\qquad + \frac{1}{r_j^2}\left(\frac{u_{j,k+1} - 2\,u_{j,k} + u_{j,k-1}}{\left(\Delta\theta\right)^2}\right), \\
&= \frac{1}{r_j}\frac{1}{\left(\Delta r\right)^2}\left[r_{j+1/2}\left(u_{j+1,k} - u_{j,k}\right) - r_{j-1/2}\left(u_{j,k} - u_{j-1,k}\right)\right]
\end{aligned}$$

$$+\frac{1}{r_j^2}\left(\frac{u_{j,k+1}-2\,u_{j,k}+u_{j,k-1}}{(\Delta\theta)^2}\right),$$

$$\begin{aligned}
= \quad & \left(\frac{r_{j+1/2}}{r_j\ (\Delta r)^2}\right)u_{j+1,k}-\left(\frac{r_{j+1/2}}{r_j\ (\Delta r)^2}+\frac{r_{j-1/2}}{r_j\ (\Delta r)^2}+\frac{2}{r_j^2\ (\Delta\theta)^2}\right)u_{j,k} \\
& +\left(\frac{r_{j-1/2}}{r_j\ (\Delta r)^2}\right)u_{j-1,k}+\left(\frac{1}{r_j^2\ (\Delta\theta)^2}\right)u_{j,k+1}+\left(\frac{1}{r_j^2\ (\Delta\theta)^2}\right)u_{j,k-1}.
\end{aligned} \tag{4.2}$$

We define

$$\alpha_j=\tfrac{r_{j-1/2}}{r_j\,(\Delta r)^2}, \qquad \gamma_j=\tfrac{r_{j+1/2}}{r_j\,(\Delta r)^2},$$

$$\varepsilon_j=\tfrac{1}{r_j^2\,(\Delta\theta)^2}, \qquad \beta_j=\gamma_j+\alpha_j+2\,\varepsilon_j.$$

Thus, (4.2) becomes

$$\nabla^2 u_{j,k}\approx\gamma_j u_{j+1,k}-\beta_j u_{j,k}+\alpha_j u_{j-1,k}+\varepsilon_j u_{j,k+1}+\varepsilon_j u_{j,k-1}.$$

For the boundary nodes, we want to apply the Robin boundary condition

$$\frac{\partial u}{\partial r}=Au+B, \tag{4.3}$$

for some constants A and B. Consider the boundary node $u_{M,k}$ where $k\neq 0$. Then (4.2) becomes

$$\begin{aligned}
\nabla^2 u_{M,k}\approx \ & \left(\frac{r_{M+1/2}}{r_M\ (\Delta r)^2}\right)u_{M+1,k}-\left(\frac{r_{M+1/2}}{r_M\ (\Delta r)^2}+\frac{r_{M-1/2}}{r_M\ (\Delta r)^2}+\frac{2}{r_M^2\ (\Delta\theta)^2}\right)u_{M,k} \\
& +\left(\frac{r_{M-1/2}}{r_M\ (\Delta r)^2}\right)u_{M-1,k}+\left(\frac{1}{r_M^2\ (\Delta\theta)^2}\right)u_{M,k+1}+\left(\frac{1}{r_M^2\ (\Delta\theta)^2}\right)u_{M,k-1}.
\end{aligned} \tag{4.4}$$

For the $u_{M+1,k}$ term, we apply an $O(\Delta r^2)$ approximation to (4.3)

$$\frac{u_{M+1,k} - u_{M-1,k}}{2\,\Delta r} \approx A\,u_{M,k} + B,$$

which implies

$$u_{M+1,k} \approx (2A\Delta r)u_{M,k} + u_{M-1,k} + 2\Delta r B.$$

Substituting into (4.4) gives

$$\begin{aligned}
\nabla^2 u_{M,k} \;\approx\; & \left(\frac{r_{M+1/2}}{r_M\,(\Delta r)^2}\right)\left((2A\Delta r)\,u_{M,k} + u_{M-1,k} + 2\Delta r B\right) \\
& - \left(\frac{r_{M+1/2}}{r_M\,(\Delta r)^2} + \frac{r_{M-1/2}}{r_M\,(\Delta r)^2} + \frac{2}{r_M^2\,(\Delta\theta)^2}\right) u_{M,k} \\
& + \left(\frac{r_{M-1/2}}{r_M\,(\Delta r)^2}\right) u_{M-1,k} + \left(\frac{1}{r_M^2\,(\Delta\theta)^2}\right) u_{M,k+1} + \left(\frac{1}{r_M^2\,(\Delta\theta)^2}\right) u_{M,k-1}.
\end{aligned}$$

Thus we have

$$\begin{aligned}
\nabla^2 u_{M,k} \;\approx\; & \left(\frac{2A\,r_{M+1/2}}{r_M\,(\Delta r)} - \gamma_M - \alpha_M - 2\,\varepsilon_M\right) u_{M,k} + (\alpha_M + \gamma_M)\,u_{M-1,k} \\
& + \varepsilon_M\,u_{M,k+1} + \varepsilon_M\,u_{M,k-1} + \frac{2B\,r_{M+1/2}}{r_M\,(\Delta r)}.
\end{aligned}$$

For $k = 0$ and $j = 1, \ldots, M-1$, we see that (4.2) becomes

$$\begin{aligned}
\nabla^2 u_{j,0} \;\approx\; & \frac{1}{r_j}\frac{1}{(\Delta r)^2}\left[r_{j+1/2}\,(u_{j+1,0} - u_{j,0}) - r_{j-1/2}\,(u_{j,0} - u_{j-1,0})\right] \\
& + \frac{1}{r_j^2}\frac{1}{(\Delta\theta)^2}\left[u_{j,1} - 2u_{j,0} + u_{j,-1}\right],
\end{aligned}$$

and we apply the periodicity condition $u_{j,N} = u_{j,0}$ and use the fact that $u_{j,-1} = u_{j,N-1}$. Thus, we find that

$$\begin{aligned}\nabla^2 u_{j,0} \;\approx\; & \left(\frac{r_{j+1/2}}{r_j\,(\Delta r)^2}\right) u_{j+1,0} - \left(\frac{r_{j+1/2}}{r_j\,(\Delta r)^2} + \frac{r_{j-1/2}}{r_j\,(\Delta r)^2} + \frac{2}{r_j^2\,(\Delta\theta)^2}\right) u_{j,0} \\ & + \left(\frac{r_{j-1/2}}{r_j\,(\Delta r)^2}\right) u_{j-1,0} + \left(\frac{1}{r_j^2\,(\Delta\theta)^2}\right) u_{j,1} + \left(\frac{1}{r_j^2\,(\Delta\theta)^2}\right) u_{j,N-1},\end{aligned}$$

or, simplifying

$$\nabla^2 u_{j,0} \approx \gamma_j\, u_{j+1,0} - \beta_j\, u_{j,0} + \alpha_j\, u_{j-1,0} + \varepsilon_j\, u_{j,1} + \varepsilon_j\, u_{j,N-1}. \tag{4.5}$$

For the node at the origin, $j = 0$, a control volume approach is used. We consider the control volume in polar coordinates defined by $D_1(r,\theta) = \{(r,\theta) \,:\, 0 \le r \le \Delta r/2,\ 0 \le \theta \le 2\pi\}$ and define the curve $C = \partial D_1 = \{(\Delta r/2, \theta) \,:\, 0 \le \theta \le 2\pi\}$. Then we can approximate the value of the u_0 with the average value of Δu over the control volume $D_1(r,\theta)$:

$$\begin{aligned}\nabla^2 u_0 \;&\approx\; \frac{1}{A(D_1)} \iint_{D_1} \Delta u \, dA, \\ &=\; \frac{4}{\pi\,(\Delta r)^2} \int_0^{2\pi} \int_0^{\Delta r/2} \nabla \cdot (\nabla u)\, dA.\end{aligned} \tag{4.6}$$

Now, we apply the Divergence Theorem in two dimensions:

$$\iint_{D_1} \nabla \cdot \boldsymbol{F} = \oint_C \boldsymbol{F} \cdot \boldsymbol{n}\, ds,$$

where $\boldsymbol{n}$ is the outward unit normal vector on the boundary and ds is the arclength

element of the curve C. Since we are in polar coordinates, we have that $\boldsymbol{n} = \hat{\boldsymbol{e}}_r$ and $ds = rd\theta$ where r is evaluated on C. Also recall that in the polar basis,

$$\nabla u = u_r\,\hat{\boldsymbol{e}}_r + \frac{1}{r}\,u_\theta\,\hat{\boldsymbol{e}}_\theta.$$

Thus, (4.6) becomes

$$\begin{aligned}\nabla^2 u_0 &\approx \frac{4}{\pi\,(\Delta r)^2}\oint_C u_r\left(\frac{\Delta r}{2},\theta\right)\,ds,\\ &= \frac{2}{\pi\Delta r}\int_0^{2\pi} u_r\left(\frac{\Delta r}{2},\theta\right)\,d\theta.\end{aligned}$$

We approximate $u_r\left(\frac{\Delta r}{2},\theta\right)$ with an $O\left(\Delta r^2\right)$ central difference scheme. Further, the integral is approximated using the Trapezoid Rule, noting that $\Delta\theta = \frac{2\pi}{N}$. Then (4.6) is equivalent to

$$\begin{aligned}\nabla^2 u_0 &\approx \frac{2}{\pi\Delta r}\int_0^{2\pi}\frac{u_{1,k}-u_0}{2\,(\Delta r/2)}\,d\theta,\\ &= \frac{2}{\pi\,(\Delta r)^2}\cdot\Delta\theta\left[\frac{1}{2}\,(u_{1,0}-u_0)+(u_{1,1}-u_0)+(u_{1,2}-u_0)\right.\\ &\qquad\left.+\cdots+(u_{1,N-1}-u_0)+\frac{1}{2}\,(u_{1,N}-u_0)\right],\\ &= \frac{2\Delta\theta}{\pi\,(\Delta r)^2}\sum_{k=0}^{N-1}(u_{1,k}-u_0),\\ &= -\frac{2N\Delta\theta}{\pi\,(\Delta r)^2}\,u_0+\frac{2\Delta\theta}{\pi\,(\Delta r)^2}\sum_{k=0}^{N-1}u_{1,k}.\end{aligned}$$

Recalling the definitions of our coefficients,

$$\alpha_j = \frac{r_{j-1/2}}{r_j\,(\Delta r)^2}, \qquad \gamma_j = \frac{r_{j+1/2}}{r_j\,(\Delta r)^2},$$

$$\varepsilon_j = \frac{1}{r_j^2\,(\Delta\theta)^2}, \qquad \beta_j = \gamma_j + \alpha_j + 2\,\varepsilon_j,$$

we can summarize the discretizations of the various grid points:

Case 1: Interior Nodes For $j = 1, \ldots, M-1$ and $k = 1, \ldots, N-1$

$$\nabla^2 u_{j,k} = \gamma_j u_{j+1,k} - \beta_j u_{j,k} + \alpha_j u_{j-1,k} + \varepsilon_j u_{j,k+1} + \varepsilon_j u_{j,k-1} \tag{4.7}$$

Case 2: Boundary Nodes For $j = M$ and $k = 1, \ldots, N-1$

$$\begin{aligned} \nabla^2 u_{M,k} \;\; = \;\; & \left(\frac{2A\,r_{M+1/2}}{r_M\,(\Delta r)} - \gamma_M - \alpha_M - 2\varepsilon_M\right) u_{M,k} + (\alpha_M + \gamma_M)\,u_{M-1,k} \\ & + \varepsilon_M\,u_{M,k+1} + \varepsilon_M\,u_{M,k-1} + \frac{2B\,r_{M+1/2}}{r_M\,(\Delta r)} \end{aligned} \tag{4.8}$$

Case 3: θ Periodicity Condition Nodes For $j = 1, \ldots, M-1$ and $k = 0$

$$\nabla^2 u_{j,0} = \gamma_j\,u_{j+1,0} - \beta_j\,u_{j,0} + \alpha_j\,u_{j-1,0} + \varepsilon_j\,u_{j,1} + \varepsilon_j\,u_{j,N-1} \tag{4.9}$$

Case 4: Origin Node For $j = 0$

$$\nabla^2 u_0 = -\frac{4}{(\Delta r)^2}\,u_0 + \frac{2\Delta\theta}{\pi\,(\Delta r)^2}\sum_{k=0}^{N-1} u_{1,k} \tag{4.10}$$

We use the following lexicographical ordering of the nodes

$$\boldsymbol{U} = [u_0,\;\; u_{1,0},\;\; \ldots,\;\; u_{1,N-1},\;\; u_{2,0},\;\; \ldots,\;\; u_{M,N-1}]\,.$$

Consider the interior portion of the discretization matrix, i.e., Cases 1 and 3. We define the $N \times N$ matrices

$$T_j = \begin{pmatrix} -\beta_j & \varepsilon_j & 0 & \cdots & 0 & \varepsilon_j \\ \varepsilon_j & -\beta_j & \varepsilon_j & 0 & \cdots & 0 \\ 0 & \varepsilon_j & -\beta_j & \varepsilon_j & 0 & \vdots \\ \vdots & \ddots & \ddots & \ddots & \ddots & 0 \\ 0 & \cdots & 0 & \varepsilon_j & -\beta_j & \varepsilon_j \\ \varepsilon_j & 0 & \cdots & 0 & \varepsilon_j & -\beta_j \end{pmatrix}.$$

Let I be the $N \times N$ identity matrix and Θ be the $N \times N$ zero matrix. Then the interior portion of the matrix has the $(M-1)N \times (M-1)N$ form

$$\begin{pmatrix} T_1 & \gamma_1 I & \Theta & \cdots & \cdots & \Theta \\ \alpha_2 I & T_2 & \gamma_2 I & \Theta & \cdots & \vdots \\ \Theta & \alpha_3 I & T_3 & \gamma_3 I & \ddots & \vdots \\ \vdots & \ddots & \ddots & \ddots & \ddots & \Theta \\ \vdots & \cdots & \Theta & \alpha_{M-2} I & T_{M-2} & \gamma_{M-2} I \\ \Theta & \cdots & \cdots & \Theta & \alpha_{M-1} I & T_{M-1} \end{pmatrix}. \tag{4.11}$$

This matrix is appended with a first row and column to account for the u_0 node. We define

$$a = \tfrac{2}{\pi(\Delta r)^2} \qquad\qquad \alpha = -\tfrac{4}{(\Delta r)^2}$$

and $\mathbf{R} = [a, \cdots, a]$ to be an $1 \times N$ vector, $\mathbf{c} = [\alpha, \cdots, \alpha]$ to be an $N \times 1$ vector, and ϑ to be the $N \times 1$ zero vector. Thus the discretization matrix becomes

$$\begin{pmatrix} \alpha & \mathbf{R} & \vartheta^T & \cdots & \cdots & \cdots & \vartheta^T \\ \mathbf{c} & T_1 & \gamma_1 I & \Theta & \cdots & \cdots & \Theta \\ \vartheta & \alpha_2 I & T_2 & \gamma_2 I & \Theta & \cdots & \vdots \\ \vartheta & \Theta & \alpha_3 I & T_3 & \gamma_3 I & \Theta & \vdots \\ \vdots & \vdots & \ddots & \ddots & \ddots & \ddots & \vdots \\ \vdots & \vdots & \cdots & \Theta & \alpha_{M-2} I & T_{M-2} & \gamma_{M-2} I \\ \vartheta & \Theta & \cdots & \cdots & \Theta & \alpha_{M-1} I & T_{M-1} \end{pmatrix}.$$

Finally we add a last row and column to account for the boundary nodes. Define

$$\psi = \frac{2\,A\,r_{M+1/2}}{r_M\,(\Delta r)} - \gamma_M - \alpha_M - 2\,\varepsilon_M.$$

Further, we define the $N \times N$ matrix

$$\Psi = \begin{pmatrix} \psi & \varepsilon_M & 0 & \cdots & 0 & \varepsilon_M \\ \varepsilon_M & \psi & \varepsilon_M & 0 & \cdots & 0 \\ 0 & \varepsilon_M & \psi & \varepsilon_M & 0 & \vdots \\ \vdots & \ddots & \ddots & \ddots & \ddots & 0 \\ 0 & \cdots & 0 & \varepsilon_M & \psi & \varepsilon_M \\ \varepsilon_M & 0 & \cdots & 0 & \varepsilon_M & \psi \end{pmatrix}.$$

Thus, the discretization matrix becomes

$$D = \begin{pmatrix} \alpha & \mathbf{R} & \vartheta^T & \cdots & \cdots & \cdots & \cdots & \vartheta^T \\ \mathbf{c} & T_1 & \gamma_1 I & \Theta & \cdots & \cdots & \cdots & \Theta \\ \vartheta & \alpha_2 I & T_2 & \gamma_2 I & \Theta & \cdots & \vdots & \vdots \\ \vdots & \Theta & \alpha_3 I & T_3 & \gamma_3 I & \Theta & \vdots & \vdots \\ \vdots & \vdots & \ddots & \ddots & \ddots & \ddots & \ddots & \vdots \\ \vdots & \vdots & \cdots & \Theta & \alpha_{M-2} I & T_{M-2} & \gamma_{M-2} I & \Theta \\ \vdots & \vdots & \cdots & \cdots & \Theta & \alpha_{M-1} I & T_{M-1} & \gamma_{M-1} I \\ \vartheta & \Theta & \cdots & \cdots & \cdots & \Theta & (\gamma_M + \alpha_M) I & \Psi \end{pmatrix},$$

where

$$\alpha_j = \tfrac{r_{j-1/2}}{r_j\,(\Delta r)^2}, \qquad \gamma_j = \tfrac{r_{j+1/2}}{r_j\,(\Delta r)^2},$$

$$\varepsilon_j = \tfrac{1}{r_j^2\,(\Delta\theta)^2}, \qquad \beta_j = \gamma_j + \alpha_j + 2\,\varepsilon_j.$$

Note that the additional term in the boundary condition

$$\omega = \frac{2\,B\,r_{M+1/2}}{r_M\,(\Delta r)}$$

will be accounted for with an additional vector in the discretized Laplacian operator.

Since we have $(M-1)N+1$ nodes, the final discretization will have the form

$$\Delta u \approx D\boldsymbol{U} + \Omega$$

where Ω is an $(M-1)N+1 \times 1$ vector of the form

$$\Omega = \begin{pmatrix} 0 \\ \vdots \\ 0 \\ \omega \\ \vdots \\ \omega \end{pmatrix}$$

and the ω-segment has dimension $N \times 1$.

Matrix Operator Formulation

Formulating this discretization as a matrix operator will allow us to more easily apply alternating direction implicit methods. As an example of this operator formulation, we will consider the case where $M = 4$ and $N = 5$. The nodes are arranged as follows

$$U = \begin{pmatrix} u_o & u_o & u_o & u_o & u_o \\ u_{10} & u_{11} & u_{12} & u_{13} & u_{14} \\ u_{20} & u_{21} & u_{22} & u_{23} & u_{24} \\ u_{30} & u_{31} & u_{32} & u_{33} & u_{34} \\ u_{40} & u_{41} & u_{42} & u_{43} & u_{44} \end{pmatrix}.$$

The discretizations in the r and θ directions are developed separately. In the θ direction, this can be represented as

$$\underbrace{\frac{1}{(\Delta\theta)^2}\begin{pmatrix} 1 & 0 & 0 & 0 & 0 \\ 0 & 1/r_1^2 & 0 & 0 & 0 \\ 0 & 0 & 1/r_2^2 & 0 & 0 \\ 0 & 0 & 0 & 1/r_3^2 & 0 \\ 0 & 0 & 0 & 0 & 1/r_4^2 \end{pmatrix}}_{R_j} \cdot U \cdot \underbrace{\begin{pmatrix} -2 & 1 & 0 & 0 & 1 \\ 1 & -2 & 1 & 0 & 0 \\ 0 & 1 & -2 & 1 & 0 \\ 0 & 0 & 1 & -2 & 1 \\ 1 & 0 & 0 & 1 & -2 \end{pmatrix}}_{D_\theta}.$$

Therefore, the matrix representation of the θ-discretization is $R_j \cdot U \cdot D_\theta$. For the r-discretization, we have the following

$$\underbrace{\frac{1}{(\Delta r)^2}\begin{pmatrix} 0 & 0 & 0 & 0 & 0 \\ r_{\frac{1}{2}}/r_1 & -2 & r_{\frac{3}{2}}/r_1 & 0 & 0 \\ 0 & r_{\frac{3}{2}}/r_2 & -2 & r_{\frac{5}{2}}/r_2 & 0 \\ 0 & 0 & r_{\frac{5}{2}}/r_3 & -2 & r_{\frac{7}{2}}/r_3 \\ 0 & 0 & 0 & 2 & -2 \end{pmatrix}}_{D_r}.$$

For the Robin boundary condition, we have the following

$$\frac{\partial u}{\partial r} \approx \underbrace{\begin{pmatrix} 0 & 0 & 0 & 0 & 0 \\ 0 & 0 & 0 & 0 & 0 \\ 0 & 0 & 0 & 0 & 0 \\ 0 & 0 & 0 & 0 & 0 \\ \alpha & \alpha & \alpha & \alpha & \alpha \end{pmatrix}}_{A} \circ U + \underbrace{\begin{pmatrix} 0 & 0 & 0 & 0 & 0 \\ 0 & 0 & 0 & 0 & 0 \\ 0 & 0 & 0 & 0 & 0 \\ 0 & 0 & 0 & 0 & 0 \\ \beta & \beta & \beta & \beta & \beta \end{pmatrix}}_{B},$$

where

$$\alpha = \frac{2A\, r_{\frac{9}{2}}}{(\Delta r) r_4}, \qquad \beta = \frac{2B\, r_{\frac{9}{2}}}{(\Delta r) r_4},$$

and $\circ$ indicates the Hadamard product of matrices or element-wise multiplication. Thus, the r-discretization is given by

$$D_r \cdot U + A \circ U + B.$$

The discretization accounting for the singularity condition at the origin can be represented as

$$\underbrace{\frac{2\Delta\theta}{\pi\,(\Delta r)^2}\begin{pmatrix} -1 & 1 & 0 & 0 & 0 \\ 0 & 0 & 0 & 0 & 0 \\ 0 & 0 & 0 & 0 & 0 \\ 0 & 0 & 0 & 0 & 0 \\ 0 & 0 & 0 & 0 & 0 \end{pmatrix}}_{P} \cdot U \cdot \underbrace{\begin{pmatrix} 1 & 1 & 1 & 1 & 1 \\ 1 & 1 & 1 & 1 & 1 \\ 1 & 1 & 1 & 1 & 1 \\ 1 & 1 & 1 & 1 & 1 \\ 1 & 1 & 1 & 1 & 1 \end{pmatrix}}_{D_0}.$$

Thus, at the origin node, the matrix representation is given by $P \cdot U \cdot D_0$. Putting these three pieces together yields the matrix representation for the Laplacian operator in polar coordinates

$$\nabla^2 U = D_r\, U + R_j\, U\, D_\theta + P\, U\, D_0 + A \circ U + B$$

Returning to the model equations (2.15)-(2.21), we see that the reaction-diffusion equations for the electric potential and extracellular glucose have the form

$$U_t = D_r\, U + R_j\, U\, D_\theta + P\, U\, D_0 + A \circ U + B + f(U)$$

This system of equations can be expensive to solve numerically. Alternating Direction Implicit (ADI) methods will be employed to solve the system more economically.

Alternating Direction Implicit (ADI) Methods

In 1955, Peaceman and Rachford [4] published a new scheme that is a perturbation of the Crank-Nicolson scheme. For parabolic problems, the idea behind this Alternating Direction Implicit (ADI) scheme was to split each time step into two half time steps. Consider the parabolic problem

$$\frac{\partial u}{\partial t} = D\left(\frac{\partial^2 u}{\partial x^2} + \frac{\partial^2 u}{\partial y^2}\right). \tag{4.12}$$

For the first half time step, $t_{n+1/2}$, we replace the second derivative in x with a second order finite difference at $t_{n+1/2}$, leaving the second derivative in y at time t_n. This procedure is then repeated for the next half time step, t_{n+1}, on the second derivative

in y, leaving the second derivative in x at time $t_{n+1/2}$. The classical ADI method for (4.12) can be written as

$$\frac{u_{j,k}^{n+\frac{1}{2}} - u_{j,k}^{n}}{\frac{\Delta t}{2}} = D\left(\delta_x^2\, u_{j,k}^{n+\frac{1}{2}} + \delta_y^2\, u_{j,k}^{n}\right), \tag{4.13}$$

$$\frac{u_{j,k}^{n+1} - u_{j,k}^{n+\frac{1}{2}}}{\frac{\Delta t}{2}} = D\left(\delta_x^2\, u_{j,k}^{n+\frac{1}{2}} + \delta_y^2\, u_{j,k}^{n+1}\right), \tag{4.14}$$

where

$$u_{j,k}^{n} = u\left(x_j, y_k, t_n\right), \qquad x_j = j\Delta x, \quad y_k = k\Delta y, \quad t_n = n\Delta t,$$

$$\delta_x^2\, u_{j,k}^{n} = \frac{u_{j-1,k}^{n} - 2u_{j,k}^{n} + u_{j+1,k}^{n}}{\Delta x^2}.$$

Peaceman and Rachford [4] showed that this method was unconditionally stable even though each individual step is unstable. Furthermore, by the Lax Equivalence Theorem, the method is convergent for linear problems. They also showed that the method is second order accurate in time and space, not first order in time as one might expect. Details of these computations can be found in Appendix C.

We would like to apply ADI methods to our two-dimensional model of the pancreatic islet. However, the parabolic partial differential equations present in the islet model are nonlinear. This will require a modification to the above 'linear' ADI method. We discuss the necessary adjustments in the next section.

Nonlinear ADI Method

We consider the differential equation

$$u_t = D\left(u_{xx} + u_{yy}\right) + f(x, y, t, u) \quad (x, y, t) \in \Omega \times (0, T], \tag{4.15}$$

with initial condition

$$u(x, y, 0) = u_0(x, y) \quad \text{for} \quad (x, y) \in \Omega, \tag{4.16}$$

and Dirichlet boundary condition

$$u(x, y, t) = g(x, y, t) \quad \text{for} \quad (x, y, t) \in \partial\Omega \times (0, T]. \tag{4.17}$$

We require that f have a bounded first partial derivative in u:

$$\left|\frac{\partial f}{\partial u}\right| \leq \lambda,$$

and we further assume that $u_o(x, y)$, $g(x, y, t)$, and $f(x, y, t, u)$ are sufficiently smooth functions. In the case where $f(x, y, t, u)$ is a linear function of u, it suffices to add the term $f_{i,j}^{n+1/2}$ to the right-hand sides of (4.13) and (4.14). However, when f is a nonlinear function of u, we must modify the ADI method of Peaceman and Rachford. Amiri and Hosseini [6] suggest adding the terms f_1 and f_2 to the standard ADI method in (4.13) and (4.14):

$$\frac{u_{j,k}^{n+\frac{1}{2}} - u_{j,k}^{n}}{\frac{\Delta t}{2}} = D\left(\delta_x^2\, u_{j,k}^{n+\frac{1}{2}} + \delta_y^2\, u_{j,k}^{n}\right) + f_1, \tag{4.18}$$

$$\frac{u_{j,k}^{n+1} - u_{j,k}^{n+\frac{1}{2}}}{\frac{\Delta t}{2}} = D\left(\delta_x^2\, u_{j,k}^{n+\frac{1}{2}} + \delta_y^2\, u_{j,k}^{n+1}\right) + f_2. \tag{4.19}$$

We want to eliminate $u_{j,k}^{n+\frac{1}{2}}$ from (4.18) and (4.19). Subtracting (4.19) from (4.18) yields

$$\frac{u_{j,k}^{n+\frac{1}{2}} - u_{j,k}^{n}}{\frac{\Delta t}{2}} - \frac{u_{j,k}^{n+1} - u_{j,k}^{n+\frac{1}{2}}}{\frac{\Delta t}{2}} = D\left(\delta_y^2\, u_{j,k}^{n} - \delta_y^2\, u_{j,k}^{n+1}\right) + (f_1 - f_2), \tag{4.20}$$

$$2u_{j,k}^{n+\frac{1}{2}} = \left(u_{j,k}^{n+1} + u_{j,k}^{n}\right) + \frac{D\Delta t}{2}\left(\delta_y^2\, u_{j,k}^{n} - \delta_y^2\, u_{j,k}^{n+1}\right) + \frac{\Delta t}{2}(f_1 - f_2), \tag{4.21}$$

$$u_{j,k}^{n+\frac{1}{2}} = \frac{1}{2}\left(u_{j,k}^{n+1} + u_{j,k}^{n}\right) + \frac{D\Delta t}{4}\left(\delta_y^2\, u_{j,k}^{n} - \delta_y^2\, u_{j,k}^{n+1}\right) + \frac{\Delta t}{4}(f_1 - f_2). \tag{4.22}$$

Rewriting (4.19), we see that

$$u_{j,k}^{n+1} - u_{j,k}^{n+\frac{1}{2}} = \frac{D\Delta t}{2}\left(\delta_x^2\, u_{j,k}^{n+\frac{1}{2}} + \delta_y^2\, u_{j,k}^{n+1}\right) + \frac{\Delta t}{2} f_2. \tag{4.23}$$

Substituting (4.22) into (4.23) yields

$$u_{j,k}^{n+1} - \frac{1}{2}\left(u_{j,k}^{n+1} + u_{j,k}^{n}\right) - \frac{D\Delta t}{4}\left(\delta_y^2\, u_{j,k}^{n} - \delta_y^2\, u_{j,k}^{n+1}\right) - \frac{\Delta t}{4}(f_1 - f_2) = \frac{\Delta t}{2} f_2$$

$$+\frac{D\Delta t}{2}\left[\frac{\delta_x^2}{2}\left(u_{j,k}^{n+1} + u_{j,k}^{n}\right) + \frac{D\Delta t}{4}\left(\delta_x^2\,\delta_y^2\, u_{j,k}^{n} - \delta_x^2\,\delta_y^2\, u_{j,k}^{n+1}\right) + \frac{\Delta t}{4}\delta_x^2\,(f_1 - f_2) + \delta_y^2\, u_{j,k}^{n+1}\right].$$

After some simplification, we have the following finite difference equation

$$\frac{u_{j,k}^{n+1}-u_{j,k}^{n}}{k}-\frac{D}{2}\left(\delta_x^2+\delta_y^2\right)\left(u_{j,k}^{n+1}+u_{j,k}^{n}\right)+\frac{D^2\Delta t}{4}\delta_x^2\,\delta_y^2\left(\frac{u_{j,k}^{n+1}-u_{j,k}^{n}}{\Delta t}\right). \tag{4.24}$$

$$=\frac{1}{2}\left(f_1+f_2\right)+\frac{D\Delta t}{4}\delta_x^2\left(\frac{f_1-f_2}{k}\right)$$

Different selections of f_1 and f_2 have been introduced, but these methods have not necessarily been of high order for the case where $f(x,y,t,u)$ is nonlinear. By selecting

$$f_1=f_2=f\left(x_i,y_j,t_{n+\frac{1}{2}},\tilde{u}_{j,k}^{n+\frac{1}{2}}\right), \tag{4.25}$$

where $\tilde{u}_{j,k}^{n+\frac{1}{2}}$ is computed in the first step of the algorithm, yields an unconditionally stable method that is second order in time and space [6]. This new ADI method is summarized as follows:

New ADI Algorithm:

1. With the solution at time level t_n, solve the following equation for $\tilde{u}_{j,k}^{n+\frac{1}{2}}$:

$$\frac{\tilde{u}_{j,k}^{n+\frac{1}{2}} - u_{j,k}^{n}}{\frac{\Delta t}{2}} = \mu\left(\delta_x^2\,\tilde{u}_{j,k}^{n+\frac{1}{2}} + \delta_y^2\,u_{j,k}^{n}\right) + f\left(x_i, y_j, t_{n+\frac{1}{2}}, u_{j,k}^{n}\right).$$

2. Evaluate f_1 and f_2 by $f_1 = f_2 = f\left(x_i, y_j, t_{n+\frac{1}{2}}, \tilde{u}_{j,k}^{n+\frac{1}{2}}\right)$.

3. Obtain $u_{j,k}^{n+1}$ from the following equations:

$$\begin{aligned}\frac{u_{j,k}^{n+\frac{1}{2}} - u_{j,k}^{n}}{\frac{\Delta t}{2}} &= \mu\left(\delta_x^2\,u_{j,k}^{n+\frac{1}{2}} + \delta_y^2\,u_{j,k}^{n}\right) + f,\\ \\ \frac{u_{j,k}^{n+1} - u_{j,k}^{n+\frac{1}{2}}}{\frac{\Delta t}{2}} &= \mu\left(\delta_x^2\,u_{j,k}^{n+\frac{1}{2}} + \delta_y^2\,u_{j,k}^{n+1}\right) + f.\end{aligned}$$

Before proving the properties of this method, we need the following lemma:

Lemma 1. *At each point $(x_i, y_j) \in \Omega$, for ζ_0 and ζ_1 satisfying either*

$$(i)\quad \frac{D}{2}\left(\delta_x^2 + \delta_y^2\right)(\zeta_1 + \zeta_0) = \frac{\zeta_1 - \zeta_0}{\Delta t} + \frac{D^2\Delta t}{4}\delta_x^2\,\delta_y^2\,(\zeta_1 - \zeta_0) + e \qquad (4.26)$$

or

$$(ii)\quad \frac{D}{2}\left(\delta_x^2\,\zeta_1 + \delta_y^2\,\zeta_0\right) = \frac{\zeta_1 - \zeta_0}{\Delta t} + e \qquad (4.27)$$

with $\zeta_1 = \zeta_0 = 0$ on the boundary $\partial\Omega$, we have

$$\|\zeta_1\| \le \|\zeta_0\| + \Delta t\|e\|$$

where

$$\|\zeta\| = \left[h^2 \sum_{(x,y)\in\Omega} \zeta_{i,j}^n \right]^{\frac{1}{2}}$$

Proof. We prove Case (ii) here. The proof of Case (i) follows similarly and the details can be found in [6]. Let

$$\zeta_\nu = \sum_{p,q=1}^{N-1} c_{p,q}^\nu \sin(\pi p\, x) \sin(\pi q\, y), \tag{4.28}$$

$$e = \sum_{p,q=1}^{N-1} e_{p,q}^\nu \sin(\pi p\, x) \sin(\pi q\, y), \tag{4.29}$$

where $\nu = 0, 1$ and $N = \frac{1}{h}$. Consider how δ_x^2 and δ_y^2 operate on ζ_ν:

$$\delta_x^2 \zeta_\nu = \delta_x^2 \left(c_{p,q}^\nu \sin(\pi p\, x_i) \sin(\pi q\, y_j) \right),$$

$$= \frac{1}{h^2} \left[c_{p,q}^\nu \sin(\pi p\, x_{i-1}) \sin(\pi q\, y_j) - 2c_{p,q}^\nu \sin(\pi p\, x_i) \sin(\pi q\, y_j) + c_{p,q}^\nu \sin(\pi p\, x_{i+1}) \sin(\pi q y_j) \right],$$

$$= \frac{c_{p,q}^\nu}{h^2} \left[\sin(\pi p\, x_i - \pi p\, h) \sin \pi q\, y_j - 2 \sin \pi p\, x_i \sin \pi q\, y_j + \sin(\pi p\, x_i + \pi p\, h) \sin \pi q\, y_j \right].$$

Applying the sum and difference identities for sine and cosine and simplifying yields

$$\delta_x^2 \zeta_\nu = \frac{c_{p,q}^\nu}{h^2} \left[2 \sin \pi p\, x_i \cos \pi p\, h \sin \pi q\, y_j - 2 \sin \pi p\, x_i \sin \pi q\, y_j \right],$$

$$= \frac{2c_{p,q}^\nu}{h^2} \left[\sin \pi p\, x_i \sin \pi q\, y_j \left(\cos \pi p\, h - 1 \right) \right],$$

$$= -\frac{2}{h^2}\,\zeta_\nu\,(1-\cos\pi p\,h) = -\frac{2}{h^2}\,\zeta_\nu\cdot 2\sin^2\left(\frac{\pi p\,h}{2}\right),$$

$$= -\frac{4}{h^2}\sin^2\left(\frac{\pi p\,h}{2}\right)\zeta_\nu^n.$$

Similarly, it can be shown that

$$\delta_y^2\,\zeta_\nu = -\frac{4}{h^2}\sin^2\left(\frac{\pi q\,h}{2}\right)\zeta_\nu^n.$$

Let

$$E_p = \frac{2D\Delta t}{h^2}\sin^2\left(\frac{\pi p\,h}{2}\right), \qquad E_q = \frac{2D\Delta t}{h^2}\sin^2\left(\frac{\pi q\,h}{2}\right),$$

and substitute (4.28) and (4.29) into (4.27):

$$\frac{D}{2}\left(\delta_x^2\,\zeta_1 + \delta_y^2\,\zeta_0\right) = \frac{1}{\Delta t}\,(\zeta_1-\zeta_0) + e,$$

$$\frac{D}{2}\left[-\frac{4}{h^2}\sin^2\left(\frac{\pi p\,h}{2}\right)\zeta_1 - \frac{4}{h^2}\sin^2\left(\frac{\pi q\,h}{2}\right)\zeta_0\right] = \frac{1}{\Delta t}\,(\zeta_1-\zeta_0) + e,$$

$$-\frac{2D\Delta t}{h^2}\sin^2\left(\frac{\pi p\,h}{2}\right)\zeta_1 - \frac{2D\Delta t}{h^2}\sin^2\left(\frac{\pi q\,h}{2}\right)\zeta_0 = \zeta_1-\zeta_0+e\Delta t,$$

$$-E_p\zeta_1 - E_q\zeta_0 = \zeta_1-\zeta_0+e\Delta t,$$

$$(1+E_p)\,\zeta_1 = (1-E_q)\,\zeta_0 - e\Delta t.$$

Letting

$$M_1 = \frac{1 - E_q}{1 + E_p}, \qquad M_2 = -\frac{1}{1 + E_p},$$

we obtain

$$\zeta_1 = M_1\,\zeta_0 + M_2 e \Delta t.$$

For any time step Δt, we see that $\|M_1\| < 1$ and $\|M_2\| < 1$. Taking the discrete L_2 norm and using the triangle inequality yields

$$\begin{aligned} \|\zeta_1\| &= \|M_1\,\zeta_0\| + \Delta t\,\|M_2 e\|, \\ &\leq \|M_1\|\|\zeta_0\| + \Delta t \|M_2\|\|e\|, \\ &\leq \|\zeta_0\| + \Delta t \|e\|, \end{aligned}$$

where the last inequality results from the realization that $\|M_1\| < 1$ and $\|M_2\| < 1$. This completes the proof of the lemma. □

Amiri and Hosseini proved that this nonlinear ADI method was unconditionally stable and second order in time and space [6]. We include their proof of these properties for completeness:

Theorem 1. *Suppose the solution u of (4.15) with initial and boundary conditions (4.16) and (4.17) has bounded fourth order derivatives. Then the New ADI method is unconditionally stable and convergent, under the discrete L_2 norm, with discretization error $O\left(h^2 + k^2\right)$.*

Proof. Let U be the solution of (4.15) and let u represent the numerical approximation

to U. Further, let $\alpha = U - u$ be the discretization error. Since $f_1 = f_2$, the last term in (4.24) vanishes and applying this new method to (4.15), the local truncation error for the first step of the algorithm becomes

$$\begin{aligned} e_{i,j}^{n} &= \phi\left(x_i, y_j, t_{n+\frac{1}{2}}, U^{n+\frac{1}{2}}\right) - \phi\left(x_i, y_j, t_{n+\frac{1}{2}}, \tilde{u}^{n+\frac{1}{2}}\right) + O\left(h^2 + \Delta t^2\right), \\ &= O\left(\tilde{\alpha}_{i,j}^{n+\frac{1}{2}} + h^2 + \Delta t^2\right), \end{aligned} \tag{4.30}$$

where $\tilde{\alpha}^{n+\frac{1}{2}} = U^{n+\frac{1}{2}} - \tilde{u}^{n+\frac{1}{2}}$. From Lemma 1, Case (i), and (4.24), we have that

$$\|\alpha^{n+1}\| \leq \|\alpha^n\| + \|e^n\|\Delta t.$$

But using (4.30), we have that

$$\|\alpha^{n+1}\| \leq \|\alpha^n\| + \lambda\left(\|\tilde{\alpha}_{i,j}^{n+\frac{1}{2}}\| + \Delta t^2 + h^2\right)\Delta t. \tag{4.31}$$

From Step 1 in the New ADI Algorithm and Lemma 1, Case (ii), we have that

$$\|\tilde{\alpha}_{i,j}^{n+\frac{1}{2}}\| \leq \|\alpha^n\| + \|e^n\|\Delta t. \tag{4.32}$$

Substitution of (4.32) into (4.31) yields

$$\|\alpha^{n+1}\| \leq (1 + \Delta t\lambda)\|\alpha^n\| + \lambda(\Delta t^2 + h^2)\Delta t. \tag{4.33}$$

Proceeding with this recursion relationship yields

$$\|\alpha^{n+1}\| \leq (1 + \Delta t\lambda)^{n+1}\|\alpha^0\| + \lambda\Delta t(\Delta t^2 + h^2)\sum_{j=0}^{n}(1 + \Delta t\lambda)^j \tag{4.34}$$

Consider the series in the last term. Let $S_n = \sum_{j=0}^{n}(1+\Delta t\lambda)^j$. This can be easily summed to

$$S_n = \frac{1-(1+\Delta t\lambda)^{n+1}}{1-(1+\Delta t\lambda)} = \frac{(1+\Delta t\lambda)^{n+1}-1}{\Delta t\lambda}. \tag{4.35}$$

Returning to (4.34), we have that

$$\begin{aligned}
\|\alpha^{n+1}\| &\leq (1+\Delta t\lambda)^{n+1}\|\alpha^0\| + \lambda\Delta t(\Delta t^2+h^2)\sum_{j=0}^{n}(1+\Delta t\lambda)^j, && (4.36)\\
&= (1+\Delta t\lambda)^{n+1}\|\alpha^0\| + \lambda\Delta t(\Delta t^2+h^2)\left(\frac{(1+\Delta t\lambda)^{n+1}-1}{\Delta t\lambda}\right), && (4.37)\\
&= (1+\Delta t\lambda)^{n+1}\|\alpha^0\| + (\Delta t^2+h^2)\left[(1+\Delta t\lambda)^{n+1}-1\right]. && (4.38)
\end{aligned}$$

Since $(n+1)k \leq T$ and recalling the limit definition of e

$$e = \lim_{n\to\infty}\left(1+\frac{1}{n}\right)^n,$$

we have that

$$\begin{aligned}
(1+\Delta t\lambda)^{n+1} &\leq \left(1+\frac{T\lambda}{n+1}\right)^{n+1}, && (4.39)\\
& && (4.40)\\
&\leq e^{\lambda T}, && (4.41)
\end{aligned}$$

which gives

$$\|\alpha^{n+1}\| \leq e^{\lambda T}\|\alpha^0\| + (\Delta t^2+h^2)\left(e^{\lambda T}-1\right), \tag{4.42}$$

where λ is a constant independent of h and Δt. This completes the proof of the theorem. $\square$

Modifications for Polar Coordinates

Pancreatic islets are roughly circular and, as a result, we will think of a distribution of β-cells over the unit disk and use polar coordinates. Recall that in polar coordinates, the Laplacian operator is expressed as

$$\nabla^2 u = u_{rr} + \frac{1}{r}\, u_r + \frac{1}{r^2} u_{\theta\theta}.$$

As previously discussed, there is a singularity condition at the origin for which a control volume approach is used. Recall the matrix operator formulation for the discretization of the Laplacian

$$\nabla^2 U = D_r\, U + R_j\, U\, D_\theta + P\, U\, D_0 + A \circ U + B,$$

where $D_r\, U$ is the r-discretization matrix, $R_j\, U\, D_\theta$ is the θ-discretization matrix, $P\, U\, D_0$ represents the origin discretization accounting for the singularity, and $A \circ U + B$ contains the information for the boundary conditions. The partial differential equation now has the form

$$U_t = D_r\, U + R_j\, U\, D_\theta + P\, U\, D_0 + A \circ U + B + f(U),$$

where $f(U)$ is a nonlinear function of U. Modifications to the New ADI Algorithm must be made to handle the polar coordinates and the mixed boundary condition.

The algorithm has the following steps:

Polar ADI Algorithm:

1. Solve the following for $\tilde{u}_{i,j}^{n+\frac{1}{2}}$:

$$\frac{\tilde{u}_{i,j}^{n+\frac{1}{2}} - u_{i,j}^{n}}{k/2} = D_r\,\tilde{u}_{i,j}^{n+\frac{1}{2}} + A \circ \tilde{u}_{i,j}^{n+\frac{1}{2}} + R_j\,u_{i,j}^{n}\,D_\theta + P\,u_{i,j}^{n}\,D_o + B + f\left(r_i, \theta_j, u_{i,j}^{n}\right)$$

2. Solve the following for $u_{i,j}^{n+\frac{1}{2}}$ (differencing in r-direction):

$$\frac{u_{i,j}^{n+\frac{1}{2}} - u_{i,j}^{n}}{k/2} = D_r\,u_{i,j}^{n+\frac{1}{2}} + A \circ u_{i,j}^{n+\frac{1}{2}} + R_j\,u_{i,j}^{n}\,D_\theta + P\,u_{i,j}^{n}\,D_o + B + f\left(r_i, \theta_j, \tilde{u}_{i,j}^{n+\frac{1}{2}}\right)$$

3. Solve the following for $u_{i,j}^{n+1}$ (differencing in θ-direction & origin):

$$\frac{u_{i,j}^{n+1} - u_{i,j}^{n+\frac{1}{2}}}{k/2} = D_r\,u_{i,j}^{n+\frac{1}{2}} + A \circ u_{i,j}^{n+\frac{1}{2}} + R_j\,u_{i,j}^{n+1}\,D_\theta + P\,u_{i,j}^{n+1}\,D_o + B + f\left(r_i, \theta_j, \tilde{u}_{i,j}^{n+\frac{1}{2}}\right)$$

Test Problem

This modified nonlinear ADI method of Amiri and Hosseini was tested on the following reaction diffusion equation in polar coordinates:

$$\begin{aligned} u_t &= \nabla^2 u - 2u, \\ \frac{\partial u}{\partial r}(t, 1, \theta) &= -u(t, 1, \theta), \\ u(0, r, \theta) &= J_1\left(\sqrt{k^2 - 1}\,r\right)\cos\theta, \end{aligned}$$

where $J_1(kr)$ is the Bessel function of the first kind and $k \approx 2.604$ so that the mixed boundary condition is satisfied with $A = -1$ and $B = 0$. The exact solution to this

partial differential equation is given by

$$u(t, r, \theta) = e^{-\left(k^2+1\right)t} J_1\left(\sqrt{k^2-1}\, r\right) \cos\theta.$$

The results of the test problem are shown in Figure 33. We can see that there is good agreement between the numerical method and the exact solution of the partial differential equation.

2D Islet Model Simulations

The 2D model of a pancreatic islet is simulated by the method of lines using the nonlinear ADI method for the two reaction-diffusion terms. Recall the model equations:

$$\frac{\partial u}{\partial \tau} = \nabla^2 u - I_{ion}(u, w, z, cr, ci, ge, gi), \tag{4.43}$$

$$\frac{dw}{d\tau} = \lambda_2 \left(n_\infty(u) - w\right), \tag{4.44}$$

$$\frac{dz}{d\tau} = \lambda_3 \left(s_\infty(u) - z\right), \tag{4.45}$$

$$\frac{dcr}{d\tau} = \alpha_1 \frac{ci^2}{ci^2 + \delta_2^2} - \alpha_2 \left(cr - \alpha_3\, ci\right), \tag{4.46}$$

$$\frac{dci}{d\tau} = -\delta_1\, \gamma_{Ca}\, m_\infty(u) \left(u - u_{Ca}\right) - \delta_3 ci + \delta_4 (cr - \alpha_3\, ci) - \delta_5 \frac{ci^2}{ci^2 + \delta_2^2}, \tag{4.47}$$

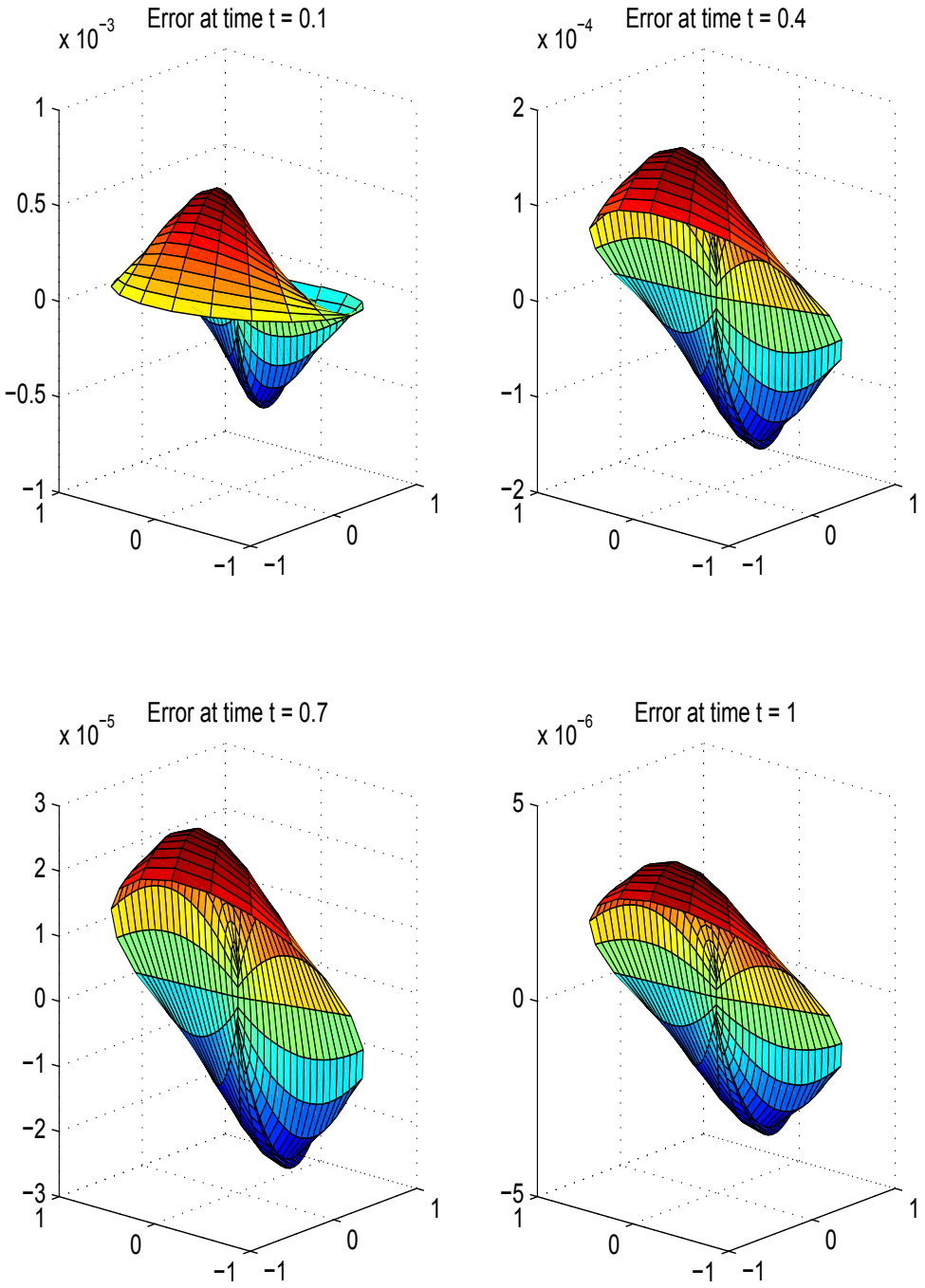

Figure 33: Error plots for test problem with discretization $dr = 1/16$ and $d\theta = 2\pi/20$. The time step was taken as $dt = 0.001$.

$$\frac{\partial ge}{\partial \tau} = \Delta_2 \nabla^2 ge - \frac{\lambda_1 \alpha_4}{\rho} \frac{ge - gi}{(ge + \alpha_4)(gi + \alpha_4)}, \tag{4.48}$$

$$\frac{\partial gi}{\partial \tau} = \lambda_1 \alpha_4 \frac{ge - gi}{(ge + \alpha_4)(gi + \alpha_4)}. \tag{4.49}$$

We want to consider the situation where different percentages of the boundary of the islet are exposed to glucose to observe how this affects the speed of the wave propagating through the islet. To do this, we will start at the steady state initial conditions of the system and apply an influx of glucose along the boundary. From (4.49), we can see that for the system to be at steady state requires that $ge = gi$. We selected a value for these glucose levels to be 0.35. Similarly, from (4.44) and (4.45), the steady state is located at $w = n_\infty(u)$ and $z = s_\infty(u)$. Looking at (4.46), we see that setting

$$\frac{dcr}{d\tau} = \alpha_1 \frac{ci^2}{ci^2 + \delta_2^2} - \alpha_2 \, (cr - \alpha_3 \, ci) = 0$$

implies that

$$\alpha_2 \, cr = \alpha_1 \frac{ci^2}{ci^2 + \delta_2^2} + \alpha_2 \, \alpha_3 \, ci,$$

$$cr = \frac{\alpha_1}{\alpha_2} \frac{ci^2}{ci^2 + \delta_2^2} + \alpha_3 \, ci.$$

Considering the intracellular calcium concentration equation (4.47), we set

$$\frac{dci}{dt} = -\delta_1 \, \gamma_{Ca} \, m_\infty(u) \, (u - u_{Ca}) - \delta_3 ci + \delta_4 (cr - \alpha_3 \, ci) - \delta_5 \frac{ci^2}{ci^2 + \delta_2^2} = 0.$$

However, note that at steady state

$$\begin{aligned}\delta_4\,(cr-\alpha_3\,ci)-\delta_5\,\frac{ci^2}{ci^2+\delta_2^2} &= \delta_4\left(\frac{\alpha_1}{\alpha_2}\frac{ci^2}{ci^2+\delta_2^2}+\alpha_3\,ci-\alpha_3\,ci\right)-\delta_5\,\frac{ci^2}{ci^2+\delta_2^2},\\ &= \delta_4\frac{\alpha_1}{\alpha_2}\frac{ci^2}{ci^2+\delta_2^2}-\delta_5\,\frac{ci^2}{ci^2+\delta_2^2}=0,\end{aligned}$$

since

$$\delta_4\,\frac{\alpha_1}{\alpha_2}=\delta_5.$$

Thus, we have that

$$-\delta_1\,\gamma_{Ca}\,m_\infty(u)\;(u-u_{Ca})-\delta_3\,ci=0,$$

which implies that

$$ci=-\frac{\delta_1}{\delta_3}\,\gamma_{Ca}\,m_\infty(u)\,(u-u_{Ca})\,.$$

Using the values $ge = gi = 0.35$, we have the following set of steady state initial conditions

$$\begin{aligned}u(r,\theta,0) &= -0.7665189111,\\ w(r,\theta,0) &= 0.0006055695,\\ z(r,\theta,0) &= 0.2501559065,\\ ci(r,\theta,0) &= 0.1303081901,\\ cr(r,\theta,0) &= 1.157647811.\end{aligned}$$

Using these initial conditions, we expose different percentages of the boundary of the islet to glucose and observe how this affects the speed of the wave propagating through the islet. In Figure 34, we show a series of snapshots of the wave moving through the pancreatic islet in the case of 25% of the boundary being exposed to glucose. While this representation of the wave is simpler to visualize, it is easier to measure the wave speed if we consider a ray through the unit disk and project into the $t - r$ plane, as shown in Figure 35. We estimate the time that it takes for the wave to reach the center of the islet to be $\tau = 0.019$.

For 12.5%, 50%, 100% percentages of the islet boundary exposed to glucose, we carry out the same simulation. The ray projections for these cases as well as for the 25% boundary case are shown in Figure 36. In dimensionless time, we estimate the time for the wave to reach the islet center. We also estimate the duration of the bursting cycle in each of these case. These values are shown in Table 5. Note

Portion of Boundary	Time to Islet Center	Time of Burst Cycle
12.5%	0.0265	0.333
25%	0.019	0.351
50%	0.018	0.337
100%	0.0255	0.318

Table 5: Propagation times for various portions of the boundary exposed to glucose. The spatial gridsize was $dr = 1/32$ and $d\theta = 2\pi/40$. The time step was $dt = 0.0001$.

that there is a different behavior at the end of the burst cycle in the case of 12.5%

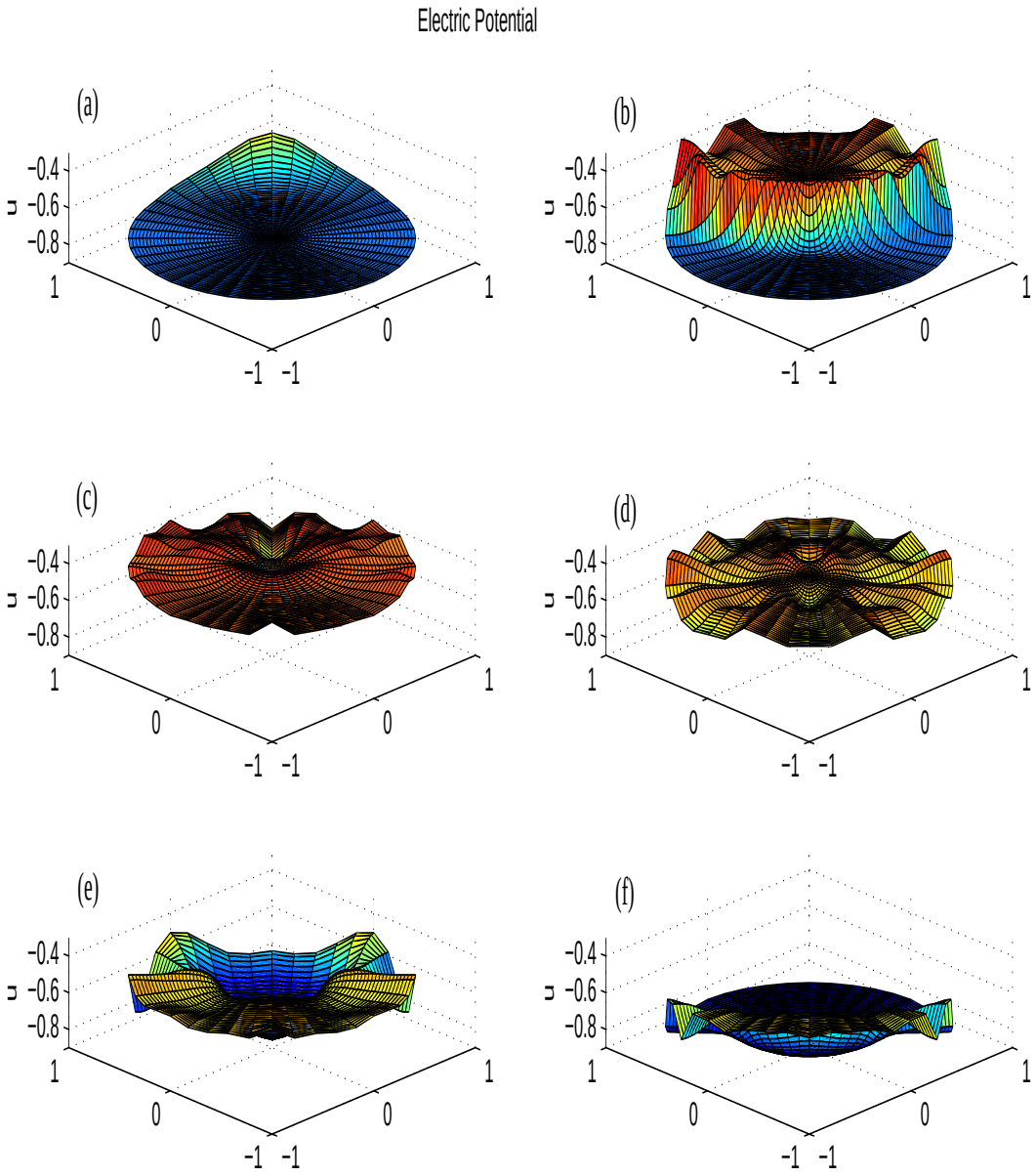

Figure 34: Simulation of wave propagating through islet with 1/4 of the boundary exposed to glucose. Reading from left to right, the snapshots are at times (a) $\tau = 0.1370$, (b) $\tau = 0.1745$, (c) $\tau = 0.2495$, (d) $\tau = 0.3495$, (e) $\tau = 0.4945$, and (f) $\tau = 0.5045$.

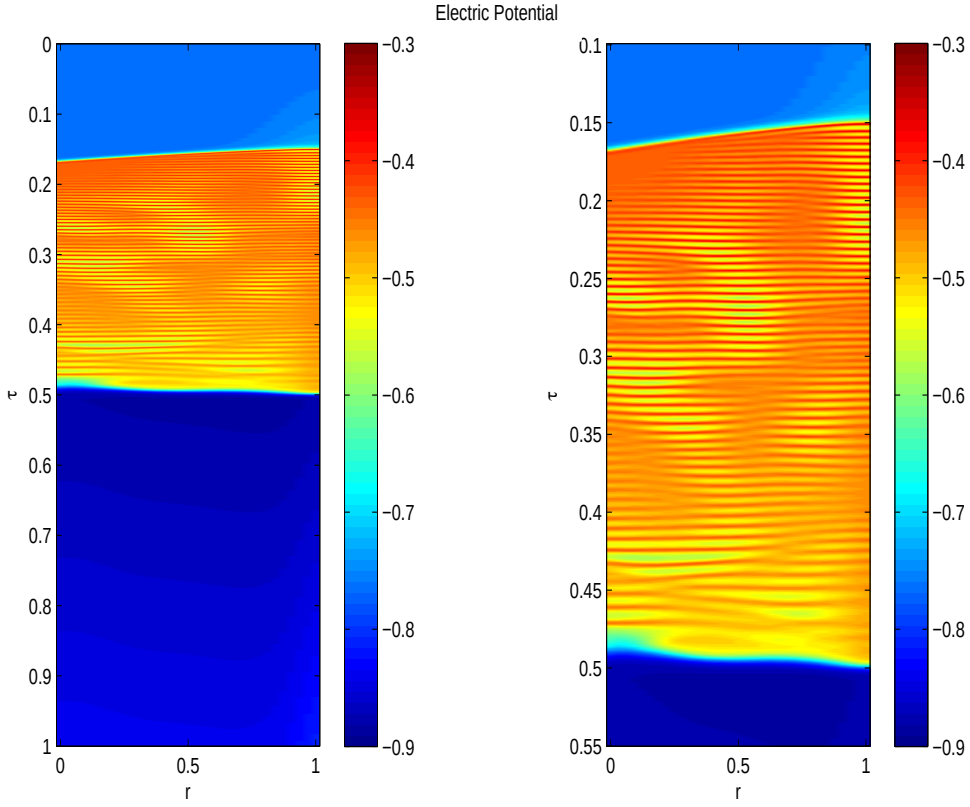

Figure 35: Ray through $\theta = 0$ with 1/4 of the boundary exposed to glucose. In the right figure, we have zoomed in on the wave to better estimate the wave speed.

of the boundary being exposed. This made it difficult to estimate the propagation times. As a result, the end of the burst cycle was taken to be the time at which there was no oscillatory behavior throughout the islet. This may account for the seemingly erroneous value for the time of the burst cycle. There appears to be a correlation between the percentage of the islet boundary exposed to glucose and the duration of the burst cycle, i.e., the more of the islet boundary that is exposed the shorter the burst cycle. This relationship is logical since the larger the portion of the boundary

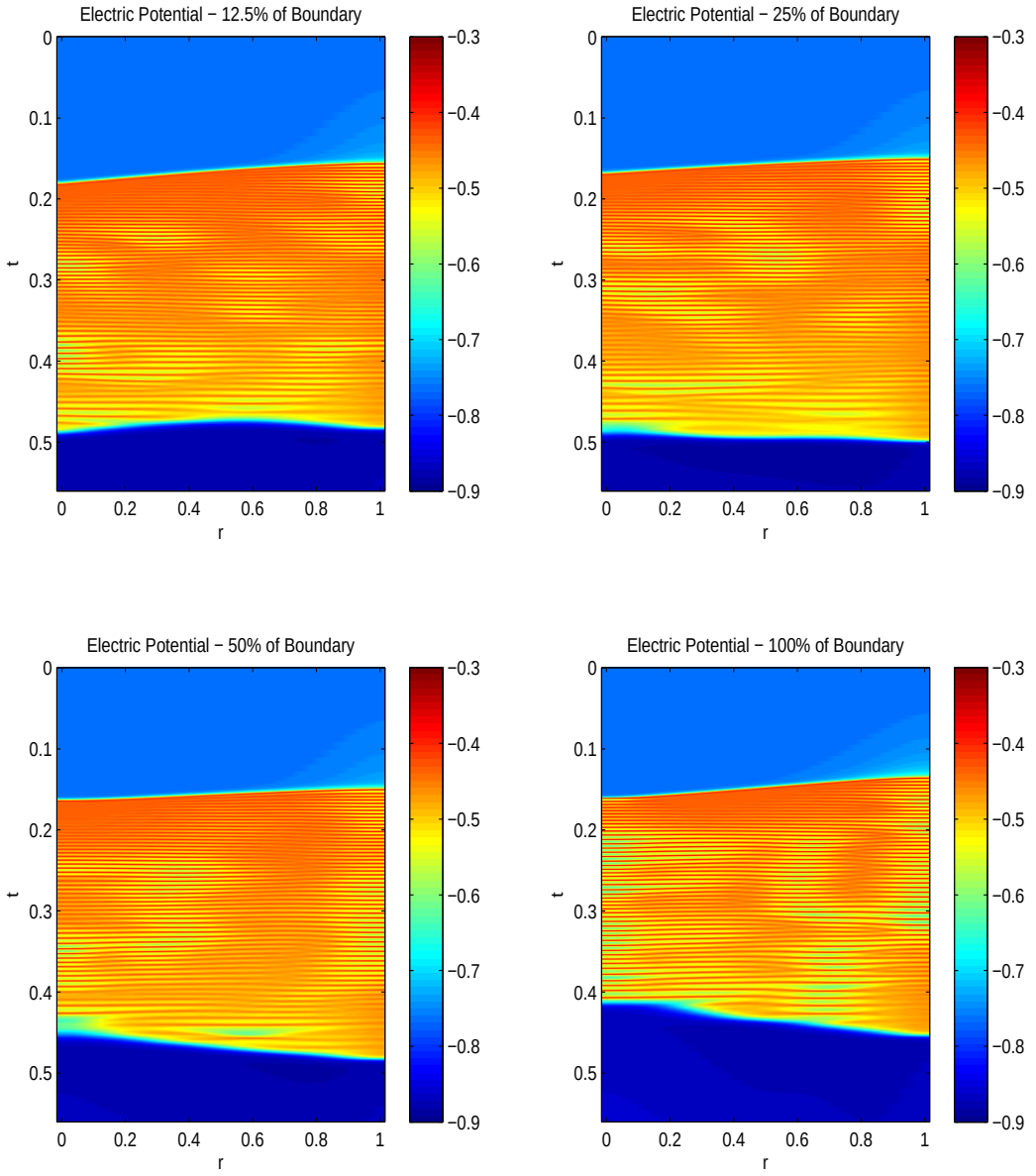

Figure 36: Rays through $\theta = 0$ with various portions of the boundary exposed to glucose.

exposed to glucose, the more β-cells will be exposed to the glucose concentration. As a result, the cascade of electrical activity will initiate over a larger range of boundary cells and cause the wave to propagate into the islet more quickly.

CHAPTER 5

DISCUSSION AND CONCLUSIONS

From the experiments of Aslanidi et. al. [1], waves of electrical activity have been observed propagating through pancreatic islets of Langerhans in response to a glucose stimulation. When glucose is transported inside a β-cell, a cascade occurs that initiates electrical activity. The glucose is metabolized to produce ATP which increases the ratio of ATP to ADP. The increase in the ATP concentration inactivates the K(ATP) channels in the cell membrane. As a result, we would anticipate a relationship between the speed of these waves of electrical activity and the conductance of the K(ATP) channel.

Using a robust model of a pancreatic islet proposed in [30], which combines the models of Sherman [21] and Bertram and Pernarowski [2], we have simulated these waves of activity. After a systematic reduction of the model equations and a conversion to traveling coordinates, the relationship between the wave speed and the model parameters was investigated. Traveling wave fronts and pulses were observed in the reduced model. Two different reductions were considered. The kinetic variables were set to their stationary values and the presence of a traveling wave front or heteroclinic orbit was observed. A relationship between the wave speed and the conductance of the ATP-modulated potassium channel was constructed. When the

slow gating variable was included in the reduced model, a homoclinic connection or traveling wave pulse was present. The homoclinic orbit was approximated by a high period periodic orbit and a similar relationship between the conductance and wave speed was determined. It was also observed that the heteroclinic connection is a good approximation for a portion of the homoclinic connection for equilibrium on the left branch of the nullcline.

For a more realistic biological comparison, the length of the interval or period was shortened. Comparisons of the speed of the wave traveling through the islet in the partial differential equation model and the model in traveling coordinates were done. There were significant differences in the wave speeds between these two models. Since the true wave speed is only being computed for the traveling coordinate system, we hypothesize that these values for the speed would be more accurate biophysically.

As pancreatic islets are roughly circular, a two-dimensional model of an islet on the unit disk was also simulated. Alternating direction implicit (ADI) methods were used for these simulations. Because the model equations are nonlinear, a modified ADI method for nonlinear parabolic differential equations proposed by [6] was adapted for polar coordinates and Robin boundary conditions. A series of simulations were done increasing the percentage of the boundary of the islet that was exposed to the glucose bath. We observed that the larger the portion of the boundary exposed to glucose, the more rapidly the electrical wave activity reached the interior of the islet. This is reasonable because of the electrical coupling of the β-cells. The more cells

on the boundary that are exposed to the glucose stimulation, the more cells in the interior that are coupled to them. The boundary cells will pull the interior cells into an excited state.

APPENDICES

APPENDIX A

DIMENSIONAL ISLET MODEL EQUATIONS AND PARAMETERS

Dimensional Islet Model Equations

Islet Model Equations:

$$\frac{\partial V}{\partial t} = D\left(\nabla^2 V\right) - \frac{1}{C} I_{ion}\left(V, n, s, Ca, Ca_{er}, Ge, Gi\right)$$

$$\frac{dn}{dt} = \frac{n_\infty(V) - n}{\tau_n}$$

$$\frac{ds}{dt} = \frac{s_\infty(V) - s}{\tau_s}$$

$$\frac{dCa}{dt} = f\left(\alpha\, I_{Ca}(V) - k_c Ca\right) + \left(J_{out} - J_{in}\right)$$

$$\frac{dCa_{er}}{dt} = \frac{1}{\sigma}\left(J_{in} - J_{out}\right)$$

$$\frac{\partial Ge}{\partial t} = p\, D_g\left(\nabla^2 Ge\right) - \frac{1}{\rho} F(Ge, Gi)$$

$$\frac{\partial Gi}{\partial t} = F(Ge, Gi)$$

Ionic Current Functions:

$$I_{ion} = I_s(V,s) + I_{Ca}(V) + I_k(V,n) + I_{KATP}(V,Gi) + I_{KCa}(V,Ca) + I_{CRAC}\,(V,Ca_{er})$$

$$I_s(V,s) = \bar{g}_s\, s\ (V - V_K)$$

$$I_{Ca}(V) = \bar{g}_{Ca} \cdot m_\infty(V) \cdot (V - V_{Ca})$$

$$I_K(V,n) = \bar{g}_K\, n\ (V - V_K)$$

$$I_{KATP}(V,Gi) = g_{K(ATP)}(Gi) \cdot (V - V_K)$$

$$I_{K(Ca)}(V,Ca) = \left(\frac{Ca^5}{Ca^5 + k_d^5}\right)(V - V_K)$$

$$I_{CRAC}\,(V,Ca_{er}) = \bar{g}_{CRAC} \cdot z_\infty\,(Ca_{er}) \cdot (V - V_{CRAC})$$

Gating Variable Functions:

$$m_\infty(V) = \frac{1}{1+exp(-(V-V_m)/s_m)} \qquad s_\infty(V) = \frac{1}{1+exp(-(V-V_s)/s_s)}$$

$$n_\infty(V) = \frac{1}{1+exp(-(V-V_n)/s_n)} \qquad z_\infty\,(Ca_{er}) = \frac{1}{1+exp((Ca_{er}-\overline{Ca_{er}})/s_z)}$$

Endoplasmic Reticulum Flux Functions:

$$J_{in}(Ca) = \frac{\nu_p}{\mu}\frac{Ca^2}{Ca^2+k_p^2} \qquad J_{out}\,(Ca,Ca_{er}) = \frac{1}{\mu}\,(p_l + p_{ip3})\,(Ca_{er} - Ca)$$

Glucose System Functions:

$$F(Ge,Gi) = V_{max}\frac{K_m(Ge-Gi)}{(K_m+Ge)(K_m+Gi)}$$

$$g_{K(ATP)}(Gi) = \bar{g}^{(o)}_{K(ATP)} + \bar{g}^{(c)}_{K(ATP)} \cdot h(Gi) \qquad h(Gi) = \frac{1}{1+exp((Gi-G_{th})/s_g)}$$

Dimensional Islet Model Parameters

Parameter	Value	Parameter	Value
a	200 μm	s_m	12 mV
d	10 μm	τ_s	20000 msec
C	5300 fF	τ_n	20 msec
g_c	100 pS	f	0.01
$\bar{g}_s$	200 pS	α	-4.5×10^{-6} $\frac{\mu\text{M}}{\text{fA msec}}$
$\bar{g}_{Ca}$	1000 pS	k_c	0.2 $\frac{1}{\text{msec}}$
$\bar{g}_k$	2700 pS	μ	250 msec
$\bar{g}_{KCa}$	1000 pS	σ	5
$\bar{g}_{CRAC}$	40 pS	$\overline{Ca_{er}}$	4 μM
V_k	-75 mV	s_c	1 μM
V_{ca}	25 mV	ν_p	0.24 μM
V_{CRAC}	-30 mV	k_p	0.1 μM
V_s	-52 mV	k_d	0.6 μM
V_n	-16 mV	p_l	0.02
V_m	-20 mV	p_{ip3}	0
s_s	5 mV	s_g	1 mM
s_n	5.6 mV	$D = \frac{g_c d^2}{C}$	1.8868 $\frac{\mu m^2}{\text{msec}}$
D_g	673 $\frac{\mu\text{m}^2}{\text{sec}}$	k	0.1 $\frac{1}{\mu\text{m}}$
p	0.3	G	11 mM
ρ	0.01	$\bar{g}^{(o)}_{KATP}$	85 pS
K_m	17 mM	$\bar{g}^{(c)}_{KATP}$	110 pS
V_{max}	0.53 $\frac{\text{mM}}{sec}$	G_{th}	5 mM

APPENDIX B

NONDIMENSIONAL ISLET MODEL EQUATIONS AND PARAMETERS

Nondimensional Islet Model Equations

Islet Model Equations:

$$\frac{\partial u}{\partial \tau} = \nabla^2 u - i_{ion}(u, w, z, cr, ci, ge, gi)$$

$$\frac{dw}{d\tau} = \lambda_2 \, (n_\infty(u) - w)$$

$$\frac{dz}{d\tau} = \lambda_3 \, (s_\infty(u) - z)$$

$$\frac{dcr}{d\tau} = \alpha_1 \frac{ci^2}{ci^2 + \delta_2^2} - \alpha_2 \, (cr - \alpha_3 \, ci)$$

$$\frac{dci}{d\tau} = -\delta_1 \, \gamma_{Ca} \, m_\infty(u) \, (u - u_{Ca}) - \delta_3 ci + \delta_4 (cr - \alpha_3 \, ci) - \delta_5 \frac{ci^2}{ci^2 + \delta_2^2}$$

$$\frac{\partial ge}{\partial \tau} = \Delta_2 \, \nabla^2 ge - \frac{\lambda_1 \, \alpha_4}{\rho} \frac{ge - gi}{(ge + \alpha_4)(gi + \alpha_4)}$$

$$\frac{\partial gi}{\partial \tau} = \lambda_1 \, \alpha_4 \frac{ge - gi}{(ge + \alpha_4)(gi + \alpha_4)}$$

Ionic Current Functions:

$$i_{ion} = i_s(u,z) + i_{Ca}(u) + i_k(u,w) + i_{KATP}(u,ge) + i_{KCa}(u,ci) + i_{CRAC}\,(u,cr)$$

$$i_s(u,z) = \gamma_s\, z\,(u+1)$$

$$i_{Ca}(u) = \gamma_{Ca} \cdot m_\infty(u) \cdot (u - u_{Ca})$$

$$i_K(u,w) = \gamma_K\, w\,(u+1)$$

$$i_{KATP}(u,gi) = \tfrac{a^2}{CD} \cdot g_{K(ATP)}(gi) \cdot (u+1)$$

$$i_{K(Ca)}(u,ci) = \gamma_{KCa}\left(\tfrac{ci^5}{ci^5+1}\right)(u+1)$$

$$i_{CRAC}(u,cr) = \gamma_{CRAC} \cdot z_\infty(cr) \cdot (u + u_{CRAC})$$

Gating Variable Functions:

$$m_\infty(u) = \tfrac{1}{1+exp(-(uV_K+V_m)/s_m)} \qquad s_\infty(u) = \tfrac{1}{1+exp(uV_K+V_s)/s_s)}$$

$$n_\infty(u) = \tfrac{1}{1+exp(uV_K+V_n)/s_n)} \qquad z_\infty(cr) = \tfrac{1}{1+exp\left(\frac{\overline{Ca_{er}}}{s_z}(cr-1)\right)}$$

Endoplasmic Reticulum Flux Functions:

$$j_{in}(ci) = \tfrac{\nu_p}{\mu}\tfrac{ci^2}{ci^2+\delta_2^2} \qquad j_{out}(ci,cr) = \tfrac{\overline{Ca_{er}}}{\mu}(p_l + p_{ip3})(cr - \alpha_3 ci)$$

Glucose System Functions:

$$\hat{f}(ge,gi) = V_{max}\,\alpha_4\,\tfrac{ge-gi}{(ge+\alpha_4)(gi+\alpha_4)}$$

$$g_{K(ATP)}(gi) = \bar{g}^{(o)}_{K(ATP)} + \bar{g}^{(c)}_{K(ATP)} \cdot h(gi) \qquad h(gi) = \tfrac{1}{1+exp(Ggi-G_{th})/s_g)}$$

Nondimensional Islet Model Parameters

Parameter	Value	Parameter	Value
$u_{Ca} = -\frac{V_{Ca}}{V_K}$	$\frac{1}{3}$	$u_{CRAC} = \frac{V_{CRAC}}{V_K}$	0.4
$\gamma_s = \frac{\bar{g}_s a^2}{CD}$	800	$\gamma_K = \frac{\bar{g}_K a^2}{CD}$	10800
$\gamma_{Ca} = \frac{\bar{g}_{Ca} a^2}{CD}$	4000	$\gamma_{KCa} = \frac{\bar{g}_{KCa} a^2}{CD}$	4000
$\gamma_{CRAC} = \frac{\bar{g}_{CRAC} a^2}{CD}$	160	$\lambda_1 = \mathbb{T}_u \frac{a^2 V_{max}}{DG}$	1.02145
$\lambda_2 = \frac{a^2}{D\tau_n}$	1060	$\lambda_3 = \frac{a^2}{D\tau_s}$	1.06
$\delta_1 = \frac{\alpha f C V_K}{k_d}$	0.029813	$\delta_2 = \frac{k_p}{k_d}$	$\frac{1}{6}$
$\delta_3 = \frac{f a^2 k_c}{D}$	42.4	$\delta_4 = \frac{a^2 (p_l + p_{ipi3}) \overline{Ca_{er}}}{k_d D \mu}$	11.3067
$\delta_5 = \frac{a^2 \nu_p}{k_d D \mu}$	33.92	$\alpha_1 = \frac{a^2 \nu_p}{\sigma D \mu \overline{Ca_{er}}}$	1.0176
$\alpha_2 = \frac{a^2 (p_l + p_{ip3})}{\sigma D \mu}$	0.3392	$\alpha_3 = \frac{k_d}{\overline{Ca_{er}}}$	0.15
$\alpha_4 = \frac{K_m}{G}$	1.54545	$\Delta_2 = \mathbb{T}_u \frac{p D_g}{D}$	0.107007

APPENDIX C

ANALYSIS OF THE LINEAR ADI METHOD

Order of Accuracy of the Linear ADI Method

We prove the order of accuracy of the method following [48]. Letting

$$r_x = \frac{\mu \Delta t}{\Delta x^2}, \qquad r_y = \frac{\mu \Delta t}{\Delta y^2},$$

we can rewrite (4.13)-(4.14) as

$$\left(1 - \frac{r_x}{2}\delta_x^2\right) u_{j,k}^{n+\frac{1}{2}} = \left(1 + \frac{r_y}{2}\delta_y^2\right) u_{j,k}^{n}, \tag{5.1}$$

$$\left(1 - \frac{r_y}{2}\delta_y^2\right) u_{j,k}^{n+1} = \left(1 + \frac{r_x}{2}\delta_x^2\right) u_{j,k}^{n+\frac{1}{2}}. \tag{5.2}$$

Taking (5.1) and operating on both sides by $\left(1 + \frac{r_x}{2}\delta_x^2\right)$ yields

$$\left(1 + \frac{r_x}{2}\delta_x^2\right)\left(1 - \frac{r_x}{2}\delta_x^2\right) u_{j,k}^{n+\frac{1}{2}} = \left(1 + \frac{r_x}{2}\delta_x^2\right)\left(1 + \frac{r_y}{2}\delta_y^2\right) u_{j,k}^{n}. \tag{5.3}$$

Noting that the operators on the left hand side commute, we can rewrite (5.3) as

$$\left(1 - \frac{r_x}{2}\delta_x^2\right) \underbrace{\left(1 + \frac{r_x}{2}\delta_x^2\right) u_{j,k}^{n+\frac{1}{2}}} = \left(1 + \frac{r_x}{2}\delta_x^2\right)\left(1 + \frac{r_y}{2}\delta_y^2\right) u_{j,k}^{n}. \tag{5.4}$$

We can use (5.2) to eliminate the indicated $u_{j,k}^{n+\frac{1}{2}}$ term in (5.4) and write the scheme as

$$\left(1 - \frac{r_x}{2}\delta_x^2\right)\left(1 - \frac{r_y}{2}\delta_y^2\right) u_{j,k}^{n+1} = \left(1 + \frac{r_x}{2}\delta_x^2\right)\left(1 + \frac{r_y}{2}\delta_y^2\right) u_{j,k}^{n}. \tag{5.5}$$

We expand the terms in (5.5)

$$u_{j,k}^{n+1} - \frac{r_y}{2}\delta_y^2\, u_{j,k}^{n+1} - \frac{r_x}{2}\delta_x^2\, u_{j,k}^{n+1} + \frac{r_x r_y}{4}\delta_x^2\,\delta_y^2\, u_{j,k}^{n+1} =$$
$$u_{j,k}^{n} + \frac{r_y}{2}\delta_x^2\, u_{j,k}^{n} + \frac{r_x}{2}\delta_x^2\, u_{j,k}^{n} + \frac{r_x r_y}{4}\delta_x^2\,\delta_y^2\, u_{j,k}^{n},$$

$$u_{j,k}^{n+1} - u_{j,k}^{n} = \frac{r_x}{2}\delta_x^2 \left(u_{j,k}^{n+1} + u_{j,k}^{n}\right) + \frac{r_y}{2}\delta_y^2 \left(u_{j,k}^{n+1} + u_{j,k}^{n}\right) - \frac{r_x r_y}{4}\delta_x^2\,\delta_y^2 \left(u_{j,k}^{n+1} - u_{j,k}^{n}\right),$$

and observe that the ADI scheme of Peaceman and Rachford can be expressed as

$$\frac{u_{j,k}^{n+1} - u_{j,k}^{n}}{\Delta t} = \frac{\mu}{2}\left(\frac{\delta_x^2}{\Delta x^2} + \frac{\delta_y^2}{\Delta y^2}\right)\left(u_{j,k}^{n+1} + u_{j,k}^{n}\right) - \frac{\mu\Delta t}{4}\frac{\delta_x^2}{\Delta x^2}\frac{\delta_y^2}{\Delta y^2}\left(u_{j,k}^{n+1} - u_{j,k}^{n}\right). \quad (5.6)$$

Expressing the ADI scheme in this form makes it clear that this two-step method is a perturbation of the two dimensional Crank-Nicolson scheme; the perturbation being the last term in (5.6). We know that the two dimensional Crank-Nicolson scheme is second order accurate in Δt, Δx, and Δy, so we only need to analyze the last term. Recall the following

$$\delta_x^2\, u_{j,k} = \Delta x^2 \frac{\partial^2 u}{\partial x^2} + \frac{1}{12}\Delta x^4 \frac{\partial^4 u}{\partial x^4} + O\left(\Delta x^6\right),$$

$$\delta_x^2\, u_{j,k}^{n+1} = \delta_x^2\, u_{j,k} + \Delta t \frac{\partial}{\partial t}\delta_x^2\, u_{j,k} + O\left(\Delta t^2\right).$$

Thus, we have

$$\begin{aligned}
\delta_y^2 \left(u_{j,k}^{n+1} - u_{j,k}\right) &= \Delta t \frac{\partial}{\partial t}\delta_y^2\, u_{j,k} + O\left(\Delta t^2\right), \\
&= \Delta t\left[\Delta y^2\, u_{tyy} + \frac{1}{12}\Delta y^4\, u_{tyyyy} + O\left(\Delta y^6\right)\right] + O\left(\Delta t^2\right), \\
&= \Delta t\,\Delta y^2\, u_{tyy} + \frac{1}{12}\Delta t\,\Delta y^4\, u_{tyyyy} + O\left(\Delta t \Delta y^6\right) + O\left(\Delta t^2\right).
\end{aligned}$$

Forming the last term in (5.6),

$$\delta_x^2\,\delta_y^2\,\left(u_{jk}^{n+1}-u_{j,k}\right) \;=\; \delta_x^2\left[\Delta t\,\Delta y^2\,u_{tyy}+\frac{1}{12}\,\Delta t\,\Delta y^4\,u_{tyyyy}+O\left(\Delta t\,\Delta y^6\right)+O\left(\Delta t^2\right)\right],$$

$$\begin{aligned}
&= \Delta t\,\Delta x^2\,\Delta y^2 u_{tyyxx}+\frac{1}{12}\,\Delta t\,\Delta y^2\,\Delta x^4 u_{tyyxxxx}+O\left(\Delta t\,\Delta y^2\,\Delta x^6\right)\\
&\quad+\frac{1}{12}\,\Delta t\,\Delta x^2\,\Delta y^4 u_{tyyyyxx}+O\left(\Delta t\,\Delta x^4\,\Delta y^4\right)\\
&\quad+O\left(\Delta t\,\Delta x^2\,\Delta y^6\right)+O\left(\Delta t^2\right).
\end{aligned}$$

We can readily see that

$$\frac{\delta_x^2\,\delta_y^2}{\Delta x^2\,\Delta y^2}\left(u_{jk}^{n+1}-u_{j,k}\right)=\Delta t u_{tyyxx}+O\left(\Delta t\,\Delta x^2\right)+O\left(\Delta t\,\Delta y^2\right)+O\left(\Delta t^2\right),$$

and since this term is multiplied by Δt in the last term in (5.6), we can see this term is second order accurate in Δt, Δx, and Δy. Therefore, we have shown that the ADI method is second order accurate in time and space.

Stability of the Linear ADI Method

Fourier analysis will be used to prove that the ADI method is unconditionally stable. We define the two dimensional discrete Fourier transform for a sequence of points $\boldsymbol{u}=u_{j,k}$, $-\infty<i,j<\infty$ as

$$\mathcal{F}(\boldsymbol{u})(\xi,\eta)=\hat{u}(\xi,\eta)=\frac{1}{2\pi}\sum_{j,k=-\infty}^{\infty}e^{-ij\xi-ik\eta}u_{j,k}. \tag{5.7}$$

We need to discern how the Fourier transform operates on spatial shifts, so we define

the shift operators

$$S_{x\pm}\left(u_{j,k}\right) = u_{j\pm1,k}, \qquad S_{y\pm}\left(u_{j,k}\right) = u_{j,k\pm1},$$

and note that

$$\mathcal{F}\left(S_{x\pm}\left(u_{j,k}\right)\right) = e^{\pm i\xi}\mathcal{F}\left(u_{j,k}\right), \qquad \mathcal{F}\left(S_{y\pm}\left(u_{j,k}\right)\right) = e^{\pm i\eta}\mathcal{F}\left(u_{j,k}\right).$$

Returning to (5.1) and taking the Fourier transform yields

$$\begin{aligned}
\left(1 - \frac{r_x}{2}\,\delta_x^2\right) u_{j,k}^{n+\frac{1}{2}} &= \left(1 + \frac{r_y}{2}\,\delta_y^2\right) u_{j,k}^{n}, \\
\hat{u}^{n+\frac{1}{2}} - \frac{r_x}{2}\left(e^{i\xi}\hat{u}^{n+\frac{1}{2}} - 2\hat{u}^{n+\frac{1}{2}} + e^{-i\xi}\hat{u}^{n+\frac{1}{2}}\right) &= \hat{u}^{n} - \frac{r_y}{2}\left(e^{i\eta}\hat{u}^{n} - 2\hat{u}^{n} + e^{-i\eta}\hat{u}^{n}\right), \\
\hat{u}^{n+\frac{1}{2}} - \frac{r_x}{2}\left(2\hat{u}^{n+\frac{1}{2}}\cos\xi - 2\hat{u}^{n+\frac{1}{2}}\right) &= \hat{u}^{n} + \frac{r_y}{2}\left(2\hat{u}^{n}\cos\eta - 2\hat{u}^{n}\right), \\
\left(1 + r_x\left(1 - \cos\xi\right)\right)\hat{u}^{n+\frac{1}{2}} &= \left(1 + r_y\left(\cos\eta - 1\right)\right)\hat{u}^{n}, \\
\left(1 + 2r_x\sin^2\frac{\xi}{2}\right)\hat{u}^{n+\frac{1}{2}} &= \left(1 - 2r_y\sin^2\frac{\eta}{2}\right)\hat{u}^{n}, \\
\hat{u}^{n+\frac{1}{2}} &= \frac{1 - 2r_y\sin^2\frac{\eta}{2}}{1 + 2r_x\sin^2\frac{\xi}{2}}\,\hat{u}^{n}.
\end{aligned}$$

Repeating this process on (5.2) yields

$$\left(1 - \frac{r_y}{2}\delta_y^2\right) u_{j,k}^{n+1} = \left(1 + \frac{r_x}{2}\delta_x^2\right) u_{j,k}^{n+\frac{1}{2}},$$

which implies that

$$\hat{u}^{n+1} = \frac{1 - 2r_x \sin^2\frac{\xi}{2}}{1 + 2r_y \sin^2\frac{\eta}{2}}\,\hat{u}^{n+\frac{1}{2}} = \frac{\left(1 - 2r_x \sin^2\frac{\xi}{2}\right)\left(1 - 2r_y \sin^2\frac{\eta}{2}\right)}{\left(1 + 2r_x \sin^2\frac{\xi}{2}\right)\left(1 + 2r_y \sin^2\frac{\eta}{2}\right)}\,\hat{u}^{n}.$$

For this two step scheme to be unconditionally stable we need to show that for all ξ and η,

$$|\rho(\xi,\eta)| = \left|\frac{\left(1 - 2r_x \sin^2\frac{\xi}{2}\right)\left(1 - 2r_y \sin^2\frac{\eta}{2}\right)}{\left(1 + 2r_x \sin^2\frac{\xi}{2}\right)\left(1 + 2r_y \sin^2\frac{\eta}{2}\right)}\right| \leq 1.$$

Expanding the numerator and denominator yields

$$|\rho(\xi,\eta)| = \left|\frac{1 - 2r_x \sin^2\frac{\xi}{2} - 2r_y \sin^2\frac{\eta}{2} + 4r_x r_y \sin^2\frac{\xi}{2}\sin^2\frac{\eta}{2}}{1 + 2r_x \sin^2\frac{\xi}{2} + 2r_y \sin^2\frac{\eta}{2} + 4r_x r_y \sin^2\frac{\xi}{2}\sin^2\frac{\eta}{2}}\right|.$$

In this form, it is clear that the denominator is larger than the numerator for all ξ and η and therefore the inequality is proven and this method is unconditionally stable. As we have shown the scheme is consistent and stable, by the Lax Equivalence Theorem, the numerical scheme is convergent.

REFERENCES CITED

[1] Aslanidi O. V., O. A. Mornev, et al. Excitation wave propagation as a possible mechanism of signal transmission in pancreatic islets of Langerhans. *Biophysical Journal*, 80:1195–1209, 2001.

[2] Bertram R. and M. Pernarowski. Glucose diffusion in pancreatic islets of Langerhans. *Biophysical Journal*, 74:1722–1731, 1998.

[3] Pernarowski M. Fast and slow subsystems for a continuum model of bursting activity in the pancreatic islet. *SIAM J. Appl. Math.*, 58(5):1667–1687, 1998.

[4] Peaceman D.W. and H. H. Rachford. The numerical solutions of parabolic and elliptic differential equations. *SIAM*, 3:28–41, 1955.

[5] Douglas Jr. J. On the numerical integration of $\frac{\partial^2 u}{\partial x^2} + \frac{\partial^2 u}{\partial y^2} = \frac{\partial u}{\partial t}$ by implicit methods. *SIAM*, 3(1):42–65, 1955.

[6] Amiri S. and S. M. Hosseini. Second-order method for solving 2D nonlinear parabolic differential equations based on ADI method. *International Journal of Modeling, Simulation, and Scientific Computing*, 1(1):133–146, 2010.

[7] Hodgkin A.L. and A. F. Huxley. A quantitaive description of membrane current and its application to conduction and excitation in the nerve. *The Journal of Physiology*, 117(4):500–544, 1952.

[8] Dean P.M. and E. K. Matthews. Glucose induced electrical activity in pancreatic islet cells. *The Journal of Physiology*, 210:255–264, 1970.

[9] Sherman A., J. Rinzel, and J. Keizer. Emergence of organized bursting in clusters of pancreatic β-cells by channel sharing. *Biophysical Journal*, 54:411–425, 1988.

[10] Chay T.R. and J. Keizer. Morphological evidence for pancreatic polarity of β-cell within islets of Langerhans. *Diabetes*, 37:616–621, 1988.

[11] Atwater I., C. M. Dawson, A. Scott, G. Eddlestone, and E. Rojas. The nature of oscillatory behavior in electrical activity from pancreatic β-cell. *Hormone and Metabolic Research supplement series*, 1980(10):100–107, 1980.

[12] Keizer J. and G. Magnus. ATP-sensitive potassium channel and bursting in the pancreatic beta cell. *Biophysical Journal*, 56:229–241, 1989.

[13] Smolen P. and J. Keizer. Slow voltage inactivation of Ca^{2+} currents and bursting mechanisms for mouse pancreatic β-cells. *J. Math. Biology*, 127:187–190, 1992.

[14] Smith P. A., F. M. Ashcroft, and P. Rorsman. Simultaneous recordings of glucose dependent electrical activity and ATP-regulated K^+-currents in isolated mouse pancreatic β-cells. *FEBS Letters*, 261(1):187 – 190, 1990.

[15] Sherman A. Theoretical aspects of synchronized bursting in β-cells. In Huizinga J. D., editor, *Pacemaker Activity and intercellular communication*, pages 323–337. CRC Press, 1995.

[16] Sherman A. and J. Rinzel. Rhythmogenic effects of weak electronic coupling in neuronal models. *Proc. Natl. Acad. Sci. USA*, 89:2471–2474, 1992.

[17] Sherman A. Contributions of modeling to understanding stimulus secretion coupling in pancreatic β-cells. *Am. J. Physiol. - Endocrinology & Metabolism*, 271:E362–E372, 1996.

[18] Keizer J. and P. Smolen. Bursting electrical activity in pancreatic β-cells caused by $Ca^{2+}-$ and voltage-inactivated Ca^{2+} channels. *Proc. Natl. Acad. Sci. USA*, 88:3897–3901, 1991.

[19] Worley III J. F., M. S. McIntyre, et al. Endoplasmic reticulum calcium store regulates membrane potential in mouse islet β-cells. *J. of Biochemistry*, 269(20):14359–14362, 1994.

[20] Bertram R., P. Smolen, et al. A role for calcium release-activated current (CRAC) in cholinergic modulation of electrical activity in pancreatic β-cells. *Biophysical Journal*, 68:2323–2332, 1995.

[21] Sherman A. Calcium and membrane potential oscillations in pancreatic β-cells. In Othmer H. G., F. R. Adler, et al., editors, *Case Studies in Mathematical Modeling: Ecology, Physiology, and Cell Biology*, pages 199–217. Prentice-Hall, 1997.

[22] Cook D.L., M. Ikeuchi, and W. Y. Fujimoto. Lowering of pH_i inhibits Ca^{2+}-activated K^+ channels in pancreatic β-cells. *Nature*, 311:269–271, 1984.

[23] Ermentrout B. *Simulating, Analyzing, and Animating Dynamical Systems: A Guide to XPPAUT for Researchers and Students*. SIAM, 2002.

[24] Atwater I., A. Goncalves, et al. Cooling dissociates glucose-induced insulin release from electrical activity and cation fluxes in rodent pancreatic islets. *The Journal of Physiology*, 384:615–627, 1984.

[25] Johnson J.H., C. B. Newgard, et al. The high K_m glucose transporter of islets of Langerhans is functionally similar to the low affinity transporter of the liver and has an identical primary sequence. *The Journal of Biological Chemistry*, 265(12):6548–6551, 1990.

[26] Whitesell R. R., A. C. Powers, et al. Transport and metabolism of glucose in an insulin-secreting cell line. *Biochemistry*, 30:11560–11566, 1991.

[27] Bonner-Weir S. Glucose diffusion in pancreatic islets of Langerhans. *Biophysical Journal*, 74:1722–1731, 1998.

[28] Rieske E., P. Schubert, and G. W. Kreutzbert. Transfer of radioactive material between electrically coupled neurons of the leech central nervous system. *Brain Research*, 84:365–382, 1975.

[29] Maki L.W. and J. Keizer. Analysis of possible mechanisms for in vitro oscillations of insulin secretion. *Am. J. Physiol.*, 268:C780–C791, 1995.

[30] Aslanidi O. V., O. A. Mornev, et al. A model for glucose-induced wave propagation in pancreatic islets of Langerhans. *J. of Theoretical Biology*, 215:273–286, 2002.

[31] Perez-Armendariz M., D. C. Spray, and M. V. L. Bennett. Biophysical properties of gap junctions between freshly dispersed pairs of mouse pancreatic beta cells. *Biophysical Journal*, 59:76–92, 1985.

[32] Sherman A. and J. Rinzel. Model for synchronization of pancreatic β-cells by gap junctions. *Biophysical Journal*, 59:547–559, 1991.

[33] Halban P., C. Wollheim, et al. The possible importance of contact between pancreatic islet cells for the control of insulin release. *Endocrinology*, 111:86–94, 1984.

[34] Smolen P., J. Keizer, and A. Sherman. Why pancreatic islets burst but single β-cells do not. *Biophysical Journal*, 64:1668–1680, 1993.

[35] Kinard T.A., G. de Vries, et al. Modulation of the bursting properties of single mouse pancreatic β-cells by artifical conductances. *Biophysical Journal*, 76:1423–1435, 1999.

[36] Watts M., J. Tabak, and R. Bertram. Mathematical modeling demonstrates how multiple slow process can provide adjustable control of islet bursting. *Islets*, 3:320–326, 2011.

[37] Pedersen M.G. Wave speeds of solutions to density dependent nonlinear Nagumo diffusion equations - inspired by oscillating gap-junction conductance in the pancreatic islets of Langerhans. *J. of Math. Biology*, 80:683–698, 1995.

[38] Pedersen M.G. A biophysical model of electrical activity in human β-cells. *Biophysical Journal*, 99:3200–3207, 2010.

[39] Keener J. and J. Sneyd. *Mathematical Physiology.* Springer-Verlag, 1998.

[40] Fitzhugh R. Impulses and physiological states in theoretical models of nerve membrane. *Biophysical Journal*, 1:445–466, 1961.

[41] Nagumo J., S. Arimoto, and S. Yoshizawa. An active pulse transmission line simulating nerve axon. *Proceedings of the IEEE*, 50:2061–2070, 1962.

[42] E. J. Doedel. AUTO: A program for the automatic bifurcation analysis of autonomous systems. *Cong. Num.*, 30:265–384, 1981. Proc. 10th Manitoba Conf. on Num. Math. and Comp., Univ. of Manitoba, Winnipeg, Canada.

[43] Doedel E. J. AUTO-07P: Continuation and bifurcation software for ordinary differential equations. Technical report, Concordia University, 2007.

[44] Doedel E. J. and J.P. Kernévez. AUTO: Software for continuation problems in ordinary differential equations with applications. Technical report, Applied Mathematics, California Institute of Technology, 1986.

[45] Doedel E.J. and M.J. Friedman. Numerical computation of heteroclinic orbits. *Journal of Computational and Applied Mathematics*, 26:155–170, 1989.

[46] Morris C. and H. Lecar. Voltage oscillations in the barnacle giant muscle fiber. *Biophysical Journal*, 35, 1981.

[47] Doedel E. J., M. J. Friedman, and A. C. Monteiro. On locating homoclinic and heteroclinic orbits. Technical report, Ithaca, NY, USA, 1993.

[48] Thomas J. W. *Numerical Partial Differential Equations: Finite Difference Methods.* Springer-Verlag, 1995.